UFL/COEL–90/018

SHORELINE CHANGES ADJACENT TO FLORIDA'S EAST COAST TIDAL INLETS

by

Paul A. Work
and
Robert G. Dean

January 1, 1990

Shoreline Changes Adjacent to Florida's East Coast Tidal Inlets

Paul A. Work and Robert G. Dean

January 1, 1990

Contents

1 Abstract

The interruption of longshore sediment transport by a tidal inlet often causes significant shoreline changes on either side of the inlet, resulting in a "shoreline signature" that is typically a complicated function of many parameters. The present study presents a method of representing shoreline changes as even and odd functions (components), providing insight regarding the importance of the various physical processes occurring at the site. The analysis technique is described and some idealized examples presented. Limitations and characteristic features of the method are examined. Results are presented and interpreted for measured shoreline changes at 18 tidal inlets on the eastern coast of Florida. This sample includes natural inlets, natural inlets that have been jettied and deepened, and constructed inlets.

The odd function is often found to be dominant in both magnitude and extent, typically showing the familiar updrift offset planform obtained by the analytical solution to the problem of interruption of longshore sediment transport by a littoral barrier. The zone of influence for the inlet often extends as far as 5–6 miles up– and downdrift of the inlet. The even and odd functions can be used to estimate the extent of this zone.

The effects of a large ebb tidal shoal, permeable inlet training structures, background erosion, and reversals in longshore sediment transport direction are discussed. Finite difference computer simulations are used to investigate the effects of wave diffraction, refraction (due to both bathymetric features and tidal currents), and breaking patterns near the inlet on the shoreline change components. Several recent studies have investigated the wave field in the vicinity of shore-normal structures and inlets, and the subject remains of considerable interest (Douglas, 1989, Winer, 1988, Yan, 1987).

Complications introduced by the inclusion of beachfills, dredging and sand bypassing, the presence of reefs and ebb tidal shoals, modifications to coastal structures, and other deviations from idealized conditions are discussed. Applicability of the method to other sites is examined.

2 Introduction

Accurate, quantitative prediction of the time–dependent response of a beach to the construction or modification of a tidal inlet remains a challenging task. Determination of the detailed wave field surrounding the inlet is necessary, and wave shoaling, refraction, diffraction, and reflection will often be of importance at any given site. The longshore and cross–shore sediment transport that is driven by these waves will cause changes in the bathymetry, which in turn modifies the wave climate. Even with the bathymetry known, directional wave data are often unavailable or inadequate for prediction of the rapidly varying wave climate throughout the region of interest.

Formation of a tidal inlet, whether by natural or human activity, typically leads to the growth of an ebb tidal shoal. Given an adequate sediment supply, the shoal will usually increase in size until a balance has been achieved between the forces due to ebb tidal currents, which tend to jet material from the inlet throat out to the shoal, and the incident waves, which tend to drive material back onshore. This process often coincides with changes in the peak ebb tidal currents as the inlet throat adjusts to an equilibrium size subsequent to creation of the inlet. The ebb tidal currents are of greater importance to shoal formation and maintenance than the flood tidal currents, since the ebb tide tends to emerge from the inlet as a relatively well–defined jet (analogous to flow from a nozzle). The flood tidal current into the inlet is less organized, analogous to flow into a nozzle. A parallel argument is applicable regarding formation of the flood tidal shoal, although wave action on the flood tidal shoal is typically much less energetic, allowing continued growth of the shoals. Since most of the material comprising the shoals is supplied by the beaches adjacent to the inlet, an evolving shoal may be considered a sediment sink when evaluating the sediment budget for the region. The shoal volumes are often quite substantial (Walton and Adams, 1976).

If the ebb shoal is forced into deep water by the construction of long inlet training structures, or if a navigation channel is dredged through it, its ability to pass sediment from one side of the inlet to the other will be reduced. If no other mechanism is available to achieve this bypassing, the result will typically be accretion on the updrift side of the inlet, with a corresponding erosion downdrift. This is particularly true for stabilized inlets. Mechanical bypassing systems have been used to counteract these trends, but sediment is typically bypassed in only one direction and the average annual bypassing rate is often less than the net annual longshore sediment transport rate on

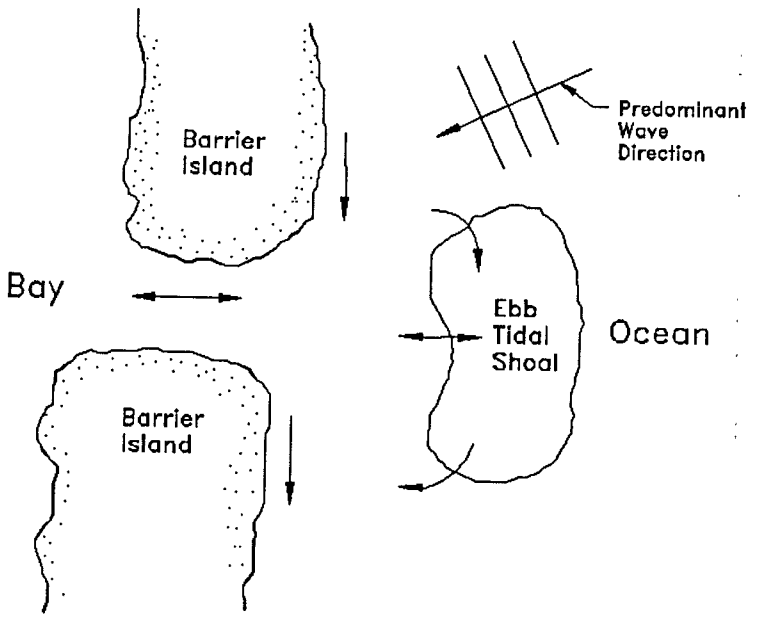

Figure 1: Schematic of inlet sand transfer processes.

the adjacent beaches.

Dredging for channel maintenance can serve as sediment bypassing if spoil is directed to the downdrift shore, or can represent a sediment loss if dumped offshore. Deep–water disposal of dredge spoil from inlets along Florida's east coast has resulted in the loss of more than 40 million yd^3 of material, much of it beach–quality sand (Dean, 1988). Management practices at most of Florida's tidal inlets now dictate placement of dredge spoil within the littoral zone, downdrift of the inlet.

Accurate assessment of the combined effect of all of the aforementioned factors remains a difficult problem. For this reason, simplifying assumptions are often employed when attempting to predict shoreline response to an inlet. These will be discussed in the following subsections.

2.1 Analytical Prediction of Shoreline Changes Adjacent to Inlets

For a stabilized inlet in a region having an appreciable net longshore sediment transport rate, the beach planform typically acquires significant updrift and downdrift offsets. Pelnard–Considère (1956) was first to obtain an analytical predictive equation for this evolution. He simplified the problem to an initially straight beach of infinite length, subject to a uniform, constant wave climate, upon which is placed (instantly) an impermeable littoral barrier of finite length. This case is of particular interest for this study, since it provides a simplified representation of the situation created when an inlet is cut through a beach and stabilized with jetties. Larson et al. (1987) review the solutions by Pelnard–Considère and other papers on the topic, and present solutions for shoreline evolution for several different sets of boundary and initial conditions.

An additional approximation is made that all contours move on– and offshore at equal rates (thus reducing the problem to specification of the location of one contour, typically the shoreline, hence the term "one–line model"). The problem can then be shown to be governed by the one–dimensional heat, or diffusion equation (Larson et al., 1987):

$$\frac{\partial y}{\partial t} = G\frac{\partial^2 y}{\partial x^2} \tag{1}$$

where x and y represent longshore and offshore coordinates, respectively (Figure 2), and G is a diffusion constant which may be expressed as:

$$G = \frac{K H_b^{\frac{5}{2}} \sqrt{\frac{g}{\kappa}}}{8(s-1)(1-p)(h_* + B)} \tag{2}$$

where

K = Dimensionless transport coefficient of order 1

H_b = Wave height at breaking

g = Gravitational constant

$\kappa = \frac{H_b}{h_b}$ (Spilling breaker assumption)

h_b = Water depth at breaking

s = Sediment specific gravity

p = Sediment porosity

h_* = Maximum depth of sediment motion, or depth of closure

B = Berm height

Equation 1 is a linear, second–order partial differential equation, and, given appropriate boundary and initial conditions, can be solved analytically to yield a function representing shoreline evolution over time.

The initial condition of a straight, undisturbed shoreline is represented by:

$$y(x,0) = 0 \quad |x| < \infty \tag{3}$$

and the boundary condition of an impermeable littoral barrier at $x = 0$ is specified as:

$$\frac{\partial y}{\partial x}\,|_{x=0} = \tan(\beta - \alpha_b) \quad t > 0 \tag{4}$$

where β is the initial azimuth of the shore–normal vector and α_b is the azimuth of the wave rays at breaking (Figure 2). This boundary condition states that the shoreline at the structure will orient itself to match the direction of the incoming waves, yielding zero longshore sediment transport at the structure, and is valid until bypassing around the end of the structure has commenced (i.e. until $y(0,t) = l$, where l denotes the length of the structure). At this point the boundary condition becomes $y(0,t) = l$, and bypassing of sediment around the tip of the barrier begins. The far–field boundary condition is given by Equation 5:

$$y(\pm\infty, t) = 0 \quad \text{for all } t \tag{5}$$

The time of bypassing, t_{bp}, may be expressed in terms of known quantities:

$$t_{bp} = \frac{\pi}{G}\frac{l^2}{4\tan^2(\beta - \alpha_b)} \tag{6}$$

The solution to Equation 1 for the stated boundary and initial conditions (Dean, 1989) is anti–symmetric about the y–axis and is given by:

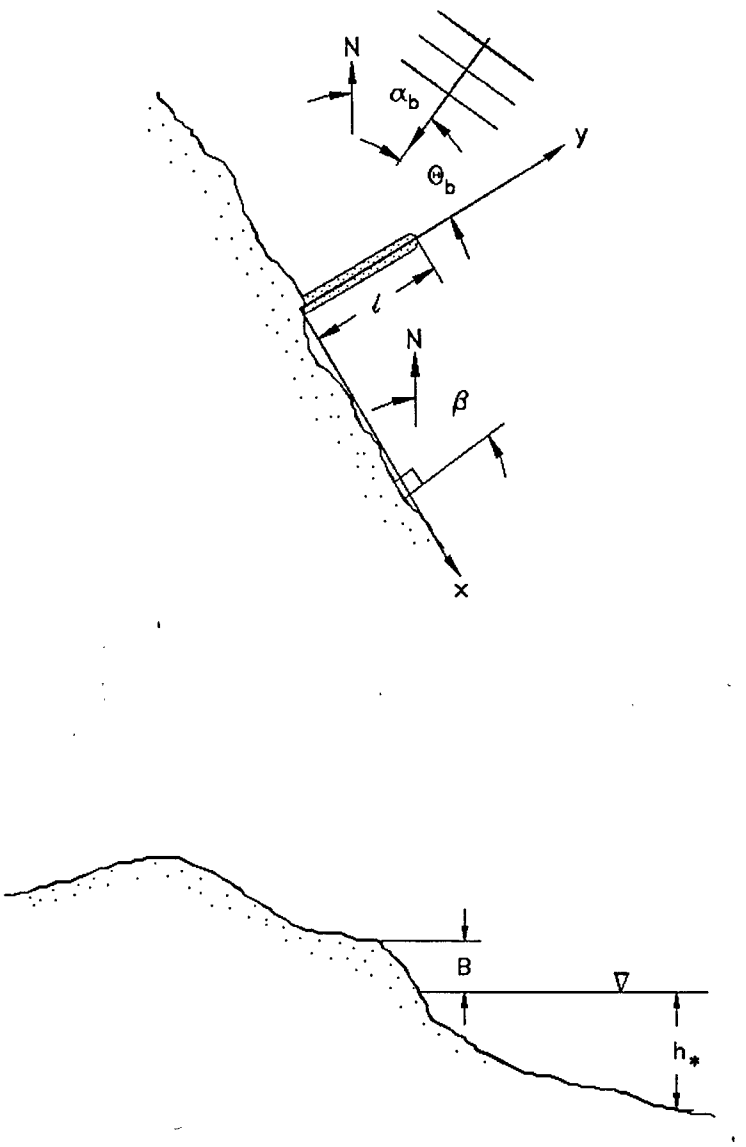

Figure 2: Coordinate geometry and beach profile definitions. $(\beta - \alpha_b)$ = wave direction, relative to shore–normal, at breaking.

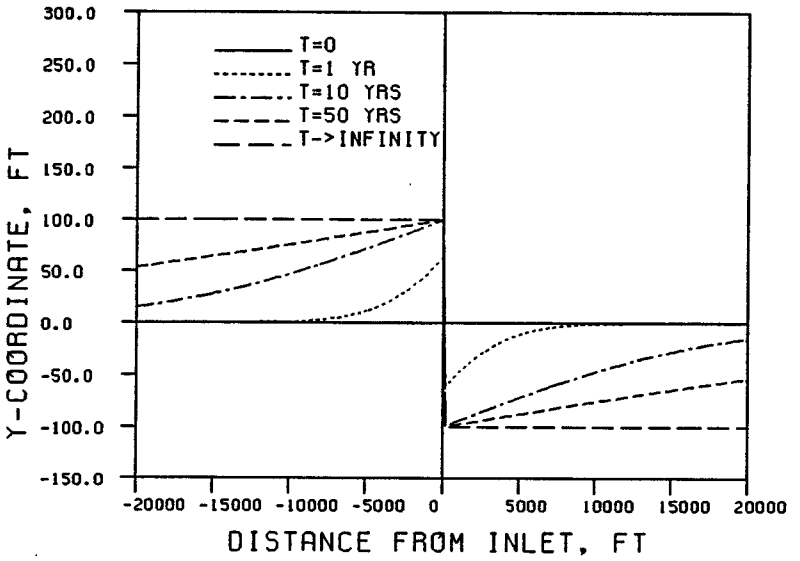

Figure 3: Analytical solution for shoreline evolution vs. time after placement of a littoral barrier. l=100 ft., H_b=3 ft., and $(\beta - \alpha_b)$=1°

$$y(x,t) = -\frac{\tan(\beta - \alpha_b)}{\sqrt{\pi}} \left[\sqrt{4Gt} \exp\left(-\frac{x^2}{4Gt}\right) - x\sqrt{\pi}\,\mathrm{erfc}\left(\frac{x}{\sqrt{4Gt}}\right) \right] \quad \text{for } t < t_{bp} \tag{7}$$

and

$$y(x,t) = \pm l\,\mathrm{erfc}\left(\frac{x}{\sqrt{4Gt}}\right) \quad \text{for } t > t_{bp} \tag{8}$$

where erfc denotes the complimentary error function (Abramowitz and Stegun, 1972).

Figure 3 shows the evolution of a shoreline after placement of a littoral barrier as represented by Equations 7 and 8. Note that the solution for $t \rightarrow \infty$ consists of two straight line segments, the updrift portion being displaced a distance of $+l$ from the initial condition, and the downdrift displaced a distance of $-l$. At this asymptotic limit, the structure does not impede the transport, i.e. the transport is uniform along the entire shoreline.

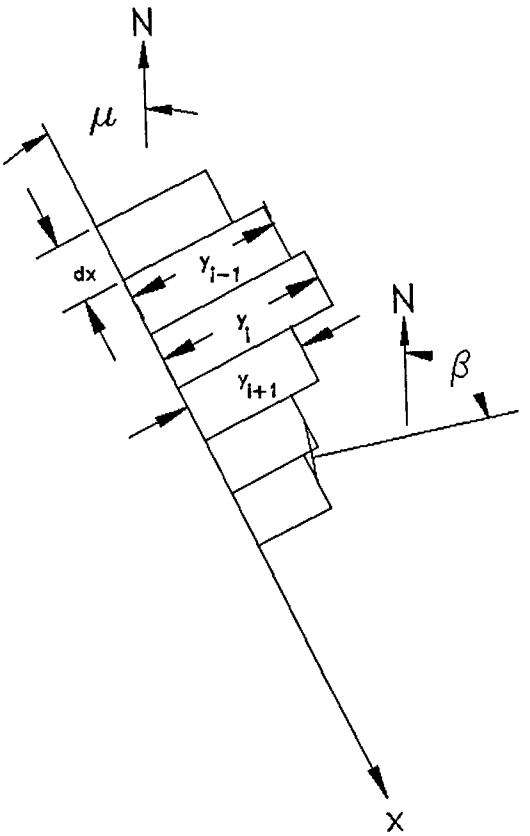

Figure 4: Geometry for finite–difference model of shoreline change.

2.2 Numerical Simulation of Shoreline Evolution

Several inlets were studied through the use of a finite–difference computer simulation of shoreline evolution. Such a model provides an effective method for treatment of a spatially and temporally varying wave climate. The problem of shoreline evolution subsequent to the placement of a littoral barrier is treated by dividing a finite domain up into N cells of equal length, Δx, as shown in Figure 4.

Rather than combining the sediment transport equation and the continuity equation to obtain one governing equation (the diffusion equation) as was done for the analytical solution, it is more convenient for this method to first compute a sediment transport rate into and out of a cell, and then compute the new shoreline position using the continuity equation. The assumption that all contours move together is retained. This is the simplest form of such a model — an explicit, one–line representation. The first step

in such a model is determination of the shoreline orientation relative to the wave direction. This was done by calculating the local azimuth of the shore–normal vector:

$$\beta_i^n = \mu - \tan^{-1}\left(\frac{(y_i^n - y_{i-1}^n)}{\Delta x}\right) + \frac{\pi}{2} \tag{9}$$

where μ is the angle of rotation of the coordinate system, and i denotes the node number, as shown in Figure 4. The time level is denoted by n, and the time step will be denoted by Δt. All angles were defined to be measured clockwise from true north.

The transport equation then becomes:

$$Q_i^n = \frac{1}{2} G_i^n (h_* + B) \sin 2(\beta_i^n - \alpha_{bi}^n) \tag{10}$$

Note that all variables are as defined in the analytical solution, but G, β, and α_b can now vary both temporally and spatially.

With the transport into and out of each cell computed, the continuity equation can be arranged to give the new shoreline position, after which a new time step is initiated:

$$y_i^{n+1} = y_i^n - \frac{\Delta t}{\Delta x} \frac{1}{(h_* + B)} (Q_{i+1}^n - Q_i^n) \tag{11}$$

A wave propagation model was used to provide an input wave climate to the shoreline evolution model. A description of the wave model is presented in section 4.2.

Many shorelines, even when in a relatively stable equilibrium form, prior to modifications by man, are not well approximated by a straight line. Rock outcrops, reefs, and other features may be responsible for more complicated, yet relatively stable, equilibrium planforms. If such a geometry is taken as the initial condition in the finite–difference model just described, for the case of no shoreline modifications, the equilibrium solution is a straight line — obviously not realistic. In this case, it is a reasonable approximation to employ an ad–hoc method, using a coordinate transformation to map the initial shoreline into a straight line, then running the model with the boundary conditions of interest, and lastly transforming the end result back by the inverse mapping. In this way, the influences of the processes preserving the initial equilibrium shoreline remain in the model. This method was not applied during this study, but is presented for future consideration.

3 Even/Odd Analysis Technique

The difficulty of reducing the limiting assumptions inherent in the analytical solution and, to a lesser degree, the numerical solutions, to an acceptable number makes an alternative viewpoint attractive. The even/odd analysis technique for investigating shoreline changes evolved from this need for a tool by which insight could be gained regarding the physical processes dominant at a site. The method has the advantage of being simple to execute, but often requires thoughtful interpretation of the results.

An even function, $y_E(x)$, is defined as any function that is symmetric about the y–axis. An odd function, $y_O(x)$, is defined as a function that is anti–symmetric about the y–axis. This can be stated mathematically as follows:

$$y_E(x) = y_E(-x) \tag{12}$$

$$y_O(x) = -y_O(-x) \tag{13}$$

The familiar cosine and sine functions are thus examples of even and odd functions, respectively.

In the present study, it was desired to divide a function, given by the shoreline change over a known time interval vs. distance from the inlet of interest, into even and odd components. This technique is presented in Berek and Dean (1982), and Dean and Pope (1987), although the characteristics of the sites studied differed from those of the sites that will be examined here. If $y_T(x)$ denotes the function to be separated into even and odd components, its even and odd components must satisfy the following equations:

$$y_T(x) = y_E(x) + y_O(x) \tag{14}$$

$$y_T(-x) = y_E(-x) + y_O(-x) \tag{15}$$

Equations 12 and 13 may be substituted into Equation 15 to yield the following:

$$y_T(-x) = y_E(x) - y_O(x) \tag{16}$$

Adding Equations 14 and 16 yields:

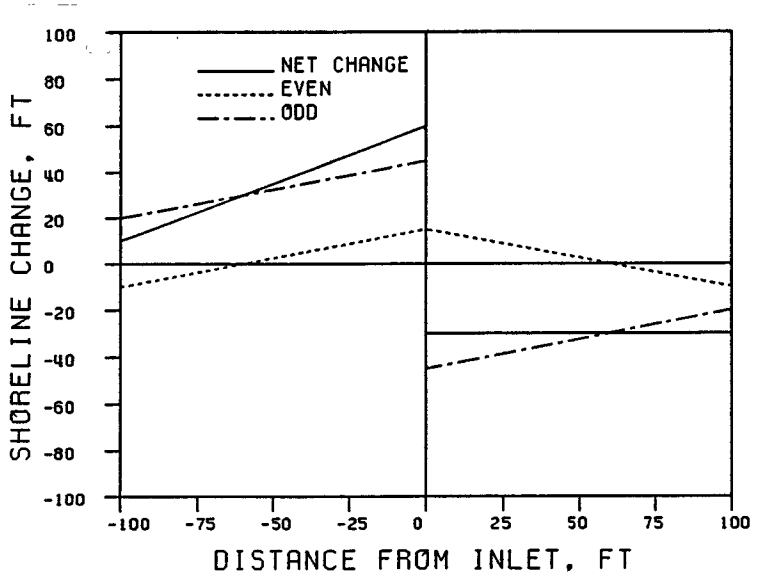

Figure 5: Function for example of even/odd analysis.

$$y_E(x) = \frac{y_T(x) + y_T(-x)}{2} \tag{17}$$

while subtracting them gives:

$$y_O(x) = \frac{y_T(x) - y_T(-x)}{2} \tag{18}$$

Note that any function $y_T(x)$, having any shape, can be divided into even and odd components.

An illustrative example is helpful. Consider the function shown in Figure 5. Note that $y_E(0) = y_T(0)$ and $y_O(0) = 0$, as will always be the case. This example demonstrates the requirement of this method that the distribution of x–coordinates for the data points be symmetrical about the y–axis, although the spacing between points need not be uniform. Also note that integrating the odd function over the domain yields zero, while integrating the even function yields the net amount of accretion or erosion that has taken place within the domain during the time period. One can usually see upon examination of the even function by eye whether any significant net erosion or accretion has taken place.

For the present study, data from historical charts, aerial photos, and surveys were provided by the Division of Beaches and Shores of the Florida Department of Natural Resources (FDNR), in the form of digitized shoreline position records. Each data point was determined by measurement of the distance from a survey monument to the MHW line. More than 3000 monuments have been placed along the sandy beach shoreline of Florida on a nominal spacing of 1000 feet.

The data provided by the FDNR gave shoreline position in terms of state plane coordinates. A coordinate transformation was then applied to place the inlet at the origin of a new, right–handed coordinate system, with the x–axis laid roughly parallel to the coast (Figure 6):

$$x = (E - E_o)\cos\delta + (N - N_o)\sin\delta \tag{19}$$

$$y = -(E - E_o)\sin\delta + (N - N_o)\cos\delta \tag{20}$$

where (E, N) denotes the coordinates of the point of interest in the state plane coordinate system, (x, y) the coordinates in the new system centered at the inlet, and (E_o, N_o) the origin of the new coordinate system in the state plane coordinate system. The angle of rotation of the new coordinate system relative to the old (measured counter–clockwise) is denoted by δ.

The average azimuth of a line normal to the shore (β in Figure 4) was also known; δ was taken as $-\beta$.

Surveys were sorted by date and geographical location. Two surveys were selected for even/odd analysis of shoreline change. A computer program was used to transform the coordinates for both surveys, as described, determine change in shoreline position, and divide the changes into even and odd components. Linear interpolation was used to ensure that the x–coordinates of the data points were distributed symmetrically about the y–axis.

3.1 Data requirements

Digitized records from two surveys of MHW–line position spanning a known time interval are required. The spatial extent of the surveys must encompass the inlet of interest; the minimum distance from the inlet to either end of either survey will determine the maximum domain for even/odd analysis. The domain should be large enough to include the "zone of influence" of the inlet, which is typically not known in advance. The length of this zone was

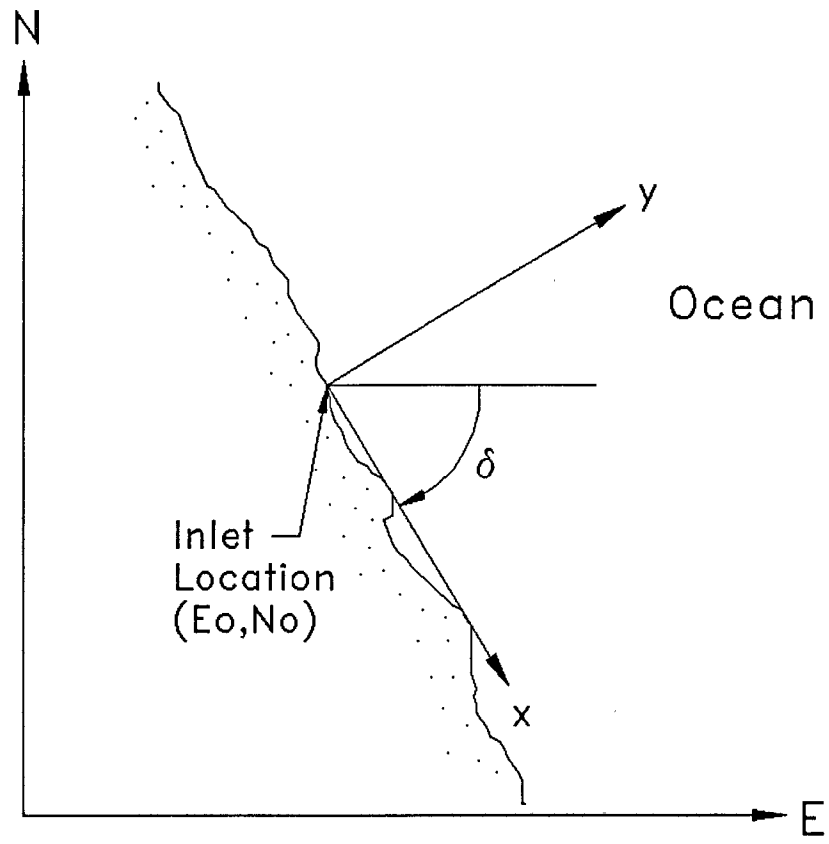

Figure 6: Definition sketch for coordinate transformation.

often found to be quite large, in some cases more than five miles up– and downdrift of the inlet.

For the case of constructed or modified inlets ("modified" meaning a natural inlet that has been dredged and/or stabilized by one or more jetties), it is usually of interest to use as a first survey a date corresponding closely to the time at which the modifications were made. Subsequent intentional modifications (such as beachfills) usually complicate the picture, so a good choice for a second survey is any survey subsequent to the first that precedes such modifications. Once the simpler case is understood, the more difficult problem including beachfills, inlet modifications, etc., may be included. It should be noted here that the method is best applied over a long time interval — "long" meaning of a duration such that the measured shoreline changes are much greater than the seasonal variations in shoreline position. This is particularly important if the exact date of the survey is not known, as is often the case with older surveys. For the east coast of Florida, this implies that, unless the exact dates of the surveys are known, shoreline changes less than 40–60 feet should be considered "noise". A similar value would be appropriate for the west coast of Florida. Seasonal variations and storm effects would appear generally as even functions. The margin of error for the charts to be used could also impose a minimum analysis time. Fortunately, for purposes of analysis, the "signal" due to inlet modification is usually large compared to seasonal shoreline variations.

3.2 Demonstration of the Method for Some Idealized Cases

Impoundment of Longshore Transport plus Uniform Erosion

Because of the complexity of the coupled longshore/cross–shore transport problem, shoreline changes are sometimes simulated by simple addition of changes induced by longshore gradients in the longshore transport rate and changes caused by cross–shore transport. Changes resulting from cross–shore transport are sometimes treated by assuming a uniform background erosion rate over the region. Impoundment updrift and erosion downdrift of a littoral barrier combined with an increase in relative local sea level along a beach having a relatively constant cross–section would be one example of a potential application of such a technique.

The analytical solution developed by Pelnard–Considère (1956; Equations 7 and 8), combined with a uniform erosion rate over the entire domain, yields shoreline change, even, and odd functions as shown in Figure 7.

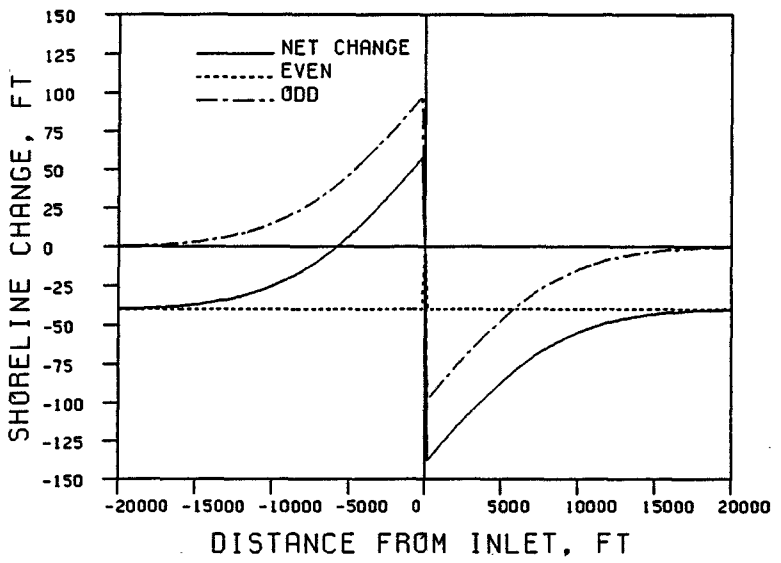

Figure 7: Pelnard–Considère solution with superimposed uniform background erosion of 40 ft. in 50 years. l=100 ft., H_b=1 ft., and $(\beta - \alpha_b)$=1°.

For this simple example, the odd component thus represents only longshore transport processes, and the even component only cross–shore processes.

The analytical solution for the response of an initially straight shoreline to a littoral barrier will always be an odd function, with the magnitude of the accretion on the updrift side matching that of the erosion on the downdrift side. In reality, at an inlet the erosion on the downdrift side is not limited by the barrier length, and may be larger or smaller in magnitude than the length of the barrier. Many factors can combine to cause the wave field to vary over the domain, which in turn will cause sediment transport gradients to exist, modifying the bathymetry, tending to ensure non–uniformity in the nearshore wave field. Refraction due to both bathymetric changes and tidal currents, reflection, and diffraction of energy into the region in the lee of the structure must all be considered. Sediment transport reversals cause deposition in the protected lee of the downdrift jetty. The asymmetry in the resulting beach planform will cause both even and odd components of shoreline change to be present, even if cross–shore transport processes are negligible at the site.

Pure Migration of the Inlet

Many unstabilized inlets migrate in the longshore direction. It is thus of interest to examine the resulting even and odd functions for the case of pure migration of the inlet, meaning translation of the inlet in the longshore direction with no changes in the shape of the beach planform either up– or downdrift of the inlet.

The preferred method of treating inlet migration for even/odd analysis is to perform different coordinate transformations for the two surveys, ensuring that the two inlet locations are both at the origin of the new coordinate system. For the case of no change in shoreline planform relative to the inlet position, such a treatment results in no accretion or erosion within the zone of influence of the inlet, and both the even and odd functions are zero. Some shoreline change may be evident at the ends of the domain if the domain for the even/odd analysis extends beyond the zone of influence for the inlet.

If one considers the migration of an inlet that cuts through a barrier island of thickness h and invokes the assumption of no shoreline changes relative to the inlet (schematized in Figure 8), the even and odd functions that result without consideration of the migration will have an amplitude of $\frac{1}{2}h$ as shown in Figure 9.

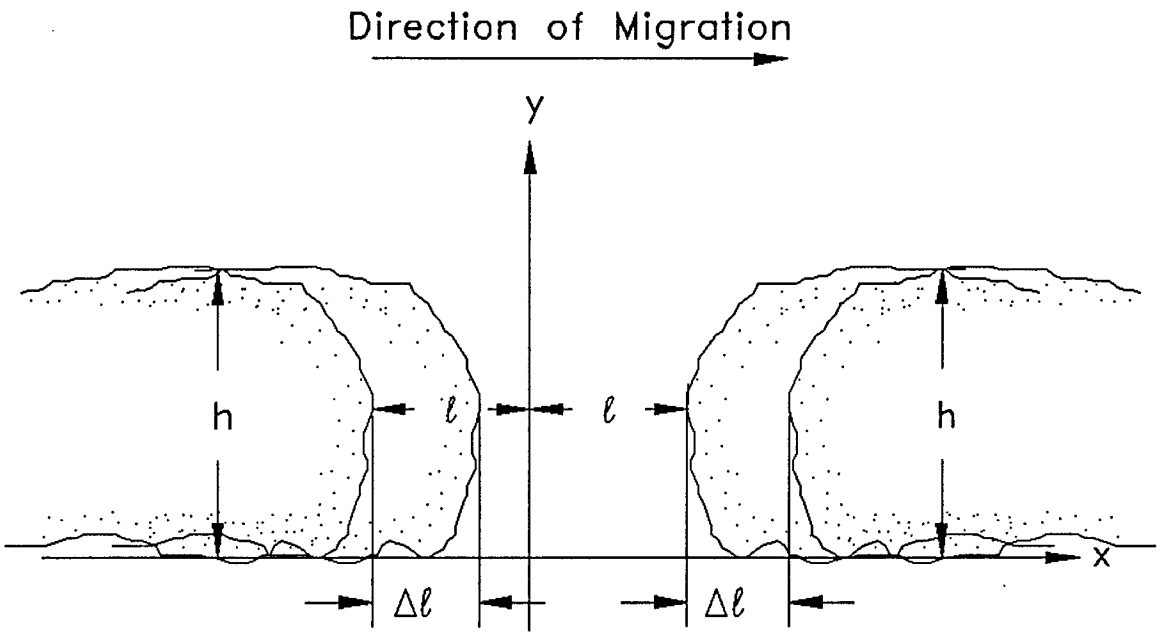

Figure 8: Initial and final shorelines — pure longshore migration of inlet.

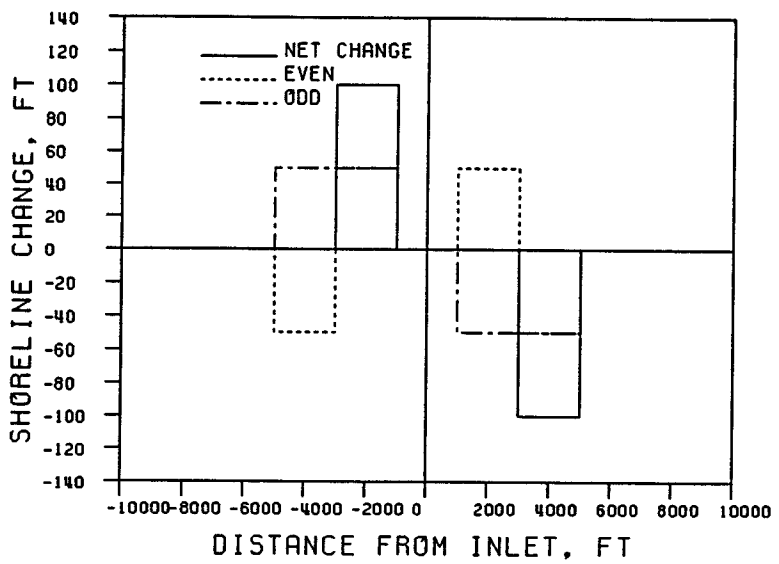

Figure 9: Net change, even, and odd functions for inlet migration of Figure 8.

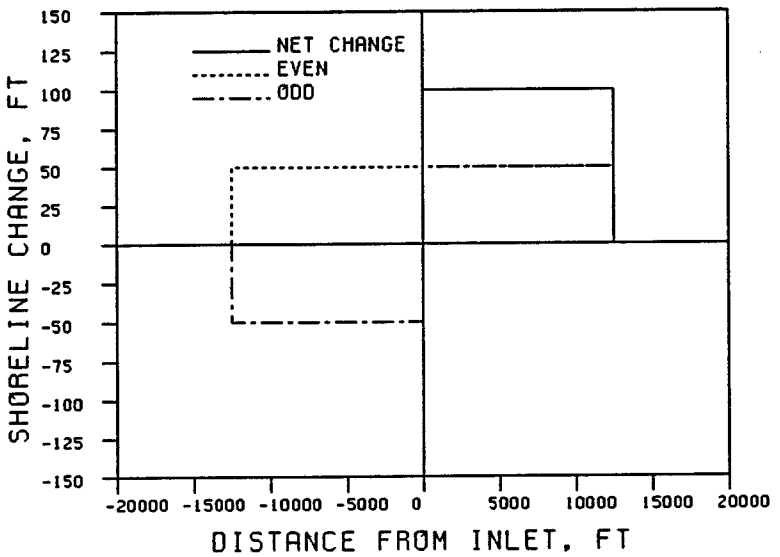

Figure 10: Shoreline change functions resulting solely from downdrift nourishment. Increase in beach width of 100 ft. along 12,500 ft. of coast.

Bypassing a Discrete Quantity of Sand Downdrift

Placing a large quantity of sand on the downdrift shore for beach nourishment purposes will introduce an asymmetry in the shoreline change function and cause both even and odd components to exist. If no other shoreline changes are present, the even and odd components will each have an amplitude equal to one–half that of the shoreline change due to the beachfill. An example is shown in Figure 10.

Selecting a Point other then the Inlet Centerline as Origin

It is important to select the inlet centerline as the origin of the coordinate system when performing the even/odd analysis. Displacement of the origin will make interpretation of the resulting components difficult, causing both even and odd functions to be present even for a case where the shoreline change is an odd function, such as the analytical solution given previously. Figure 11 illustrates the resulting even and odd components if the analytical solution to the problem of shoreline change due to the interruption of

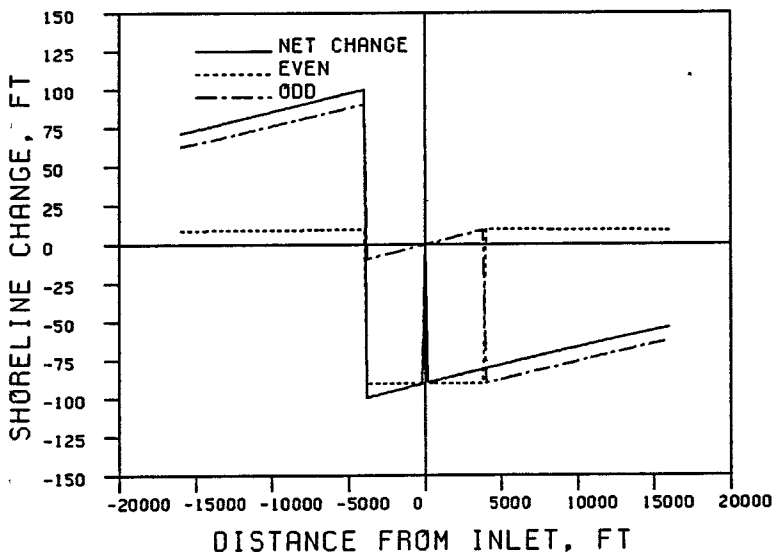

Figure 11: Even and odd functions: Analytical solution with origin shifted 4000 ft.

longshore transport by a littoral barrier is analyzed with the origin displaced.

Determining the Zone of Influence of the Inlet

The even and odd functions, as well as the net shoreline change function from which they are obtained, are also useful for estimating the extent of the "zone of influence" of the inlet. This was done, for several inlets to be presented in Section 5, by plotting the integral of the square of the amplitude of the given function vs. distance from the inlet. This integral was approximated by Equations 21 and 22:

$$Y_E(x_n) = \sum_{i=1}^{n} [y_E(x_i)]^2 (x_i - x_{i-1}) \tag{21}$$

$$Y_O(x_n) = \sum_{i=1}^{n} [y_O(x_i)]^2 (x_i - x_{i-1}) \tag{22}$$

where x_0=0.

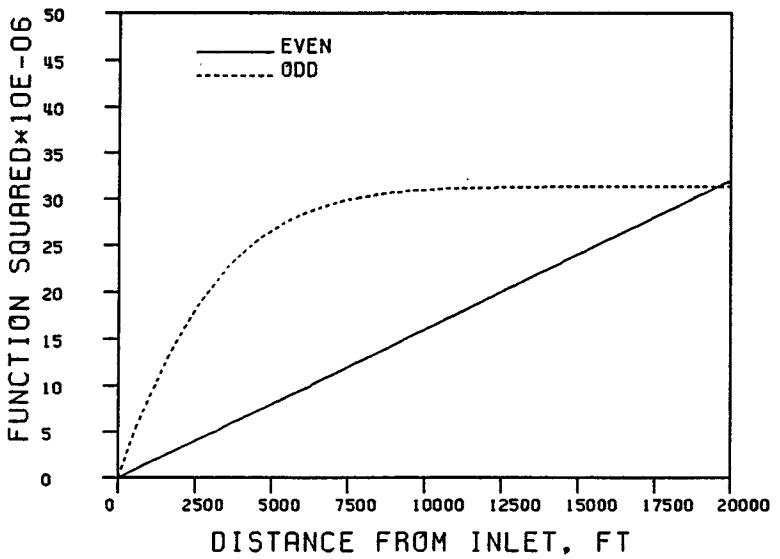

Figure 12: Cumulative sum of the square of even and odd functions from Figure 7.

An example is shown in Figure 12, where the even and odd functions correspond to those obtained in the previous example of the analytical solution plus a uniform background erosion. Note that the line corresponding to the even function has a constant slope and does not level off, reflecting the uniformity of the even function over the domain. The curve obtained from the odd function, however, increases rapidly and approaches an asymptote. There is no point at which the slope of this curve reaches zero, but the extent of the region affected by the inlet can be estimated if one assumes some arbitrary definition of negligible change. This could be where the slope of the curve reaches one percent of its maximum slope, or some other value. Repeating this method using real data will impose some limitations due to "noise" in the shoreline change signal.

A limitation in using only the even and odd functions for determination of the zone of influence is that, due to their symmetry, the result will be a zone that is symmetric about the inlet. This will not always be realistic, so it may also be useful to generate a similar graph using the net shoreline change function for each side of the inlet. Consideration of all three plots should help clarify the limits of the zone of influence. This could be useful

when attempting to identify the best location(s) for placement of material for beach renourishment.

4 Comparing Results of Even/Odd Analysis with Simulated Shoreline Changes

An obvious goal arising from a study of measured shoreline changes is to gain predictive capability regarding future changes. For this reason, both the analytical solution and the numerical simulation of shoreline response to a littoral barrier were compared to the measured shoreline changes at several inlets. The methodology underlying each comparison follows.

4.1 Determination of Best-fit Parameters for Analytical Solution

The assumptions inherent in the analytical solution (Equations 7 and 8) are often not well–suited to the situation in the field. A significant problem is the prediction of bypassing of sediment around the the littoral barrier. The behavior of the analytical solution is such that it predicts no bypassing until the updrift shoreline has accreted an amount equal to the structure length. All sediment bypassed around the tip of the structure then moves onto the downdrift beach, slowing erosion of this region slightly, and satisfying continuity exactly. Other problems with the analytical solution arise through the assumption of uniform (both temporally and spatially) wave climate, neglecting spatial variation in the wave climate arising from wave refraction, diffraction, and breaking, particularly due to the presence of an ebb tidal shoal. Tidal currents are also neglected.

The situation in the field rarely involves an impermeable structure. The permeability often varies over the length of the structure and changes with time as physical modifications (due to both natural processes and intentional actions) take place. The three–dimensionality of the bathymetry causes sand to be transported around the updrift jetty and into the inlet, even though the MHW shoreline is landward of the tip of the jetty. The amount of transport vs. MHW shoreline location relative to the jetty tip depends on the beach profile and thus sediment size. All of these factors combine to suggest that an "effective" jetty length be used when modelling shoreline changes.

The rate of bypassing to the downdrift shore rarely matches the rate at which sediment is entering the inlet from the updrift shore. In Florida, much of this material has historically been dredged from the inlet and placed offshore, outside of the littoral zone, although recent years have seen a trend toward disposal on the downdrift beaches at many inlets. The continuity

assumption employed in the analytical solution is thus often violated, since the inlet and its associated shoals behave as sediment sinks.

One possible method for analytical prediction of the shoreline change at such an inlet would be to use the full analytical solution, including bypassing (Equations 7 and 8), for the updrift shoreline, and the pre–bypassing solution (Equation 7) for the downdrift shoreline. This method assumes that the inlet acts as a complete sediment sink, and retains the assumption that both jetties are impermeable. This would lead to a shoreline planform that would deviate from the anti–symmetrical shape of the full analytical solution.

For the present study, it was decided to compare the analytical solution to the odd component of shoreline change, since the odd component is less influenced by seasonal fluctuations, sea–level rise, and any other processes tending to affect the entire domain uniformly. The odd function represents a combination of shoreline changes up– and downdrift, so it is not logical to use different solutions up– and downdrift when determining parameters for a best–fit between the odd component of shoreline change and the analytical solution. It was therefore decided to use only the pre–bypassing solution (Equation 7) for the best–fit analysis.

Two parameters were allowed to vary to obtain the best–fit between the analytical solution and the odd component of shoreline change: the diffusion coefficient, G (given by Equation 2), containing the breaking wave height, and $\tan\theta_b$, representative of the wave direction relative to shore–normal, where $\theta_b = (\beta - \alpha_b)$. All other parameters were assumed to be known and not varying. The best fit was defined as existing when the error term, ϵ^2, was minimized:

$$\epsilon^2 = \frac{1}{N}\sum_{i=1}^{N}[y_A(x_i) - y_O(x_i)]^2 \tag{23}$$

Here x_i denotes the value of x, the longshore coordinate, at the ith data point, $y_O(x_i)$ is the value of the odd function at $x = x_i$, $y_A(x_i)$ is the value of the analytical solution at $x = x_i$, and N is the number of points on one side of the inlet at which $y_O(x)$ is known. Either the updrift or downdrift shorelines may be used, since both functions are anti–symmetric about the y–axis, and the data points are distributed symmetrically about the y–axis.

The best fit between $y_A(x)$ and $y_O(x)$ will occur when the derivative of the error, ϵ^2, with respect to both variables is zero:

$$\frac{\partial \epsilon^2}{\partial G} = \frac{2}{N}\sum_{i=1}^{N}[y_A(x_i) - y_O(x_i)]\frac{\partial y_A(x_i)}{\partial G} = 0 \tag{24}$$

$$\frac{\partial \epsilon^2}{\partial \tan\theta_b} = \frac{2}{N}\sum_{i=1}^{N}[y_A(x_i) - y_O(x_i)]\frac{\partial y_A(x_i)}{\partial \tan\theta_b} = 0 \tag{25}$$

This system of two equations is nonlinear in G, and is most readily solved by defining an iterative process:

$$y_A^{k+1}(x_i) = y_A^k(x_i) + \frac{\partial y_A^k}{\partial G}|_{x_i}(\Delta G)^k + \frac{\partial y_A^k}{\partial \tan\theta_b}|_{x_i}(\Delta \tan\theta_b)^k \tag{26}$$

where k denotes the iteration number.

The pre–bypassing analytical solution (Equation 7), is given by:

$$y_A(x) = \frac{\tan\theta_b}{\sqrt{\pi}}\left[\sqrt{4Gt}\exp\left(\frac{-x^2}{4Gt}\right) - x\sqrt{\pi}\mathrm{erfc}\left(\frac{x}{\sqrt{4Gt}}\right)\right] \tag{27}$$

This is taken to represent the shoreline change between the time the inlet is first stabilized ($t = 0$) and some later time, t_{end}. The first survey used to determine the odd function may, however, not correspond to $t = 0$, but may be from some later time, t_{start}. Thus $y_A(x)$ in Equation 26 should be taken to correspond to the shoreline change between time t_{start} and time t_{end}, or:

$$\begin{aligned} y_A(x) &= \frac{\tan\theta_b}{\sqrt{\pi}}\left\{\left[\sqrt{4Gt_{end}}\exp\left(\frac{-x^2}{4Gt_{end}}\right) - x\sqrt{\pi}\mathrm{erfc}\left(\frac{x}{\sqrt{4Gt_{end}}}\right)\right]\right. \\ &- \left.\left[\sqrt{4Gt_{start}}\exp\left(\frac{-x^2}{4Gt_{start}}\right) - x\sqrt{\pi}\mathrm{erfc}\left(\frac{x}{\sqrt{4Gt_{start}}}\right)\right]\right\} \end{aligned} \tag{28}$$

Note that as $t_{start} \to 0$, Equation 28 reverts to Equation 27.

Differentiating 28 with respect to G, one obtains:

$$\frac{\partial y_A}{\partial G} = \frac{\tan\theta_b}{\sqrt{\pi}}\left[\exp\left(\frac{-x^2}{4Gt_{end}}\right)\sqrt{\frac{t_{end}}{G}} - \exp\left(\frac{-x^2}{4Gt_{start}}\right)\sqrt{\frac{t_{start}}{G}}\right] \tag{29}$$

and differentiating Equation 28 with respect to $\tan\theta_b$,

$$\frac{\partial y_A}{\partial \tan\theta_b} = \frac{1}{\sqrt{\pi}}\left\{\left[\sqrt{4Gt_{end}}\exp\left(\frac{-x^2}{4Gt_{end}}\right) - x\sqrt{\pi}\,\mathrm{erfc}\left(\frac{x}{\sqrt{4Gt_{end}}}\right)\right]\right.$$
$$\left. - \left[\sqrt{4Gt_{start}}\exp\left(\frac{-x^2}{4Gt_{start}}\right) - x\sqrt{\pi}\,\mathrm{erfc}\left(\frac{x}{\sqrt{4Gt_{start}}}\right)\right]\right\} \quad (30)$$

Equation 26 may be substituted into Equations 24 and 25, which are then rearranged to yield:

$$\sum_{i=1}^{N}(y_O - y_A^k)_{x_i}\left(\frac{\partial y_A^k}{\partial G}\right)_{x_i} = (\Delta G)^k \sum_{i=1}^{N}\left(\frac{\partial y_A^k}{\partial G}\right)^2_{x_i}$$
$$+ (\Delta \tan\theta_b)^k \sum_{i=1}^{N}\left(\frac{\partial y_A^k}{\partial \tan\theta_b}\frac{\partial y_A^k}{\partial G}\right)_{x_i} \quad (31)$$

$$\sum_{i=1}^{N}(y_O - y_A^k)_{x_i}\left(\frac{\partial y_A^k}{\partial \tan\theta_b}\right)_{x_i} = (\Delta G)^k \sum_{i=1}^{N}\left(\frac{\partial y_A^k}{\partial G}\frac{\partial y_A^k}{\partial \tan\theta_b}\right)_{x_i}$$
$$+ (\Delta \tan\theta_b)^k \sum_{i=1}^{N}\left(\frac{\partial y_A^k}{\partial \tan\theta_b}\right)^2_{x_i} \quad (32)$$

With the specification of an initial guess for both G and $\tan\theta_b$, each of the 5 different summations above may be computed, leaving a system of two equations in two unknowns, $(\Delta G)^k$ and $(\Delta \tan\theta_b)^k$. Upon solution for $(\Delta G)^k$ and $(\Delta \tan\theta_b)^k$, new guesses for G and $\tan\theta_b$ are computed:

$$G^{k+1} = G^k + (\Delta G)^k \quad (33)$$

$$(\tan\theta_b)^{k+1} = (\tan\theta_b)^k + (\Delta \tan\theta_b)^k \quad (34)$$

This process is then repeated until the values of G and $\tan\theta_b$ yielding the minimum error are obtained.

Figure 13 illustrates the goodness–of–fit between the analytical solution and the odd component of shoreline change at Sebastian Inlet for the period 1946–1970. This inlet was open during the years 1924–1942 and from 1948–present. For the computation of shoreline change by the analytical solution, the starting time, t_{start}, was taken as 22 years (1924–1946), and the ending

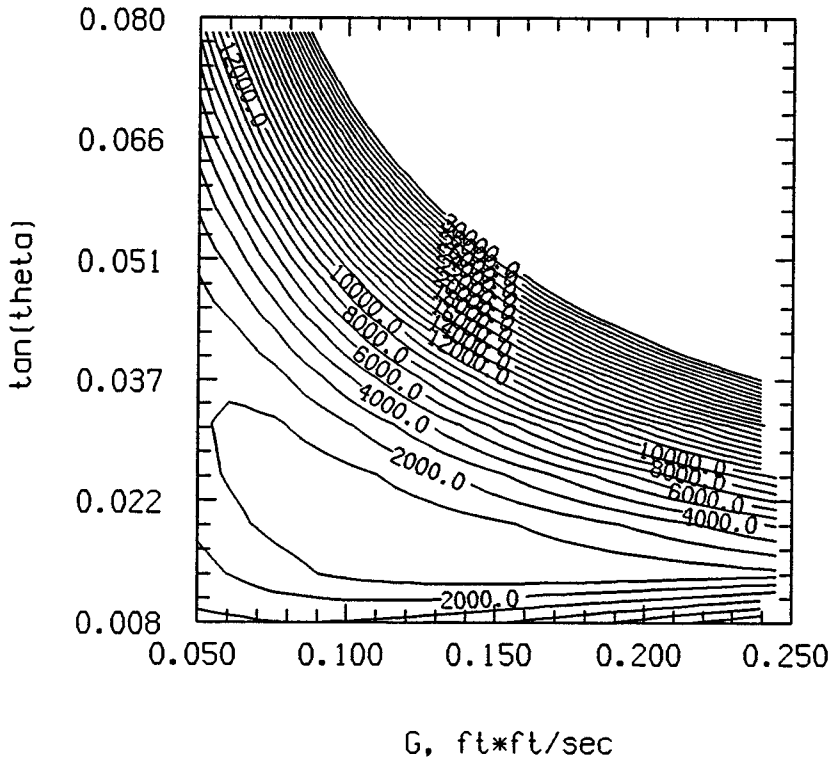

Figure 13: Sebastian Inlet: 1946–1970. Contours of equal error between analytical solution and odd component of shoreline change.

time, t_{end}, as 46 years (1924–1970). The closure of the inlet from 1942–1948 has been neglected in this analysis. Note in Figure 13 that the error increases rapidly as $\tan\theta_b$ is varied, but is much less sensitive to changes in G (and hence changes in wave height, H_b). Attempting to extrapolate a long–term breaking wave height from such an analysis is thus not recommended.

4.2 Wave Propagation and Shoreline Change Model

The numerical model was developed in the hope of improving the quality of the predicted shoreline changes by representing the complex wave climate near the inlet more accurately. The model consists of a finite difference wave propagation routine to simulate the wave transformation over the offshore bathymetry, coupled with the one–line model for the change in shoreline position discussed in Section 2.2. In this way the effects of the offshore bathymetry on the nearshore wave climate, and hence the varying longshore sediment transport rate, could be predicted.

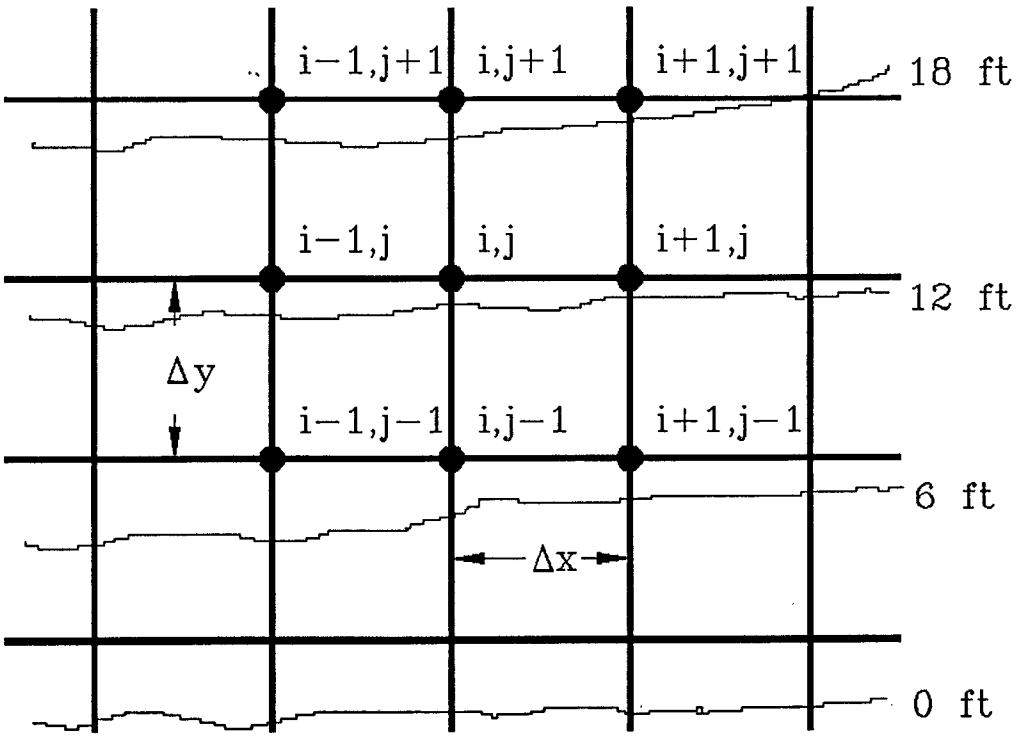

Figure 14: Computational mesh superimposed over offshore bathymetry.

The wave transformation model was initiated by laying a computational mesh over the bathymetry of interest, aligned with the general trend of the shoreline, as shown in Figure 14. The spacing between computational nodes in the x–direction is constant and is denoted by Δx. The y–direction spacing, Δy, is also constant, but need not equal Δx. The landward limit of the mesh was placed in a small, non–zero depth of water to avoid singularities during the wave height calculations. The seaward limit was taken far enough offshore to allow the assumption of uniform wave climate along this boundary.

The wave transformation processes addressed by the model include wave refraction due to both bathymetric features and tidal currents, shoaling, wave breaking, and diffraction of wave energy into the sheltered area, or "shadow zone", created by a shore–normal littoral barrier. Linear wave theory was assumed valid and wave breaking was considered the only mechanism for energy dissipation. The incident waves were assumed to possess, at any given time, only one direction and one (absolute) frequency.

Modelling of Tidal Currents

For the simulation of tidal currents, it was assumed a priori that they would be strong relative to any wave–driven currents, allowing the further assumption that the current field would be unaffected by the waves. The flood tide was simulated by placing a sink at the inlet and directing all flow toward it:

$$u_{i,j} = \frac{Q_o}{\pi R_{i,j} h_{i,j}} \cos\theta_{c_{i,j}} \tag{35}$$

$$v_{i,j} = \frac{Q_o}{\pi R_{i,j} h_{i,j}} \sin\theta_{c_{i,j}} \tag{36}$$

where

$R_{i,j} = \sqrt{(x_{i,j} - x_o)^2 + (y_{i,j} - y_o)^2}$
$\theta_{c_{i,j}} = \frac{3\pi}{2} - \tan^{-1}\left[\frac{y_{i,j}-y_o}{x_{i,j}-x_o}\right]$
$u_{i,j}$ = x–component of velocity vector at node i,j.
$v_{i,j}$ = y–component of velocity vector at node i,j.
x_o,y_o = location of center of inlet.
$h_{i,j}$ = water depth at node i,j.
Q_o = volumetric flowrate through inlet.

An example of the resulting flowfield during flood tide is shown in Figure 15.

The ebb tidal current distribution was modelled using a solution to the diffusion equation to simulate the mixing of the tidal jet as it moved offshore:

$$u_{i,j} = \frac{-Q_o\sqrt{\varepsilon}}{2 \cdot W \cdot h_{i,j}\sqrt{\pi(y_{i,j} - y_o)}} \left\{ \exp\left(- \left[\frac{W}{4\sqrt{\varepsilon(y_{i,j} - y_o)}} \left(\frac{2|x_{i,j} - x_o|}{W} + 1 \right) \right]^2 \right) \right.$$
$$\left. - \exp\left(- \left[\frac{W}{4\sqrt{\varepsilon(y_{i,j} - y_o)}} \left(\frac{2|x_{i,j} - x_o|}{W} - 1 \right) \right]^2 \right) \right\} \tag{37}$$

$$v_{i,j} = \frac{Q_o}{2 \cdot W \cdot h_{i,j}} \left\{ \mathrm{erf}\left[\frac{W}{4\sqrt{\varepsilon(y_{i,j} - y_o)}} \left(\frac{2|x_{i,j} - x_o|}{W} + 1 \right) \right] \right.$$

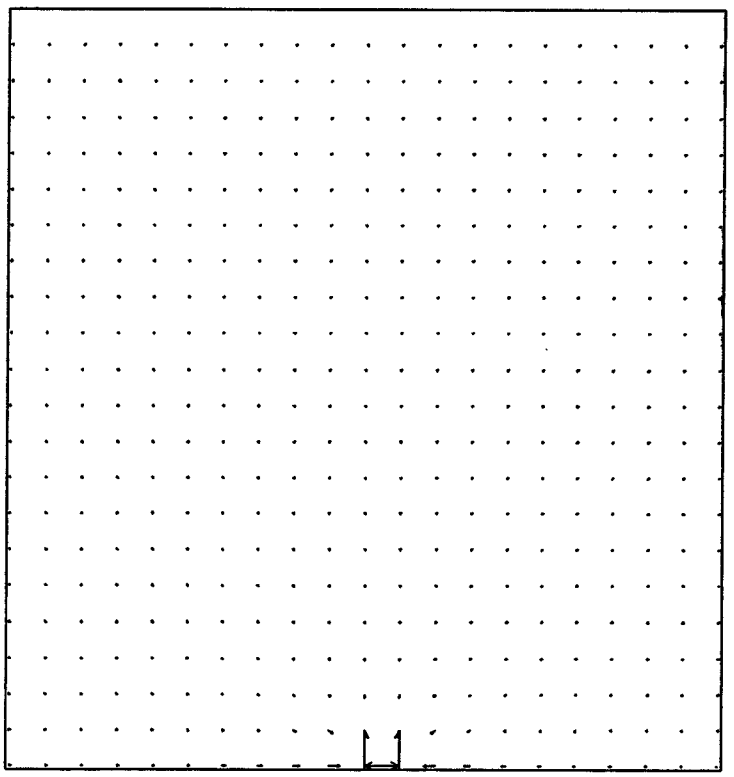

Figure 15: Flood current distribution around inlet.

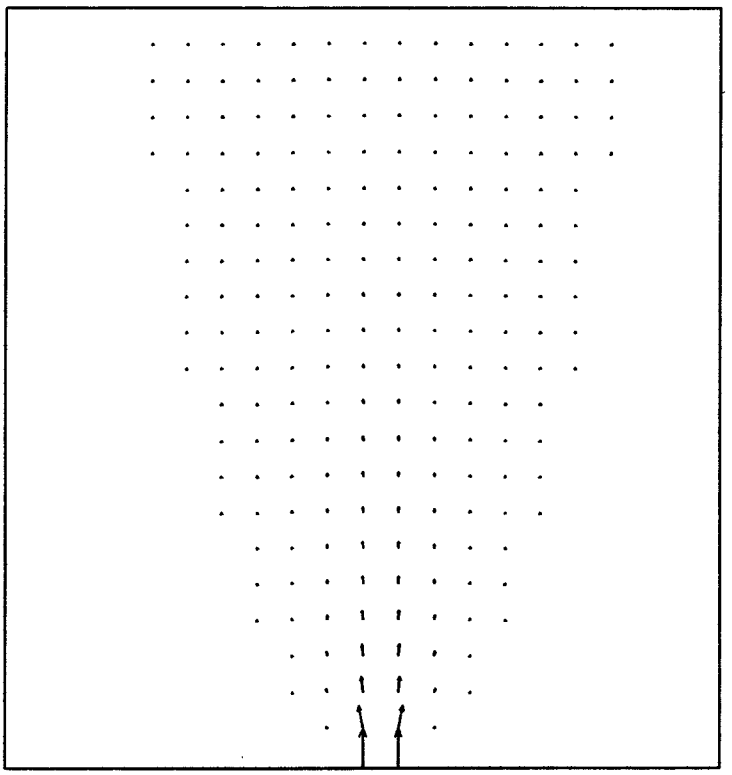

Figure 16: Example ebb tidal current distribution.

$$- \quad \text{erf}\left[\frac{W}{4\sqrt{\varepsilon(y_{i,j}-y_o)}}\left(\frac{2|x_{i,j}-x_o|}{W}-1\right)\right]\Bigg\} \tag{38}$$

where W is the inlet width and ε is a mixing rate parameter.

Equation 38, with the term $(y_{i,j} - y_o)$ replaced by time, t, has been used to predict the evolution of a rectangular beachfill over time (Larson et al., 1987). An example of the current field as represented by Equations 37 and 38 is shown in Figure 16. While obviously not providing completely faithful representations of the tidal currents, it was felt that these approximations were consistent with the other assumptions required for use of the model.

Computation of Wave Direction and Height

Because of the highly non–linear nature of the governing equations, an iterative solution technique was devised to compute the wave parameters of interest. With the presence of tidal currents, an intrinsic frquency must be

defined (Mei, 1989):

$$\begin{aligned} \sigma &= \omega - \vec{k} \cdot \vec{u} \\ &= \omega - ku\cos(\theta_w - \theta_c) \end{aligned} \tag{39}$$

where

σ = intrinsic frequency
ω = absolute frequency = $\frac{2\pi}{T}$
$\vec{u}$ = mean current vector
$\vec{k}$ = wavenumber vector
$\theta_w - \theta_c$ = angle between wavenumber and current vectors

The magnitude of the wavenumber vector, k, can be determined from the dispersion relationship:

$$\sigma^2 = gk\tanh kh \tag{40}$$

where g is the gravitational constant, and h is the local water depth.

The calculation procedure was initiated by first obtaining estimates for the wavenumber vector, $\vec{k}$, and wave celerity, at each mesh point, assuming zero mean current and straight and parallel bathymetric contours. These estimates were then used to obtain new estimates for $\vec{k}$, including the effects of tidal currents. The magnitude of the wavenumber vector was determined by solving Equation 40, while the direction was computed by applying irrotationality of the wavenumber vector:

$$\nabla \times \vec{k} = 0 \tag{41}$$

which may also be written:

$$\frac{\partial(k\sin\theta_w)}{\partial x} = \frac{\partial(k\cos\theta_w)}{\partial y} \tag{42}$$

where $\vec{k} = k\cos\theta_w\hat{\imath} + k\sin\theta_w\hat{\jmath}$, and θ_w is measured counter–clockwise from the x–direction. In finite difference form, the solution for $\theta_{w_{i,j}}$ was taken as:

$$\theta_{w_{i,j}} = \cos^{-1}\left(\frac{D_T}{k_{i,j}}\right) \tag{43}$$

where

$$D_T = D_1 + D_2 + D_3 \tag{44}$$

$$D_1 = \tau\left[(k\cos\theta_w)_{i-1,j+1} + (k\cos\theta_w)_{i+1,j+1}\right] \tag{45}$$

$$D_2 = (1-2\tau)\left[(k\cos\theta_w)_{i,j+1}\right] \tag{46}$$

$$D_3 = -\frac{\Delta y}{2\Delta x}\left[(k\sin\theta_w)_{i+1,j} - (k\sin\theta_w)_{i-1,j}\right] \tag{47}$$

The wavenumber field was re–computed until it satisfied the governing equations to within a reasonable tolerance.

The governing equation for the wave height distribution within the domain, assuming quasi–steady–state conditions, is conservation of wave action:

$$\nabla\cdot\left[\frac{E}{\sigma}\left(\vec{u}+\vec{C_g}\right)\right] = 0 \tag{48}$$

which may also be written as

$$\frac{\partial\left[\frac{H^2}{\sigma}\left(u+C_g\cos\theta_w\right)\right]}{\partial x} = \frac{-\partial\left[\frac{H^2}{\sigma}\left(v+C_g\sin\theta_w\right)\right]}{\partial y} \tag{49}$$

where C_g denotes the group velocity of the waves and H the local wave height. This was solved iteratively by application of Equation 50:

$$H_{i,j} = \sqrt{\frac{E_T\sigma_{i,j}}{(v+C_g\sin\theta_w)_{i,j}}} \tag{50}$$

where

$$E_T = E_1 + E_2 + E_3 \tag{51}$$

$$E_1 = \tau\left\{\left[\frac{H^2}{\sigma}(v+C_g\sin\theta_w)\right]_{i-1,j+1} + \left[\frac{H^2}{\sigma}(v+C_g\sin\theta_w)\right]_{i+1,j+1}\right\} \tag{52}$$

$$E_2 = (1-2\tau)\left[\frac{H^2}{\sigma}(v+C_g\sin\theta_w)\right]_{i,j+1} \tag{53}$$

$$E_3 = \frac{\Delta y}{2\Delta x}\left\{\left[\frac{H^2}{\sigma}(u + C_g \cos\theta_w)\right]_{i+1,j} - \left[\frac{H^2}{\sigma}(u + C_g \cos\theta_w)\right]_{i-1,j}\right\} \quad (54)$$

The wave height at each point was checked to see if it exceeded a limit of $H_{i,j} = 0.78 \cdot h_{i,j}$, and if so, was truncated to this limit. This was intended to address roughly the effect of energy losses due to wave breaking.

Wave Diffraction

Wave diffraction was included by use of a model by Perlin and Dean (1983), which uses the constant–depth solution for wave height in the vicinity of a rigid barrier given by Penney and Price (1952). The diffraction routine was used to calculate wave height only at those computational nodes lying within the geometric wave shadow cast by the jetty. This resulted in the neglect of wave diffraction if the wave angle deviation from shore–normal and/or the structure length were small, as was typically the case (see Figure 17). The reader is referred to the referenced papers for details of the solution.

Sediment Transport/Shoreline Position Calculations

The wave propagation model provided, at discrete intervals along the shoreline, a wave height and direction that could then be used to compute local longshore transport rates. If the wave had broken prior to reaching the landward limit of the wave propagation mesh, this breaking wave height was used to compute the local longshore sediment transport rate:

$$Q = \frac{K H_b^{\frac{5}{2}} \sqrt{\frac{g}{\kappa}}}{16(s-1)(1-p)} \sin\left[2(\beta - \alpha_b)\right] \quad (55)$$

where all variables are as defined in Section 2. (The breaking wave height referenced here is exclusive of waves breaking on a shoal or bar; H_b was defined as a wave that begins breaking on that portion of the beach profile where the depth changes monotonically).

If the wave had not broken by the time it reached the landward limit of the wave propagation mesh, Equation 55 was modified to give the sediment transport rate in terms of this nearshore wave, having direction α_R, height H_R, group velocity C_{gR}, and celerity C_R:

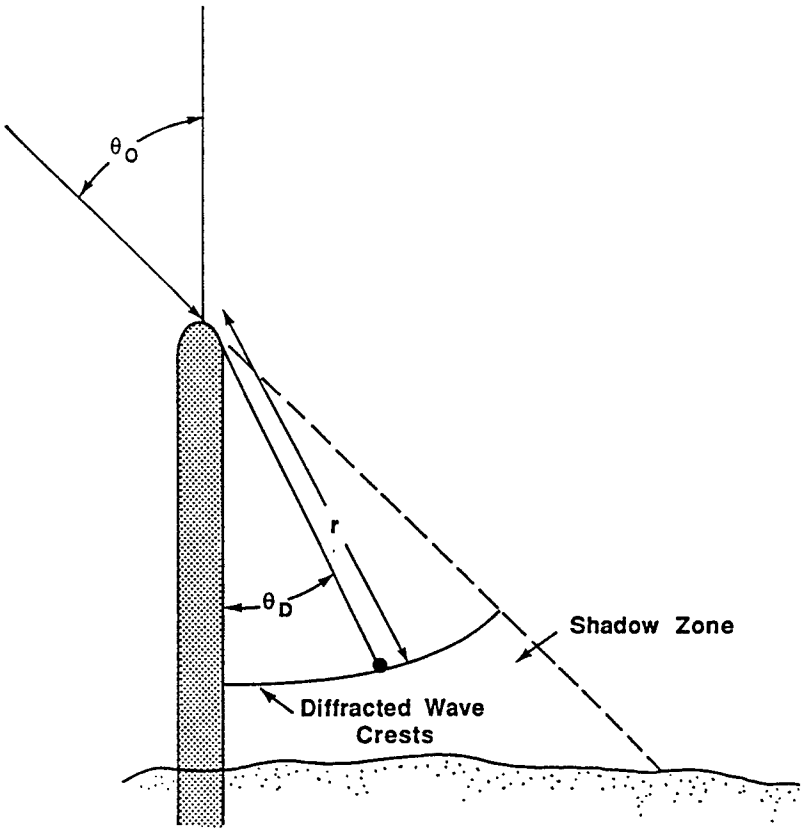

Figure 17: Geometry governing wave diffraction problem.

$$Q = \frac{K H_R^{2.4} C_{gR}^{1.2}}{8(s-1)(1-p)} \left(\frac{g}{\kappa}\right)^{0.4} \frac{1}{C_R} \sin(\beta - \alpha_R) \cos^{1.2}(\beta - \alpha_R) \qquad (56)$$

This assumes that the contours between the location of the last known wave (the landward limit of the mesh) and the shore are straight and parallel to the shoreline, and that wave energy flux is conserved until breaking. Equations 55 and 56 thus allowed specification of a distinct longshore sediment transport rate for each of the computational nodes along the shoreline. The new shoreline position was then computed, and a new time step begun.

Selection of Input Data for Numerical Model

Use of digitized survey data for the offshore bathymetry caused wave energy to be focused on selected areas that, in nature, are often more erosion-resistant than adjacent areas. It was therefore decided to use an idealized bathymetry, including an elliptical shoal, with the depth at any point within the domain given by:

$$h_{i,j} = h_o + A y_{i,j}^{\frac{2}{3}} - S \qquad (57)$$

where

$$S = a_s \exp\left\{-\left[\left(\frac{x_{i,j} - x_s}{x_{decay}}\right)^2 + \left(\frac{y_{i,j} - y_s}{y_{decay}}\right)^2\right]\right\} \qquad (58)$$

h_o = depth at landward limit of computation mesh
A = beach profile shape parameter
a_s = amplitude of shoal
x_s, y_s = coordinates of center of shoal
x_{decay}, y_{decay} = shoal shape parameters

The location, height, and horizontal dimensions of the shoal were adjusted to approximate those determined from available sources. For an inlet where the shoal size was known to have changed markedly over the time period of interest, the amplitude of the shoal was varied linearly with time.

Refraction due to bathymetric features typically dominated over that due to tidal currents. Figure 18 shows the simulated shoreline changes from

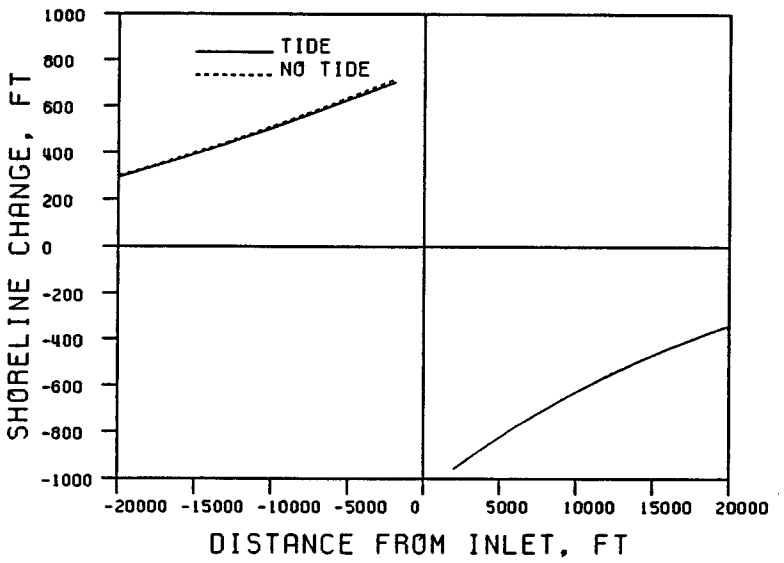

Figure 18: Predicted shoreline: tide vs. no tide. No shoal in either case.

two model runs without shoals, with and without tidal currents. Moderate tidal currents had little effect on the results.

Selection of input wave data was difficult, because of a lack of high–quality directional wave data. Therefore the wave height and direction used as input were determined from the values of G and $\tan\theta_b$ found by the best–fit analysis described in Section 4.1. These values represent long–term averages, so were used throughout the duration of the model run. The wave gages maintained by the Coastal and Oceanographic Engineering Laboratory, University of Florida, were used to provide wave period input for the model. The wave period was taken as the mean period of the peak of the energy spectrum averaged over the entire period of record for the gage, which for most of the sites is 4–5 years.

In the field, the ebb tidal shoal is often responsible for significant energy dissipation, sheltering the region in its lee as storm waves break on the shoal. In the model, wave breaking on the shoal was rarely observed, due to the long–term average incident wave heights used. The waves used as input, being much smaller than typical storm waves, would generally not break until they had travelled past the shoal. The primary influence of the shoal was thus on the nearshore wave direction. The incident wave di-

rection obtained from the best–fit analysis did not deviate drastically from shore–normal, so that the diffraction solution was rarely employed. Additionally, sediment transport reversals, common at many of Florida's tidal inlets during summer, were never simulated. Future wave data collection efforts including the measurement of wave direction should help provide a substantial improvement.

5 Presentation of Results

In this section, even/odd analysis of shoreline changes at 18 inlets on the east coast of Florida presented. (Lack of historical shoreline position data prevented the inclusion of St. Mary's Inlet in the study). For the constructed and stabilized natural inlets, the first survey dates were selected to coincide as closely as possible with the cutting of the inlet and/or the construction of stabilizing structures. Results of analyses for other time intervals are presented where relevant or of particular interest.

Most of the historical information regarding the various inlets was obtained from Marino and Mehta (1986) and Dean and O'Brien (1987a, 1987b). Littoral drift estimates attributed to USAE are U.S. Army Corps of Engineers estimates from Dean and O'Brien (1987a, 1987b), and estimates attributed to Walton are from Walton (1976), also found in Dean and O'Brien (1987a, 1987b).

In the sections that follow, results are presented in an order that was deemed best to illustrate useful application of the even/odd analysis technique. Some of the inlets do not easily lend themselves to such an analysis, but each is presented in the interest of objectivity.

Florida's East Coast Inlets

Figure 19 shows the relative locations of each of Florida's east coast inlets. Some general patterns along the east coast of Florida are worthy of note. Prior studies have concluded that each of the 19 inlets along Florida's eastern coast has a net longshore sediment transport rate directed to the south. Proceeding from north to south, there is a general trend toward decreasing wave height, net longshore sediment transport rate, and shoal size. The decrease in wave height is in large part due to sheltering by the Bahama Bank.

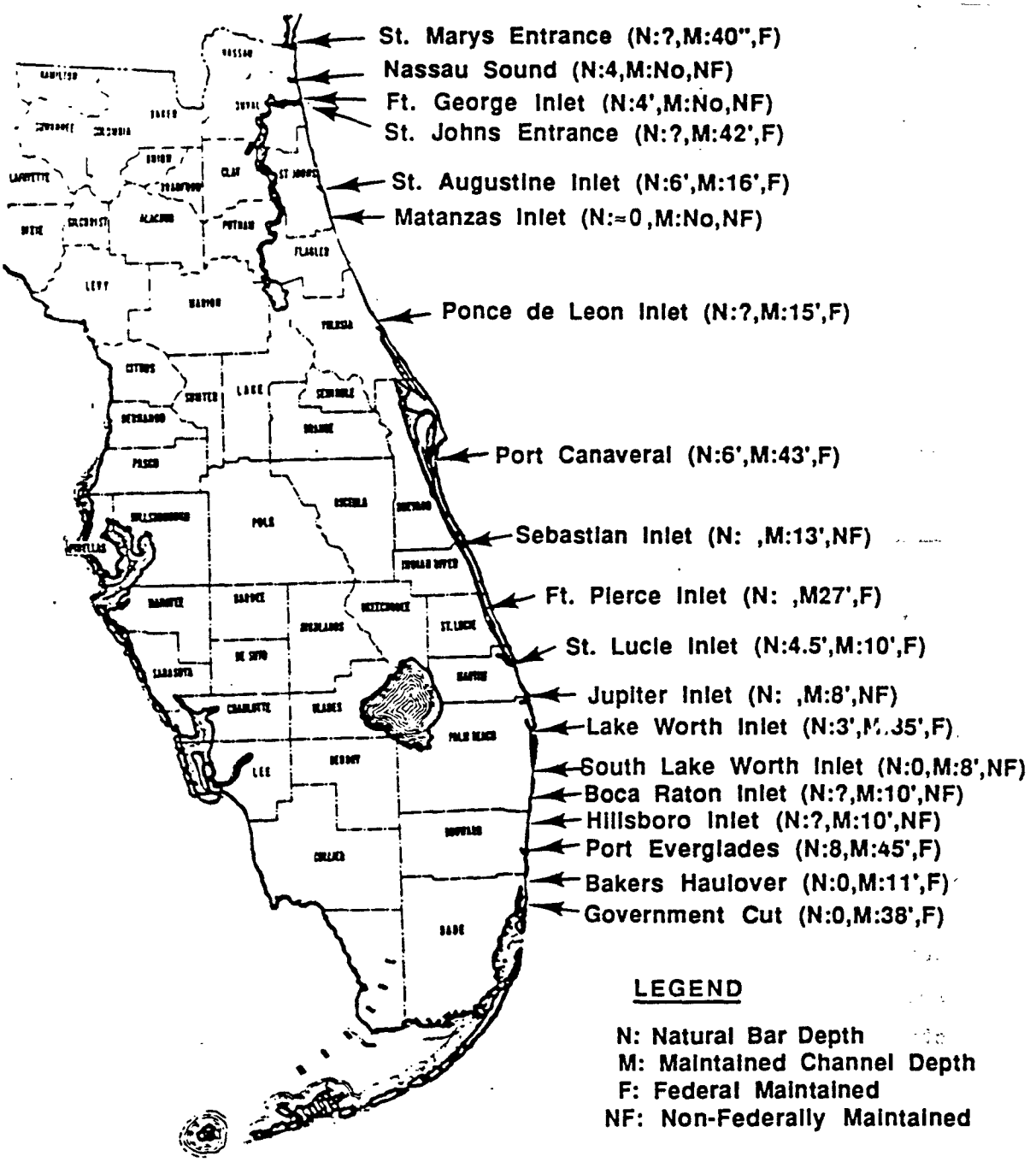

Figure 19: Locations of Florida's east coast inlets.

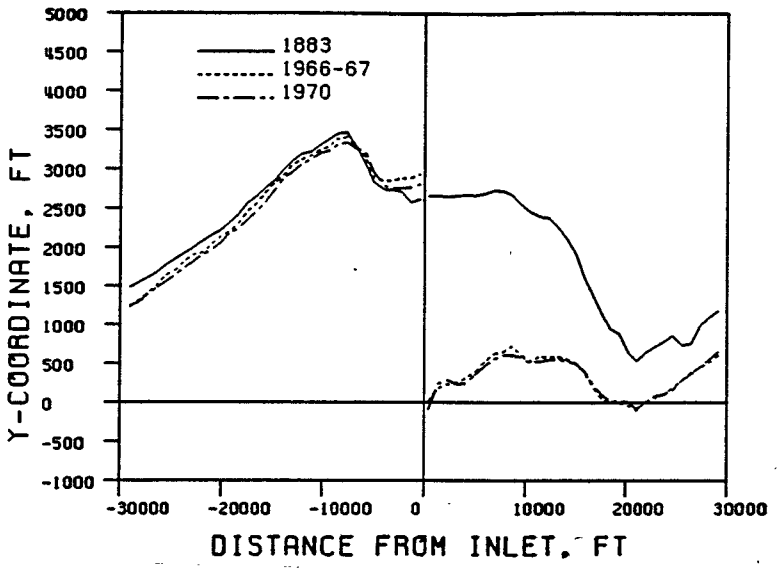

Figure 20: St. Lucie Inlet: Shoreline position vs. time.

5.1 St. Lucie Inlet

St. Lucie Inlet was constructed in 1892 by dredging from the Indian River through the barrier island to the Atlantic Ocean. It now forms the boundary between Hutchinson Island, to the north, and Jupiter Island, to the south. The nearest inlets are Ft. Pierce Inlet, 22.4 miles to the north, and Jupiter Inlet, 16.3 miles to the south. The north jetty was completed in 1929, and the south jetty was added in 1982. The net longshore sediment transport rate has been estimated at 200,000 (Walton) to 230,000 yd^3/yr (USAE) to the south. Several beach nourishment projects have been undertaken. Approximately 1.1 million yd^3 were dredged from the inlet in 1928 and most of this material was placed on the south beach. The period 1965–1985 saw another 1.9 million yd^3 of beach nourishment projects for the beach south of the inlet, including 400,000 yd^3 on 3000 feet of the south beach in 1984–85. The updrift beach is afforded some protection by a reef running close to shore for more than a mile updrift of the inlet. Despite this fact, erosion has occurred over this region since at least 1967, as may be seen in Figure 20.

The plots of shoreline position versus time show that erosion has been very significant downdrift of St. Lucie Inlet, where the shoreline has re-

treated over 2500 feet since the cutting of the inlet. Much of this material was probably incorporated into the ebb and flood tidal shoals which have formed, and account for approximately 21.7 million yd^3 (1964) and 3.0 million yd^3 (1977), respectively.

Written accounts (Walton, 1974a) indicate that significant erosion took place on both sides of the inlet shortly after it was cut. Plots of shoreline change from 1883–1967 (Figure 21) show that the north jetty had by 1967 caused enough accretion for the shoreline north of the inlet to return approximately to its pre–inlet (i.e. 1883) position. Erosion downdrift continued at a rapid rate; the erosion rate for this portion of Jupiter Island was, for many years, the highest in the state. The presence of the south jetty should help reduce the erosion rate on the south side of the inlet by reducing sediment losses into the channel during periods of transport reversal.

Even/odd analysis of the shoreline changes at St. Lucie Inlet provides a good example of the utility of the method. Note the similarity between the net, even, and odd functions shown in Figure 21 and those in Figure 7, the example of the analytical solution for impoundment of longshore transport by a littoral barrier with superimposed background erosion. Figure 22 compares the odd function with the best–fit case for the analytical solution; the fit is quite good.

Figure 23 demonstrates the relative magnitudes of the even and odd functions. They are of almost equal magnitude, and indicate that the zone of influence for the inlet extends approximately 6 miles up– and downdrift.

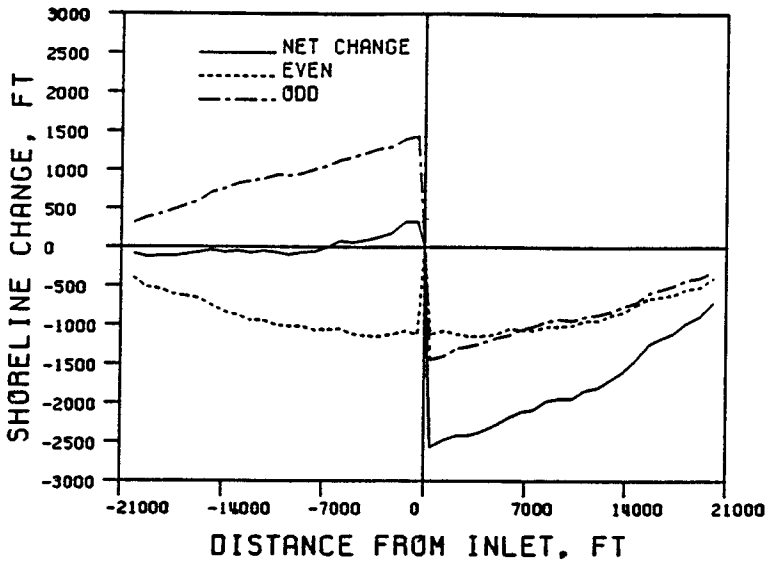

Figure 21: St. Lucie Inlet: even/odd analysis: 1883–1967.

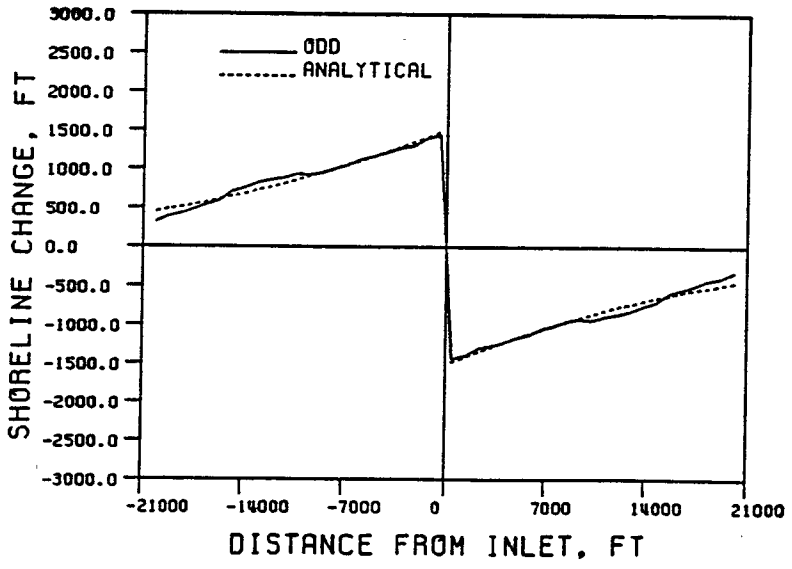

Figure 22: St. Lucie Inlet: Odd function (1883–1967) vs. analytical solution. G_{best}=0.131 ft^2/sec, $(\theta_b)_{best}$=4.4°.

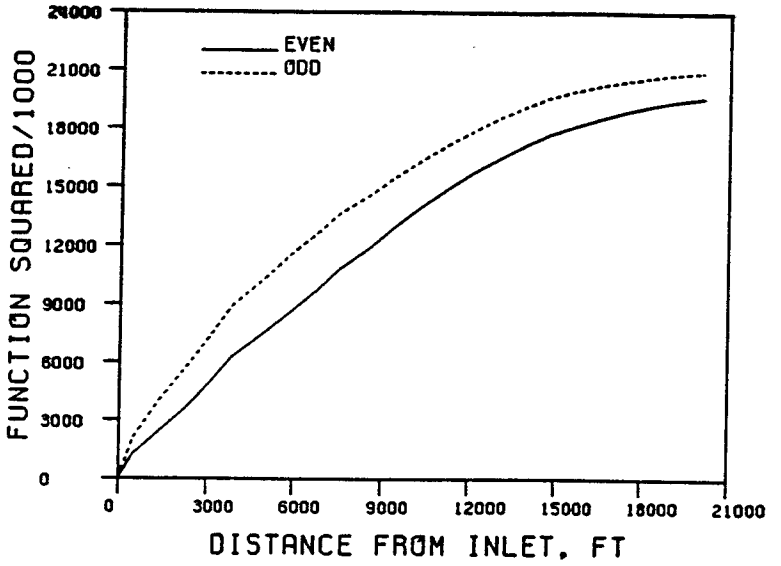

Figure 23: St. Lucie Inlet: integral of square of even and odd functions, 1883–1967.

5.2 Ft. Pierce Inlet

Ft. Pierce Inlet was cut in 1921 to replace a natural inlet 2.7 miles to the north that had closed in the early 1900's. This inlet, known as Indian River Inlet, began closing after the cutting of St. Lucie Inlet, 22.4 miles to the south, in 1892. The shoaling of Indian River Inlet was likely due to reduced tidal flow as St. Lucie Inlet increased in cross–sectional area, thus discharging a greater proportion of both the tidal prism and the fresh–water outflow from the St. Lucie River. The nearest inlet to the north is presently Sebastian Inlet, which is 28.5 miles distant.

Small jetties (400 feet long, 600 feet apart) were built at Ft. Pierce prior to the cut; they proved inadequate and were replaced in 1926 with jetties 900 feet apart, 1800 feet long on the north, and 1200 feet long on the south side of the inlet. Periodic dredging has been required for channel maintenance and to increase the channel depth from its initial depth of 4 feet to its present depth of 27 feet. Most of the dredge spoil has been dumped at sea. A beachfill project of approximately 700,000 yd^3 was completed in 1971 using material from an offshore borrow site. The project nourished approximately one mile immediately south of the inlet (Walton, 1977, 1974b). Estimates

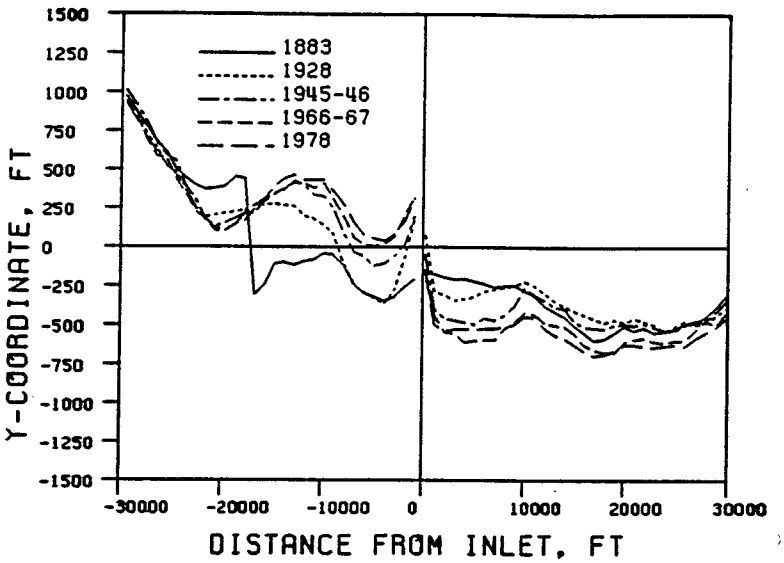

Figure 24: Ft. Pierce Inlet: Shoreline position vs. time.

of the net longshore sediment transport rate range from 140,000 yd^3/yr (Walton) to 225,000 yd^3/yr (USAE) to the south. An ebb tidal shoal of approximately 29.4 million yd^3 (1975) has formed offshore. Some of this material was probably part of the ebb tidal shoal for Indian River Inlet prior to its closure.

Ft. Pierce Inlet is, in some respects, an ideal case for study: cut by man, essentially constant configuration since the late 1920's, and isolated from other present–day inlets. "Smoothing" of the shoreline at the location of the former Indian River Inlet resulted in large changes in shoreline position after this inlet closed. The change between erosion and accretion can be seen in Figure 24 to occur between -15,000 and -20,000 feet, corresponding roughly to the position north of Ft. Pierce Inlet at which Indian River Inlet existed.

By 1928, the discontinuity in the shoreline planform due to the prior existence of Indian River Inlet had been smoothed to a more stable shape. Even/odd analysis of shoreline change for the period 1928–1967 (Figure 25) shows the updrift offset pattern expected when a shore–normal littoral barrier is constructed on a beach that has any significant net longshore sediment transport. The even function is quite small relative to the odd, emphasizing the dominant role of the blockage of longshore sediment transport by

the jetties. The fact that the average value of the even function is slightly negative indicates that some sediment has been lost from the domain. Such losses could be attributed to leakage through the jetties into the channel, with subsequent loss due to dredging, and sea–level rise.

Figure 26 provides a measure for comparison of the even and odd functions for this interval, and indicates that the zone of influence for the inlet is on the order of 20,000 ft.

The comparison between the odd function and the best–fit analytical solution for the interval 1928–1967 is illustrated in Figure 27. The wave height and direction obtained from this analysis were used to obtain the input wave climate for the numerical model. It should be noted that the error surface (discussed in Section 4.1) for this case is relatively flat, reducing the degree of confidence associated with the estimates of wave height and direction determined by this method.

Ft. Pierce Inlet provides an example of the problem of selection of an effective jetty length for use in analytical or numerical prediction of shoreline change. Both jetties are quite long, with the north jetty being approximately 1800 feet in length, but use of this length in the model produced drastically unrealistic results. For the interval 1928–1967, approximately 1300 feet of accretion on the updrift side of the inlet was predicted, compared to roughly 360 feet of measured shoreline change at the updrift jetty for this interval. This illustrates a limitation of the model: the jetty is treated as an impermeable structure, so that no bypassing can occur until the shoreline accretes beyond the tip of the structure. Also, if the time interval is sufficient for bypassing around the tip of the jetty to occur, then the accretion updrift of the jetty will be equal to the jetty length. For this reason, a second simulation was performed, using a jetty length such that the predicted shoreline change immediately updrift of the jetty matched the measured shoreline change at this location. Results are shown in Figure 28.

The model results shown here include the effects of refraction due to both tidal currents and the ebb tidal shoal. Sensitivity tests indicated that refraction due to tidal currents had a very small effect on the results, and that even the shoal exerted a relatively minor influence on the results for this case.

As with the even function based on the measured data (Figure 25), the average value of the simulated even function over the entire domain is negative, indicating a loss of sediment. This is due to the assumption in the

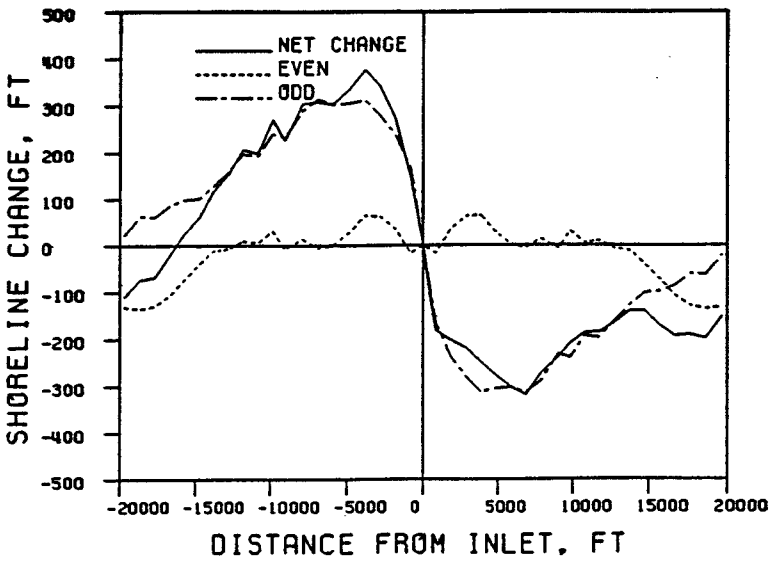

Figure 25: Ft. Pierce Inlet: even/odd analysis: 1928–1967.

model that sediment passing around the jetty never reaches the downdrift shore (as would be the case with channel dredging and disposal offshore).

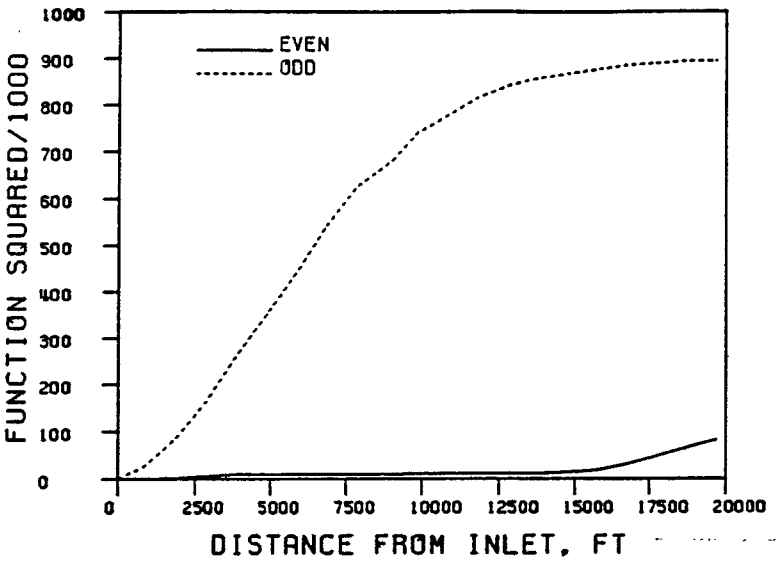

Figure 26: Ft. Pierce Inlet: integral of square of even and odd functions, 1928–1967.

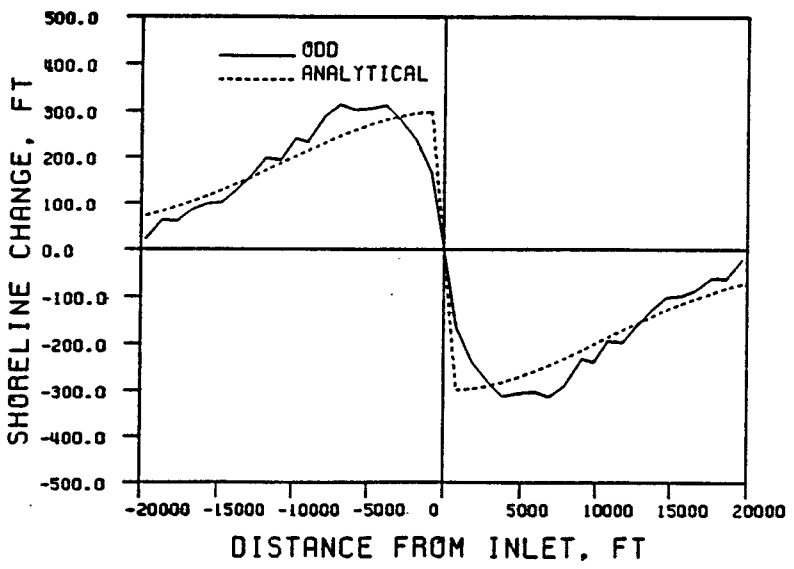

Figure 27: Ft. Pierce Inlet: Comparison of odd function (1928–1967) to analytical solution. G_{best}=0.110 ft^2/sec, $(\theta_b)_{best}$=2.3°.

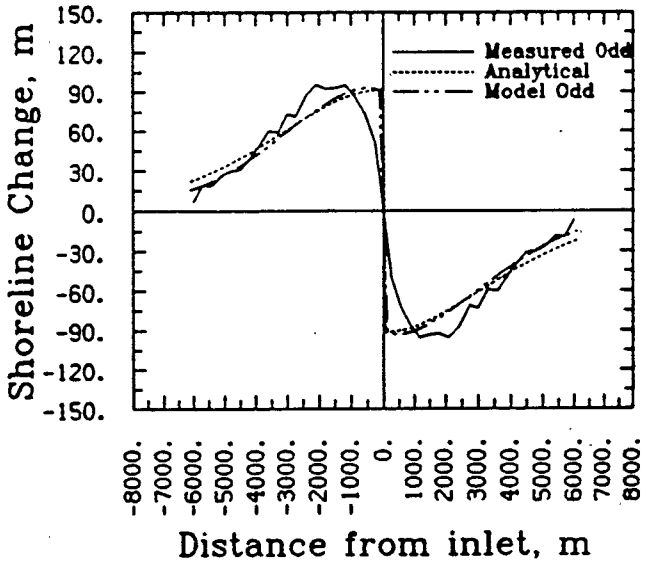

Figure 28: Ft. Pierce Inlet: Model simulation vs. measured changes, 1928–1967.

5.3 Lake Worth Inlet

Lake Worth Inlet was cut in 1917 at what is believed to have been the site of a relict natural inlet. Constructed inlets had existed about 8000 feet north and 5000 feet north of the present Lake Worth Inlet location during the intervals 1876–1886 and 1887–1924, respectively (Walker and Dunham, 1977). The nearest inlet to the north is Jupiter Inlet (12.1 miles); South Lake Worth Inlet is the nearest southerly inlet (15.6 miles).

Construction of rock jetties on both sides of the inlet was completed in 1925. The typical updrift offset planform developed, prompting construction of a sand bypassing plant in 1958, reducing, but not eliminating, the need for maintenance dredging. Most of the dredge spoil, prior to 1970, was disposed of at sea or placed within Lake Worth to form what is now Peanut Island. Dredge spoil has been placed on the south beach since 1970. A coffer dam currently surrounds the intake for the sand bypassing pump, restricting the amount of material that can be bypassed. Dredging records indicate that from 1929–1986, 5.2 million yd^3 was dredged. Of this total, 1.5 million yd^3 was dredged for channel maintenance and placed on the south beach. The size of the ebb tidal shoal has been estimated at 3.9 million yd^3 (1967).

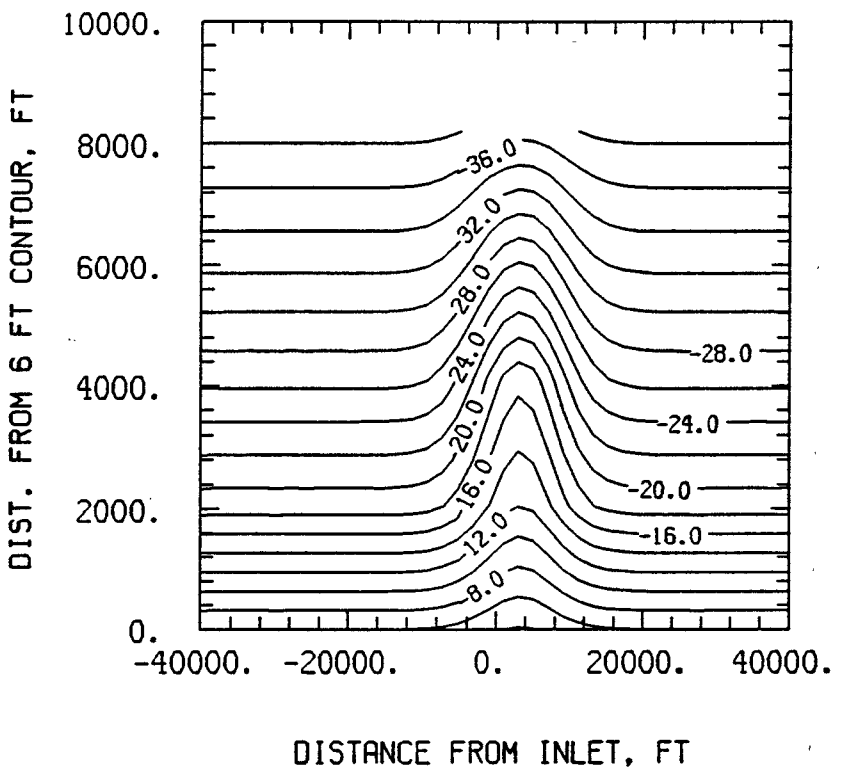

Figure 29: Ft. Pierce Inlet: Idealized bathymetry used in model simulation.

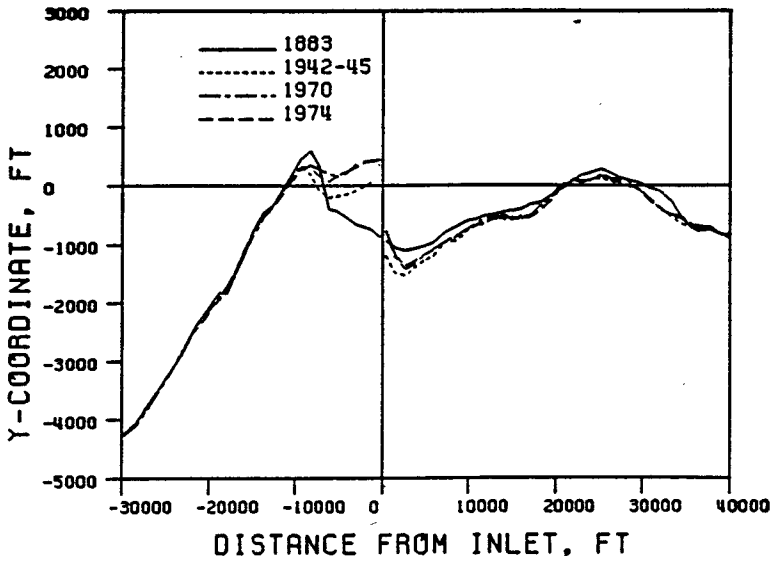

Figure 30: Lake Worth Inlet: Shoreline position vs. time.

Inspection of the plots of shoreline change (Figures 31, 32) reveals that the bypassed quantities have not been sufficient to counteract the updrift accretion/downdrift erosion pattern. Most of the significant shoreline changes have been restricted to within +/-10,000 feet of the inlet. The even function indicates a net gain of sediment within this region, with the accretion concentrated in the two miles immediately updrift of the inlet. A rocky outcrop approximately 8000 feet north of the inlet is the cause of the anomaly that appears there. Some nearshore rock is also apparent on the downdrift side.

The net littoral transport rate for this site has been estimated at 230,000 yd^3/yr (U.S. Army Corps of Engineers) and 380,000 yd^3/yr (Walton) to the south. The current average bypassing rate for the sand transfer plant is approximately 70,000 yd^3/yr. These figures and the plots of shoreline change would indicate that this bypassing rate should be increased significantly to mitigate the erosion problem on the downdrift shore.

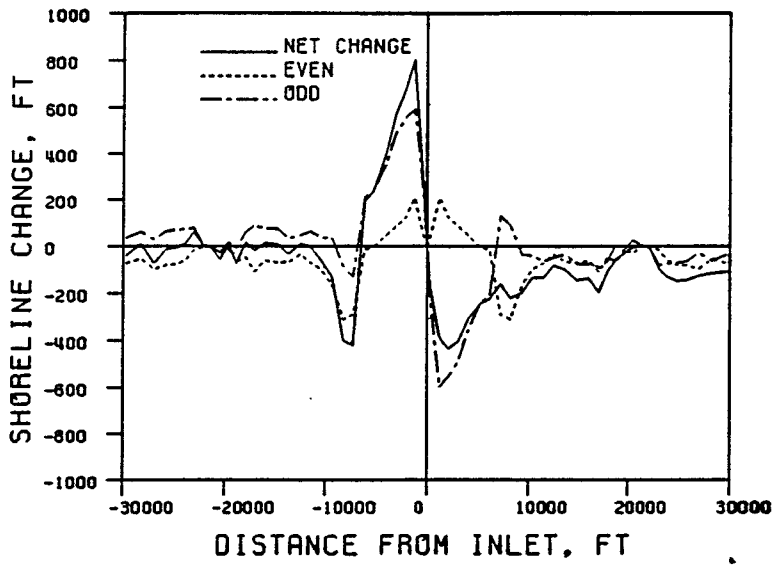

Figure 31: Lake Worth Inlet: Even/Odd analysis of shoreline change, 1883–1942/45.

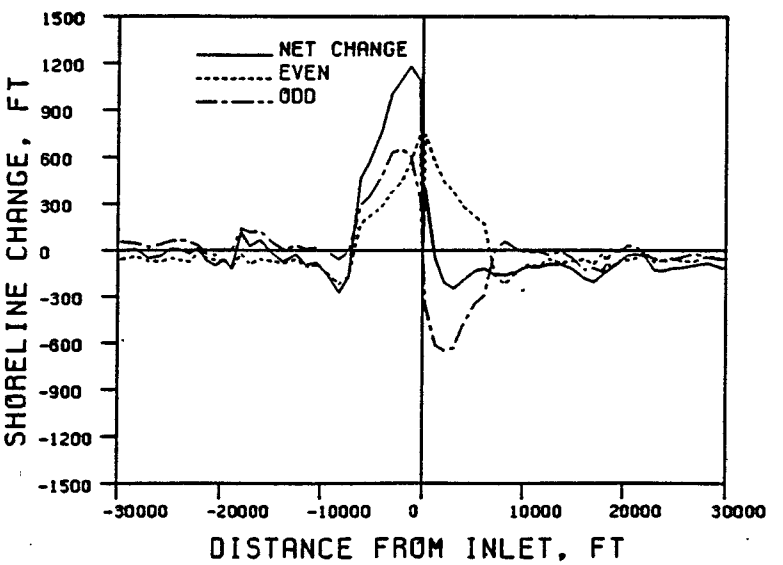

Figure 32: Lake Worth Inlet: Even/Odd analysis of shoreline change, 1883–1974.

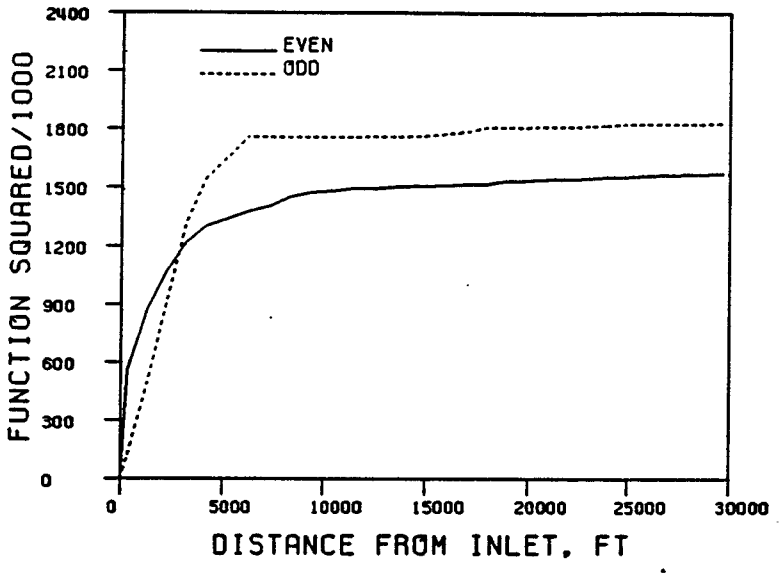

Figure 33: Lake Worth Inlet: integral of square of even and odd functions, 1883–1974.

5.4 South Lake Worth Inlet

South Lake Worth Inlet was cut in 1927 in an attempt to improve water quality in Lake Worth. Lake Worth Inlet lies 15.6 miles to the north and Boca Raton Inlet 14.5 miles to the south. Jetties were built at the time of construction, and then raised to +12 feet MLW in 1936. Intelligent long–range planning resulted in the construction of a sand transfer plant in 1937.

Wartime fuel shortages discontinued operation of the sand transfer plant from 1942–1945, during which time the inlet was nearly closed (COEL, 1965). Since that time, the plant has been upgraded twice, in 1948 and 1967, resulting in larger bypassing rate capabilities. The 1967 modifications included relocation of the sand transfer plant 118 ft. seaward of its former location and extension of the north jetty by 400 feet. The plant currently bypasses approximately 60,000 yd^3/yr.

The net littoral transport rate for South Lake Worth Inlet has been estimated at 230,000 yd^3/yr (USAE) to 280,000 yd^3/yr (Walton) to the south. The size of the ebb tidal shoal has been estimated at 1.4 million yd^3 (1969).

Figure 35 shows the results of even/odd analysis for the period 1927–

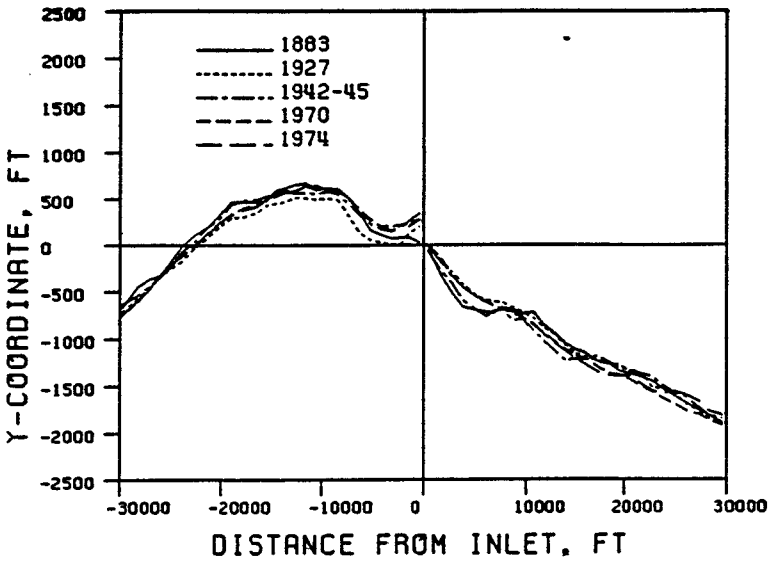

Figure 34: South Lake Worth Inlet: Shoreline position vs.time.

1942/45. A clear updrift offset has developed. The even function is quite small and indicates little change in the quantity of sediment within the vicinity. The exact date of the latter survey is not known, so it is not clear whether the offset is due to inadequate bypassing while the sand transfer plant was in operation, or whether most of the offset developed after the operation of the plant was ceased in 1942. It is likely that both mechanisms are partially responsible.

A large amount of sediment was dredged from the bay shoals and deposited on the south beach in 1964. This, in conjunction with the resumed operation of the sand transfer plant in 1945, explain the offset shown in Figure 36, 1942/45–1970. The longer–term results, shown in Figure 37 for the period 1927–1974, show that there has been a net gain in the amount of sediment within the domain, but that the bypassed quantity has not been sufficient to negate the updrift offset pattern.

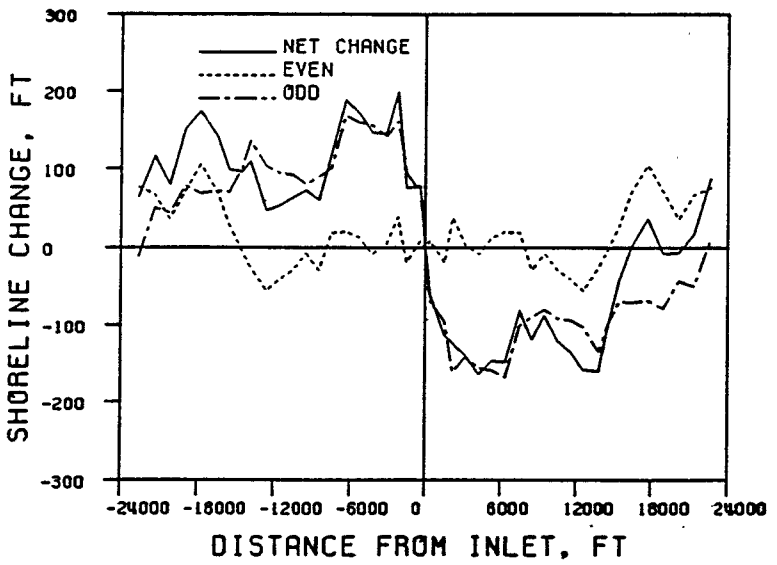

Figure 35: South Lake Worth Inlet: Even/Odd analysis of shoreline change, 1927–1942/45.

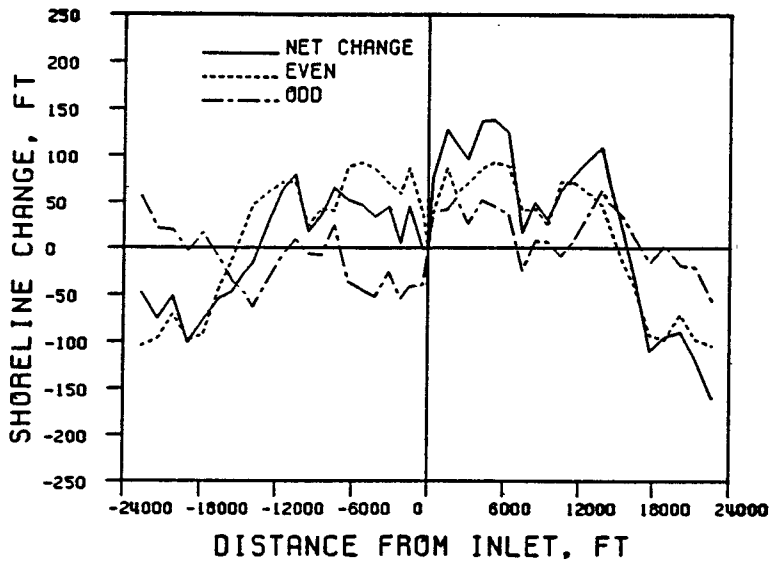

Figure 36: South Lake Worth Inlet: Even/Odd analysis of shoreline change, 1942/45–1970.

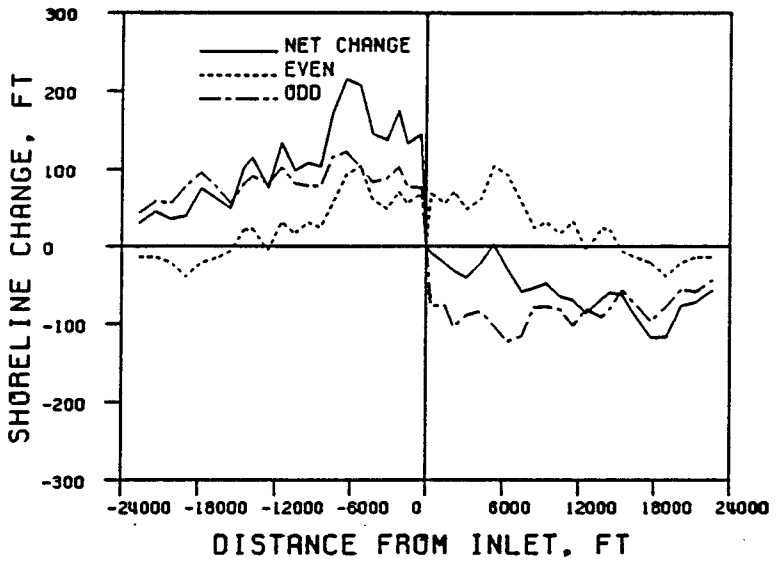

Figure 37: South Lake Worth Inlet: Even/Odd analysis of shoreline change, 1927–1974.

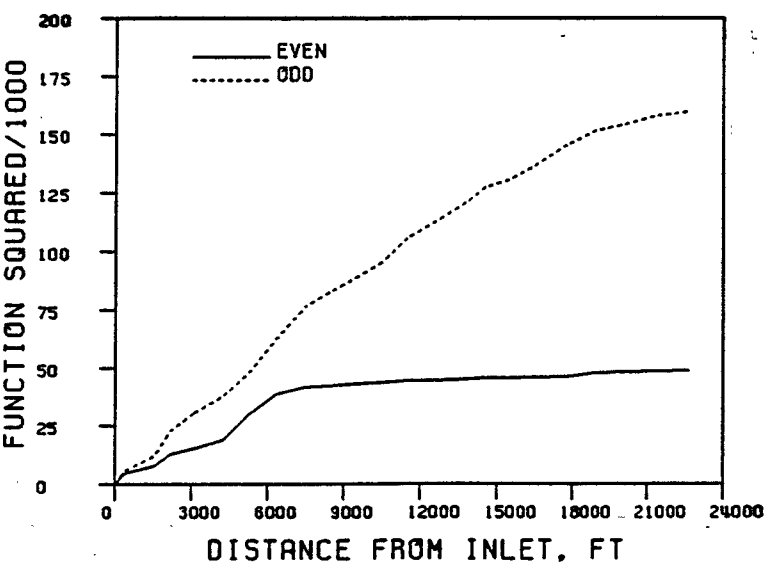

Figure 38: South Lake Worth Inlet: integral of square of even and odd functions, 1927–1974.

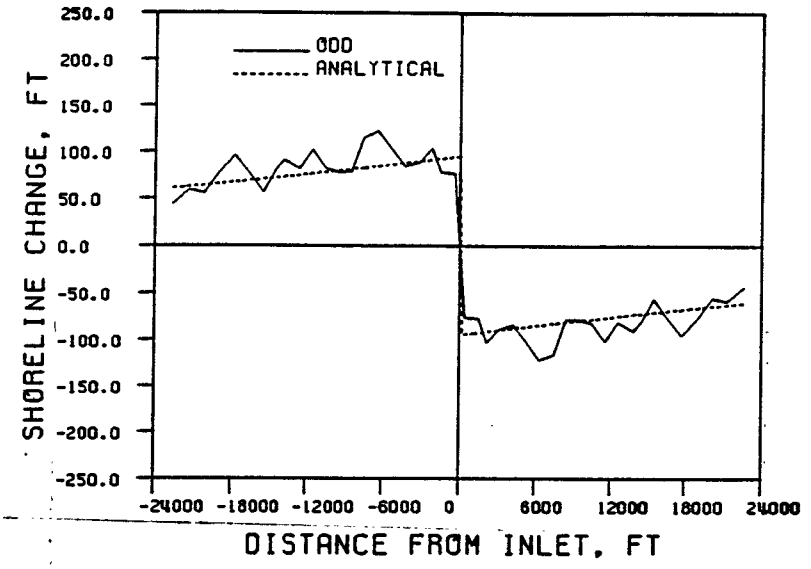

Figure 39: South Lake Worth Inlet: Comparison of odd function (1927–1974) to analytical solution. G_{best}=1.82 ft^2/sec, $(\theta_b)_{best}$=0.1°.

5.5 Sebastian Inlet

Several early attempts were made to establish Sebastian Inlet at its present location. The first, cut in 1886, closed rapidly, and a subsequent effort in 1918, that included the construction of rock jetties, was closed within hours of completion by a northeaster. Another cut was made in 1924; this lasted until 1941 or 1942. An inlet cut in 1947 closed in February, 1948 (Mehta et al., 1976).

In October, 1948, Sebastian Inlet was reopened on its present alignment. A new north jetty was built in the early 1950's, and both jetties have since been improved several times. The present configuration includes a long north jetty, short south jetty, and a sand trap approximately 2500 feet west of the inlet throat. The nearest tidal inlets are Port Canaveral, 38.9 miles to the north, and Ft. Pierce Inlet, 28.5 miles to the south.

A small beachfill project (22,000 yd^3) was conducted from 1977–79 to nourish the south beach. Another beachfill was done 1985–86 (quantity unknown). These have not adequately compensated for the blockage of longshore sediment transport (net rates estimated at 160,000 (Walton) to 300,000 yd^3/yr (USAE), to the south), as a well–defined updrift offset has

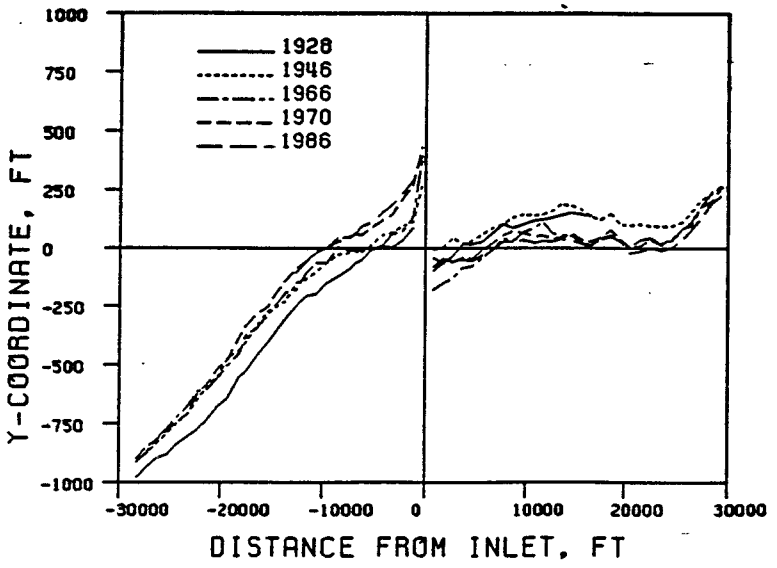

Figure 40: Sebastian Inlet: Shoreline position vs. time.

developed. This may be clearly seen in Figure 40. The net shoreline change and its even and odd components are shown in Figure 41 for the interval 1946–1970. The negative average value of the even function indicates a loss of sediment from the domain, probably resulting from shoal formation and growth.

A comparison of the 1946–1970 odd function with the analytical solution is shown in Figure 43.

The ebb tidal shoal associated with Sebastian Inlet is quite small, estimated at less then 100,000 yd^3 (1974). Sizeable flood tidal shoals exist, containing over 2 million yd^3 (1940).

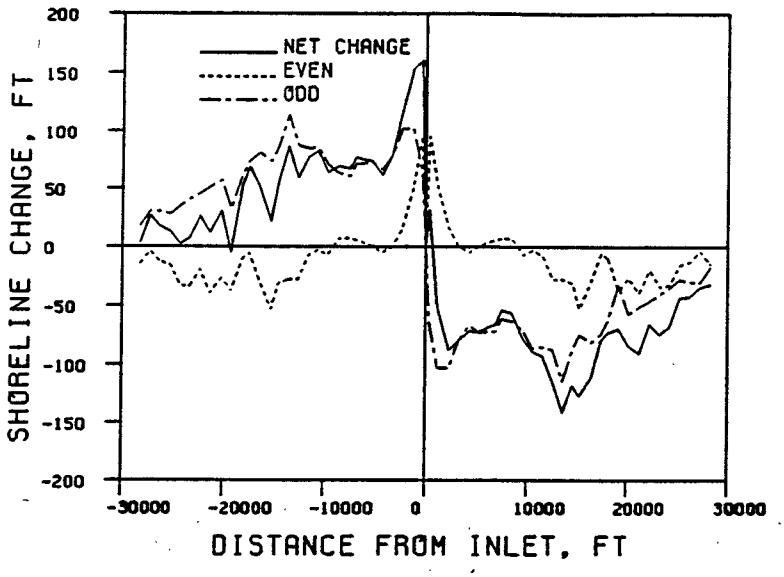

Figure 41: Sebastian Inlet: Even/Odd analysis of shoreline change, 1946–1970.

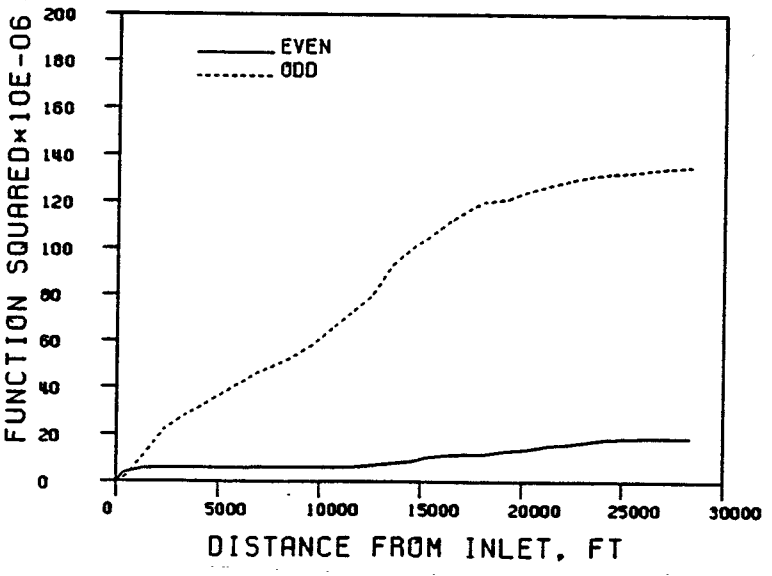

Figure 42: Sebastian Inlet: integral of square of even and odd functions, 1946–1970.

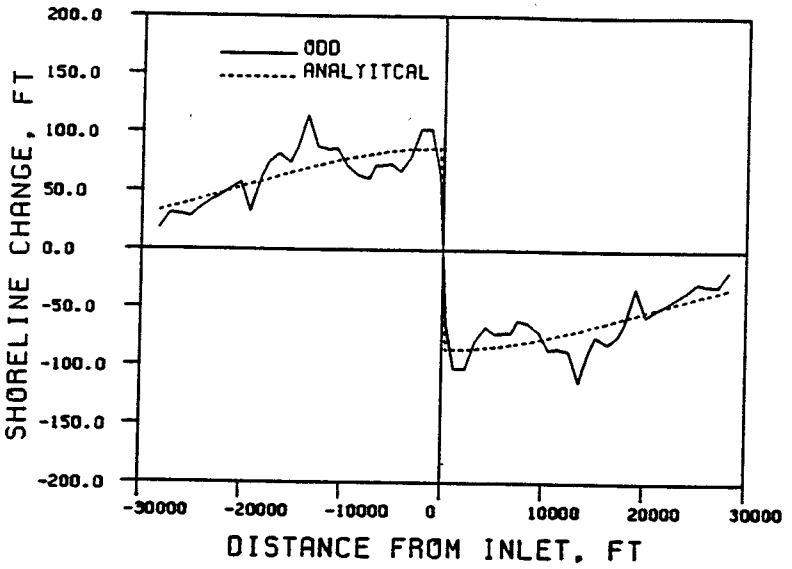

Figure 43: Sebastian Inlet: Comparison of odd function (1946–1970) to analytical solution. G_{best}=0.203 ft^2/sec, $(\theta_b)_{best}$=0.8°.

5.6 Port Canaveral

Construction of Port Canaveral was commenced in 1951 by dredging into the barrier island south of Cape Canaveral. Shoaling of the channel proceeded so rapidly that little progress could be made and work was suspended pending jetty construction (Hunt, 1980). Rock jetties 1150 feet long were constructed in 1953–54. The port is federally maintained, and currently has a project depth of 43 feet. The nearest neighboring inlets are Ponce de Leon Inlet, 49.9 miles to the north, and Sebastian Inlet, 38.9 miles to the south.

Detailed dredging records are available for Port Canaveral. The maintenance dredging rate is quite high; 10 million yd^3 was dredged for maintenance purposes during the period 1953–1985. Estimates of the net rate of longshore sediment transport range from 250,000 yd^3/yr (Walton) to 360,000 yd^3/yr (USAE) to the south, with northward transport common during the summer. The ebb tidal shoal contains approximately 5.6 million yd^3 of material, and nearby Cape Canaveral Shoal contains in excess of 100 million yd^3.

Typical of other capes along the eastern coast of the United States (i.e. Cape Hatteras), the Cape Canaveral region is quite dynamic in its response

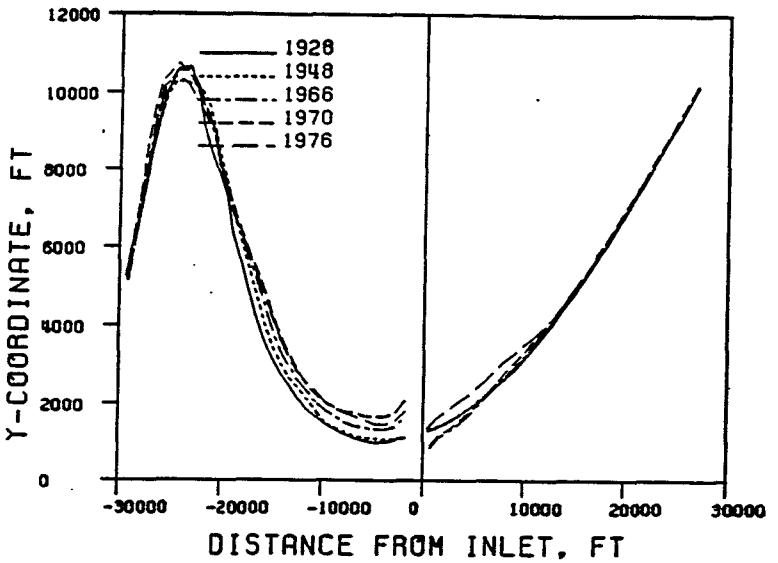

Figure 44: Port Canaveral: Shoreline position vs. time.

to disturbances. Prior to construction of the port, the south beach was accreting at approximately 1 ft/yr. Shortly after construction of the jetties, the region immediately south of the south jetty was eroding at 16 ft/yr. The result can be seen in Figure 44, where a very clear updrift offset planform has evolved. Figure 45 shows the net change, even, and odd functions for the interval 1948–1970. Note the large amount of impounded material updrift of the jetty. This accretional zone extends approximately 3.5 miles updrift, to the location of the tip of Cape Canaveral, beyond which the shoreline orientation changes significantly.

The downdrift erosional area shown in Figure 45 extends slightly more than one mile south of the inlet. The even function indicates a significant increase in the volume of sediment stored in the updrift and downdrift beaches, due to the fact that the updrift beach is impounding more sediment than the downdrift beach is losing. A likely explanation for this may be formulated by examining the large change in shoreline orientation between the updrift and downdrift beaches. Updrift of the inlet, the azimuth of a line normal to shore averages 120 degrees (measured clockwise from North), while a similar line downdrift of the inlet averages 90 degrees. Thus waves approaching shore from a direction north of east will tend to cause larger longshore transport rates on the updrift beach than on the downdrift beach. Refraction will

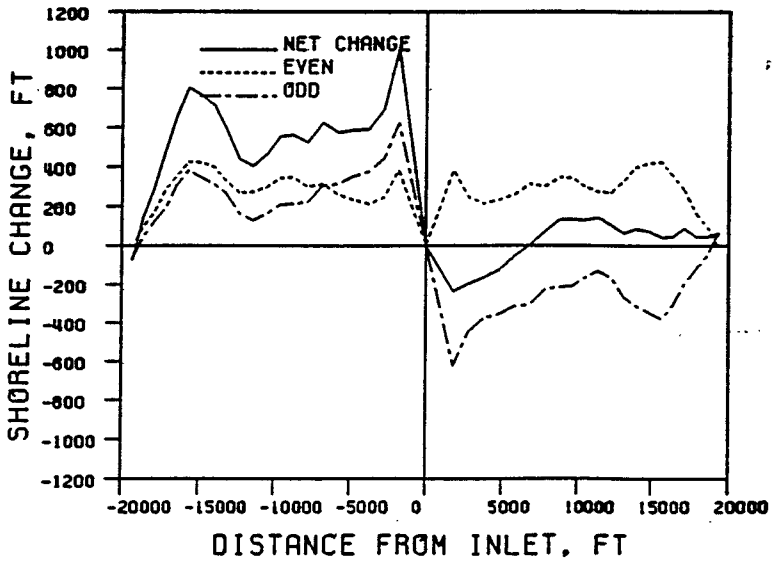

Figure 45: Port Canaveral: Even/Odd analysis of shoreline change, 1948–1970.

mitigate this tendency to some degree. The accretional trend that existed prior to the construction of the inlet also explains some of the increase in the volume of material stored in the beaches.

Approximately 2.5 million yd^3 was placed on the south beach in 1974; this material has since travelled south as a "wave". This explains the recovery of the downdrift shore between the 1970 and 1976 surveys as shown in Figure 44. The corresponding shoreline change functions are shown in Figure 46. Note the similarity to the earlier example for an idealized beachfill (Figure 10).

The U.S. Army Corps of Engineers has plans to initiate a sand bypassing project to reduce erosion rates along the south beach, but no construction has yet taken place.

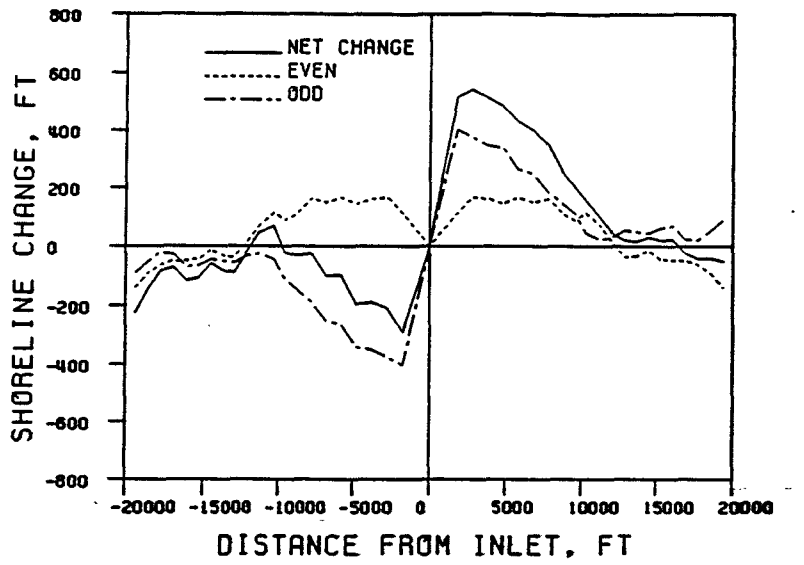

Figure 46: Port Canaveral: Even/Odd analysis of shoreline change, 1970–1976.

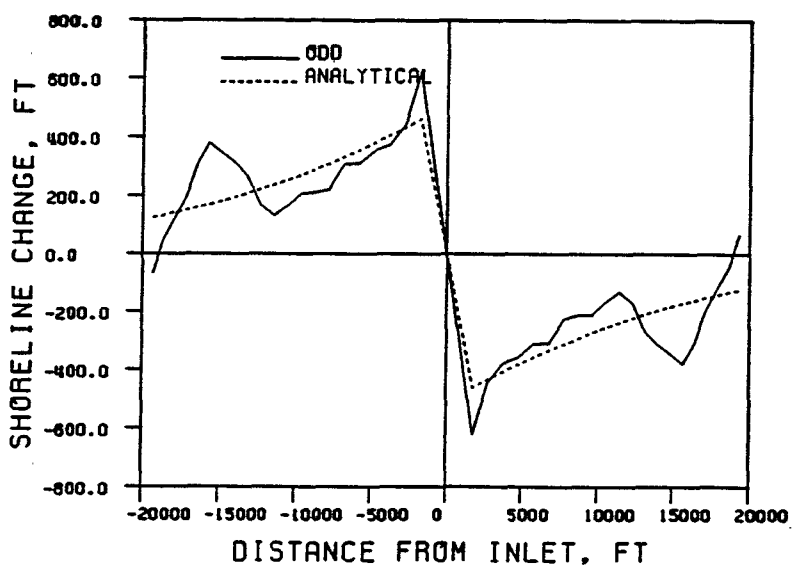

Figure 47: Port Canaveral: Comparison of odd function (1948–1970) to analytical solution. G_{best}=0.37 ft^2/sec, $(\theta_b)_{best}$=1.8°.

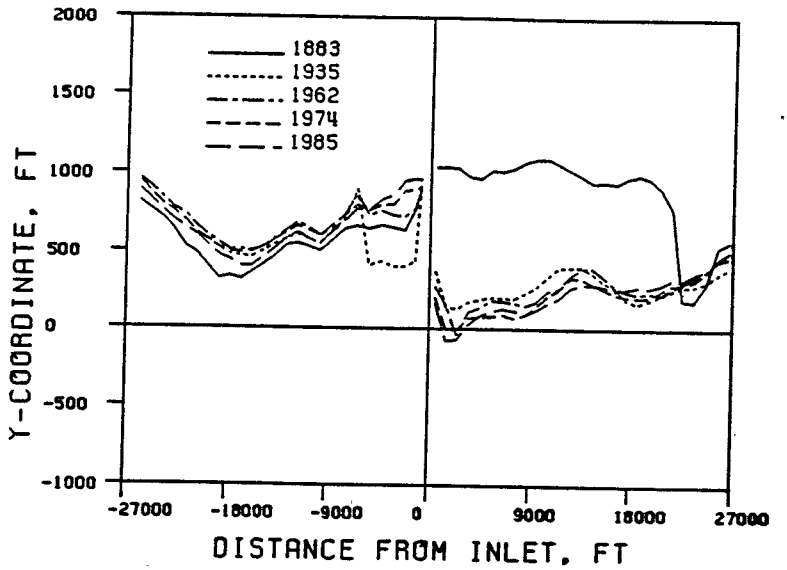

Figure 48: Port Everglades: Shoreline position vs. time.

5.7 Port Everglades Inlet

Two natural inlets existed in the vicinity of Port Everglades Inlet when it was cut in 1928: New River Inlet, located approximately 6200 feet to the north, and Dania Inlet, approximately 10,000 feet to the south. These are the 1936 locations; both inlets were known to migrate over distances of several miles. New River Inlet closed naturally in 1937, Dania Inlet closed naturally between 1936 and 1944. The nearest neighboring inlets are presently Hillsboro Inlet, 11.5 miles to the north, and Baker's Haulover, 13.3 miles to the south.

A 1450–foot north jetty and a 1250–foot south jetty were both completed in 1931 at Port Everglades. The longshore transport rate for this region has been estimated at 50,000 yd^3/yr (USAE) and 270,000 yd^3/yr (Walton) to the south. Figure 48 provides a dramatic example of shoreline response to a littoral barrier. There has been substantial erosion downdrift of the inlet, requiring beach nourishment, since it was cut.

No measureable ebb tidal shoal has formed as a result of the cutting of Port Everglades Inlet. Channel and boat basin geometries, when maintained by dredging, essentially preclude the formation of a flood tidal shoal. Of the 8 million yd^3 dredged from the inlet between 1934–1984, 3.2 million yd^3 has

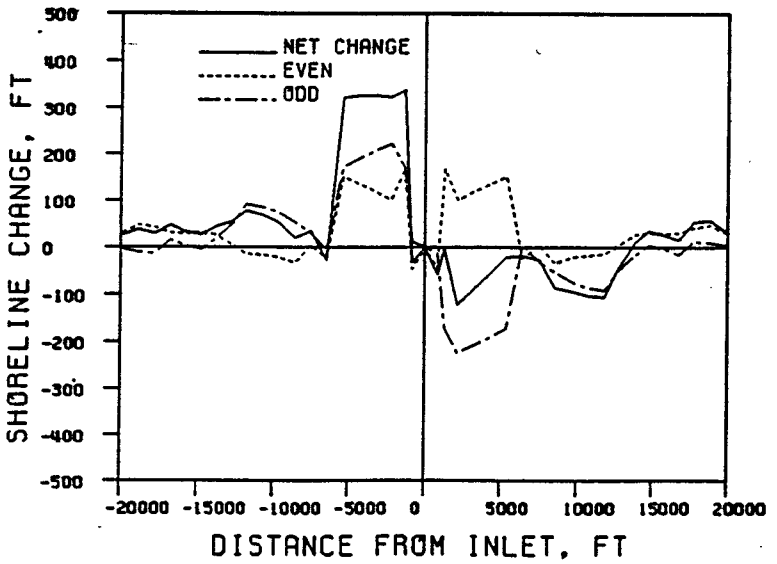

Figure 49: Port Everglades: Even/Odd analysis of shoreline change, 1935–1962.

been used as beachfill, on the south side of the inlet.

The shoreline change plots initially appear complicated, but are explainable after consideration of the history of the area. The large amount of accretion updrift of the inlet is shown in Figure 49 for the period 1935–1962 is due to deposition in the area downdrift of New River Inlet after its closure. During this same period, the shoreline downdrift of Port Everglades Inlet has responded to the inlet construction by eroding over much of the two miles immediately downdrift. Figure 50 shows the shoreline change and its components for the period 1962–1985. By 1962, the "hole" downdrift of New River Inlet had largely been filled, so the shoreline changes shown in Figure 50 reflect the common updrift offset pattern. Figure 51 shows the shoreline change for the entire period for which data are available (1883–1985) and matches the updrift offset pattern well. Note the similarity to both Figure 7, the example of the analytical solution plus uniform background erosion, and Figure 21 for St. Lucie Inlet.

The average value of the even function is strongly negative, reflecting the role of the "hole" downdrift of New River Inlet as a sediment sink until full. A comparison of the odd function vs. the analytical solution for this time period is shown in Figure 52.

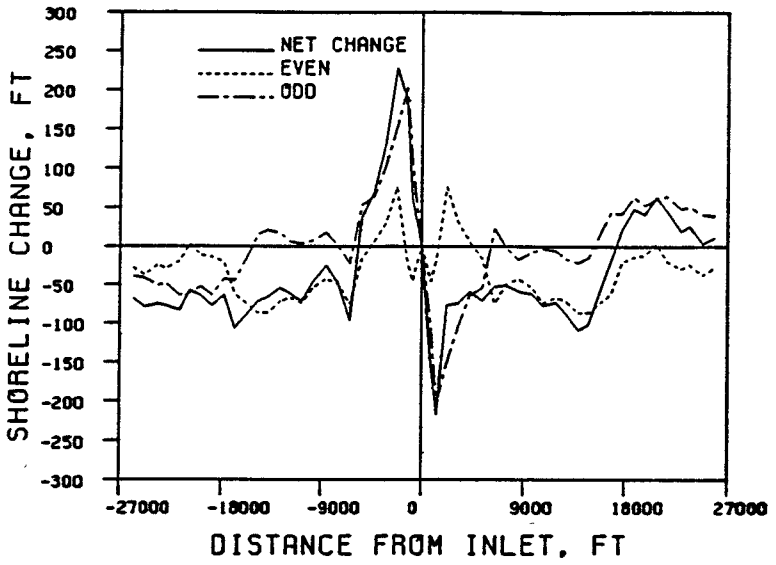

Figure 50: Port Everglades: Even/Odd analysis of shoreline change, 1962–1985.

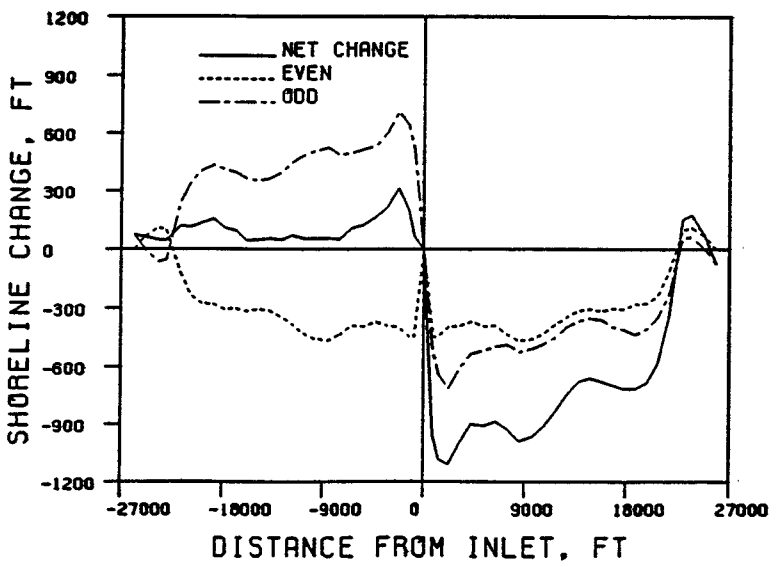

Figure 51: Port Everglades: Even/Odd analysis of shoreline change, 1883–1985.

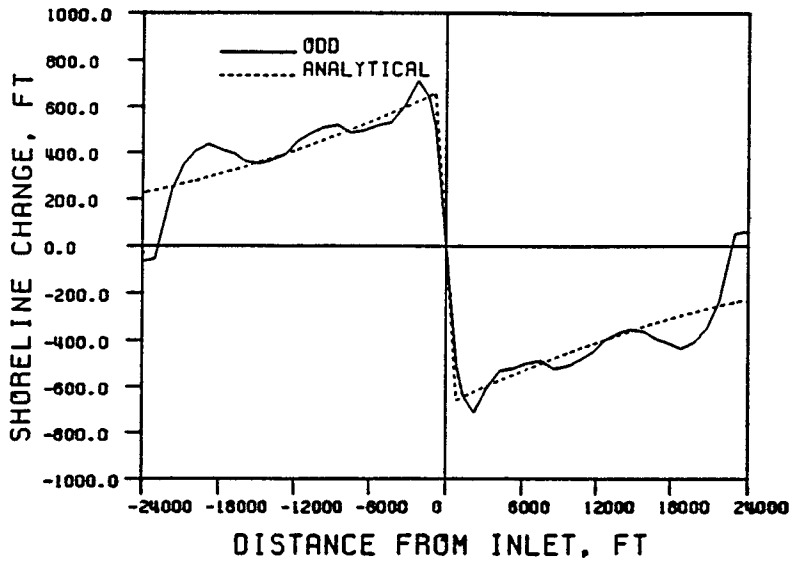

Figure 52: Port Everglades: Comparison of odd function (1883–1985) to analytical solution. G_{best}=0.29 ft^2/sec, $(\theta_b)_{best}$=1.5°.

5.8 Matanzas Inlet

Matanzas Inlet is a natural inlet that was in existence as early as the mid–sixteenth century. It has not been dredged and has no training structures other than bridge abutments. St. Augustine Inlet lies 14.7 miles to the north and Ponce de Leon Inlet 47.2 miles to the south.

The first bridge across Matanzas Inlet was completed in 1926. Dredging of the Matanzas Relocation Cut (part of the Intracoastal Waterway) in 1932 had a significant effect on the subsequent evolution of Rattlesnake Island (the sheltered island shown at center of photo) and the flood shoals associated with Matanzas Inlet. In 1964, Hurricane Dora broke through Rattlesnake Island, creating a more direct connection between Matanzas Inlet and the Intracoastal Waterway, again significantly changing tidal flow patterns. This opening was closed in 1977 by construction of a sheet pile dike.

A storm in the spring of 1989, caused a small breakthrough in the barrier island about 4000 feet south of Matanzas Inlet; this was quickly closed by bulldozer. The shoreline north of this breakthrough is heavily armored for roughly one–half mile.

The cross–section of the inlet has varied considerably over time, but

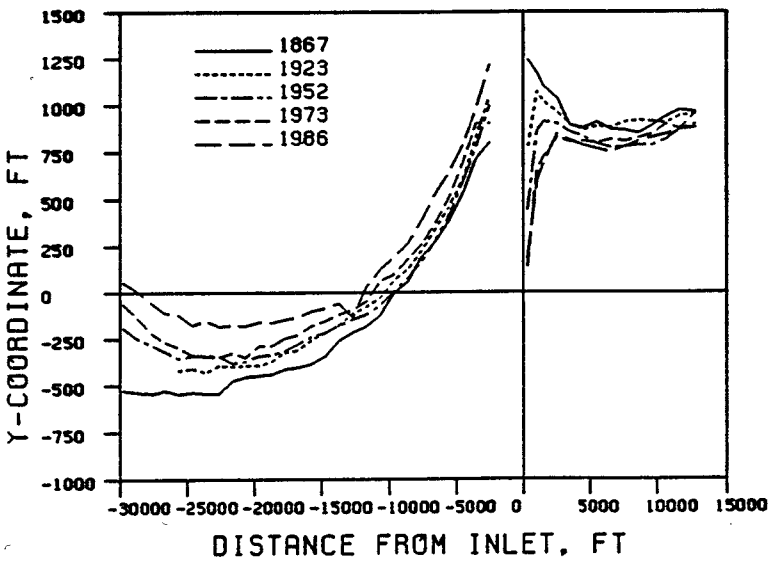

Figure 53: Matanzas Inlet: Shoreline position vs. time.

consistently has its deepest portion near the southern bridge abutment. This abutment apparently helps prevent a trend toward southward migration of the inlet that would otherwise exist. Outcrops of the Anastasia Formation, composed of loosely cemented shell material, are also evident along some sections of the downdrift shoreline; this may also play a role in the prevention of southward migration.

The ebb shoal has been estimated at 6.3 million yd^3 (1978), and the flood shoal at 400,000 yd^3. This latter figure is somewhat misleading as some of the material that would otherwise be considered part of the flood shoal has been incorporated into Rattlesnake Island as it has grown in size.

The net littoral transport rate has been estimated at from 290,000 yd^3/yr (Walton) to 440,000 yd^3/yr (USAE) to the south. Mehta and Jones (1977) estimate that an average of 71,000 yd^3 enters the inlet each year. This, combined with inadequate passing of sand across the ebb tidal shoal, has led to accretion along the updrift shore and erosion downdrift. Figure 54 shows the shoreline change and its even and odd components for the period 1923–1986. The net shoreline change has the typical updrift offset planform, although the magnitude of the changes is considerably less than those observed at some stabilized inlets having lower longshore sediment transport rates (i.e. St. Lucie Inlet, Ft. Pierce Inlet, Port Everglades). The positive

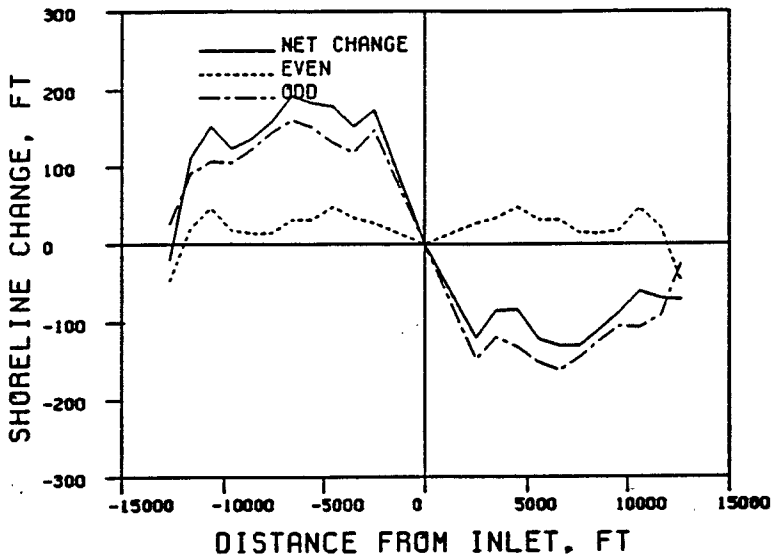

Figure 54: Matanzas Inlet: Even/Odd analysis of shoreline change, 1923–1986.

average value of the even function indicates a net gain of sediment within the domain during the time interval; this would probably not be the case were the downdrift shore not revetted. Lack of data prevented analysis of a domain larger than that shown in Figure 54; more data would be required to confidently establish the zone of influence for the inlet. Analytical and numerical simulations of the shoreline changes were not attempted because of the complex boundary conditions required.

It appears that the erosion that is experienced downdrift of Matanzas Inlet could be mitigated by bypassing the material that is captured by the inlet. This would slow or halt the growth of Rattlesnake Island and would help maintain the position of the downdrift shore.

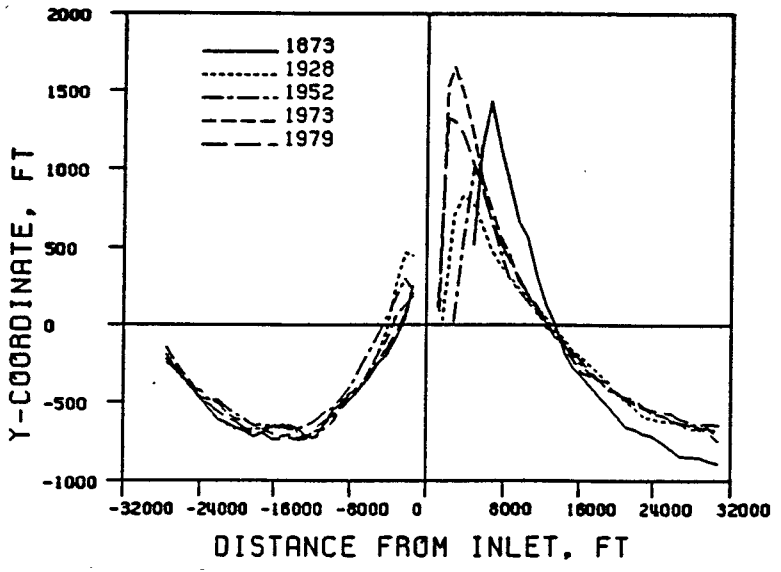

Figure 55: Ponce de Leon Inlet: Shoreline position vs. time.

5.9 Ponce de Leon Inlet

Ponce de Leon Inlet is a natural tidal inlet pre–dating the arrival of Spanish settlers in Florida in the 1500's. It was first dredged in 1943, but jetty construction was not initiated until 1968. North and south jetties 4000 feet long were completed in 1971, with the north jetty incorporating a weir section 1800 feet in length. This weir section was closed by placement of rock in 1984. The channel is maintained to a depth of 15 feet. The nearest tidal inlets are Matanzas Inlet, 47.2 miles to the north, and Port Canaveral, 49.9 miles to the south.

The net longshore sediment transport rate has been estimated at 180,000 (Walton) to 500,000 yd^3/yr (USAE) to the south; transport reversals are common during summer. 3.6 million yd^3 have been dredged from the inlet; most was placed within the 30 ft. contour north (updrift) of the inlet. The size of the ebb tidal shoal has been estimated at 22.5 million yd^3 (1974).

Plots of shoreline change for intervals bracketing the construction of the jetties show a reversal from the updrift offset pattern typically seen at stabilized inlets. Several factors are responsible for this. The offshore, rubble mound segment of the north jetty was constructed prior to the weir section, constraining any longshore currents and the flood tidal currents to

a smaller cross–sectional area, increasing flow velocities, and therefore enhancing sediment transport immediately updrift of the inlet. This situation was partially remedied by construction of the weir section, but its elevation of 0.0 ft. MLW still allowed (by design) some longshore transport to pass at higher tidal stages or when wave setup or storm surge elevated the mean water level. Erosion of the updrift shore should thus be expected if sediment were to pass over the weir at an average rate greater than the average net longshore transport rate. The net result, shown in Figure 56 for the years 1952/56–1973/75, has been erosion of the updrift shore, despite the placement of dredge spoil along this reach. Figure 57 shows results for 1952/56–1988; disposal of dredge spoil on the updrift shore has returned it to its 1952/56 position.

The very large accumulation of sand immediately downdrift of the south jetty is most easily interpreted by examination of the position of the south jetty relative to the existing shoreline at the time of construction, as shown in Figure 58. The orientation of the jetty formed a somewhat sheltered pocket into which some of the dredge spoil from the inlet was placed, partially filling it. This pocket has also trapped material that has entered it during periods of transport reversal. Additionally, refraction analysis (Purpura and Chiu, 1977) indicates that this area is, for several combinations of incident wave period and deep–water direction, a convergent nodal zone, making the shoreline bulge somewhat self–maintaining. Some of this material may be derived from the ebb tidal shoal, since the ebb tidal jet is now better defined, constrained by the jetties, allowing wave action to force some shoal material onshore.

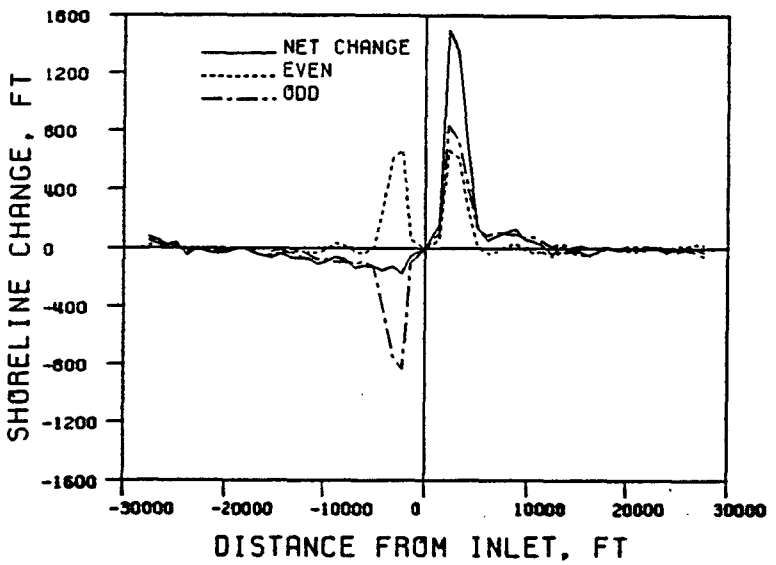

Figure 56: Ponce de Leon Inlet: Even/Odd analysis of shoreline change, 1952/56–1973/75.

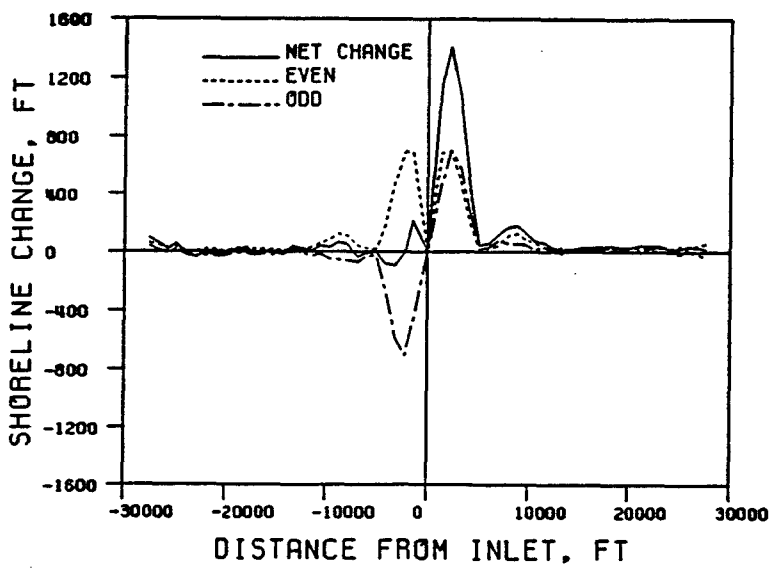

Figure 57: Ponce de Leon Inlet: Even/Odd analysis of shoreline change, 1952/56–1988.

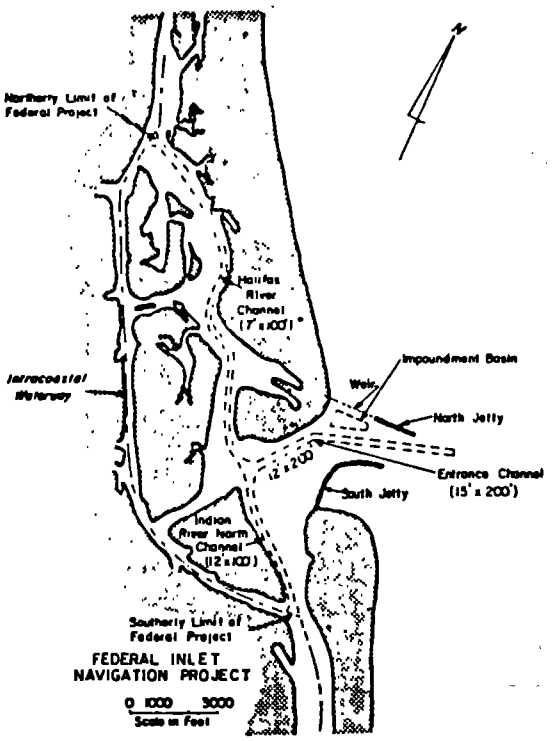

Figure 58: Ponce de Leon Inlet: South jetty alignment. Adapted from Jones and Mehta, 1978.

5.10 St. Augustine Inlet

St. Augustine Inlet existed as a meandering, natural inlet prior to the cutting of a new inlet 2.5 miles to the north in 1940. This new inlet was stabilized by construction of a jetty along its northern limit in 1941. The old inlet was shoaling by 1946. A southern jetty was added in 1957. The nearest inlets are St. John's River Entrance, 34.5 miles to the north, and Matanzas Inlet, 14.7 miles to the south.

The net longshore sediment transport rate for this site has been estimated at 380,000 to 440,000 yd^3/yr to the south (Walton and USAE, respectively); reversals are common in summer. The channel is presently maintained at a depth of 16 feet. Most of the material that has been dredged since the new inlet was constructed has been disposed of somewhere within the ebb shoal area, where it presumably could be moved ashore by wave action or re–enter the inlet.

A large ebb tidal shoal at St. Augustine Inlet has been documented since the early 1900's. Its size as of 1979 has been estimated at 110.4 million yd^3. Much material from the southern portion of the shoal, which was formerly directly offshore of the old inlet, has moved landward to form what is now

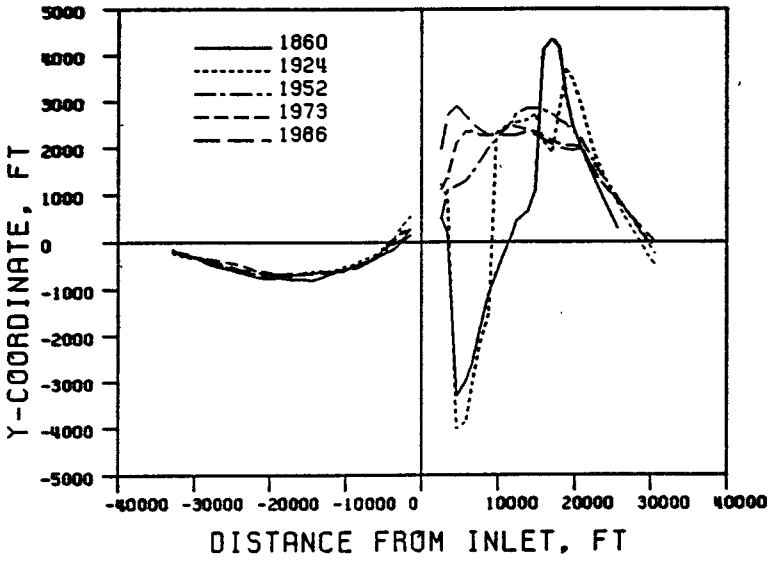

Figure 59: St. Augustine Inlet: Shoreline position vs. time.

known as Conch Island. This explains the significant accretion that is shown south (downdrift) of the current inlet position in Figure 59. This accretional zone lies within the lee of the ebb tidal shoal, and extends approximately two miles downdrift of the present inlet location. Downdrift of this area is a zone that has experienced substantial erosion. Shoreline changes updrift of the inlet have been comparatively small. The shoreline change for 1952–1986, and its even and odd components, are shown in Figure 60. Note that it is qualitatively similar to the previous example illustrating the shoreline change components for a beachfill (Figure 10) shown previously, since there has been little change updrift and much accretion downdrift. The relatively high permeability of the north jetty has resulted in minimal impoundment of sediment updrift of the jetty. Leakage of sediment through the the north jetty has resulted in the formation of Porpoise Point, a large depositional feature extending into the channel from the north (see photo). This feature has sustained long enough that houses have been built upon it, within the region defined by the two jetties.

It is also of interest to note that the volume that has moved ashore to form Conch Island (estimated at 7.3 million yd^3, Marino and Mehta, 1986) represents less than one–tenth of the estimated volume contained in the ebb tidal shoal.

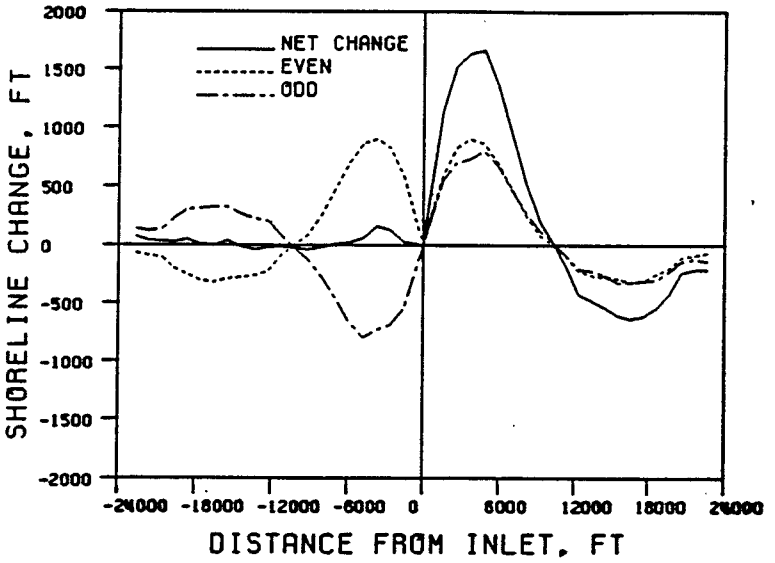

Figure 60: St. Augustine Inlet: Even/Odd analysis of shoreline change: 1952–1986.

5.11 Jupiter Inlet

Jupiter Inlet connects the Loxahatchee River to the Atlantic Ocean. It is a natural inlet that has been in existence for at least 300 years. Prior to stabilization, it was subject to occasional closure and migration. The last significant migration occurred between 1913–1922, when the inlet moved northward approximately 1250 feet. The frequency of the inlet closures increased with the construction of St. Lucie Inlet 16.3 miles to the north in 1892, and Lake Worth Inlet 12.1 miles to the south in 1917. These inlets diverted tidal flow away from Jupiter Inlet.

Jupiter Inlet was stabilized in 1922 by the construction of rock jetties 400 feet long and 350 feet apart. The north jetty was extended 200 feet, and the south jetty 75 feet, in 1929. Both jetties were modified again in the late 1960's. Regular maintenance dredging has been required to keep the inlet open. The inlet closed in 1942 and was not re–opened until 1947. From 1952–1977, over 1.1 million yd^3 was dredged from the inlet and placed on the south beach. Much of this material came from the dredging of a sand trap 1000 feet west of the inlet in 1966. Sand is currently bypassed mechanically to the south beach at an average rate of 44,000 yd^3/yr. Note

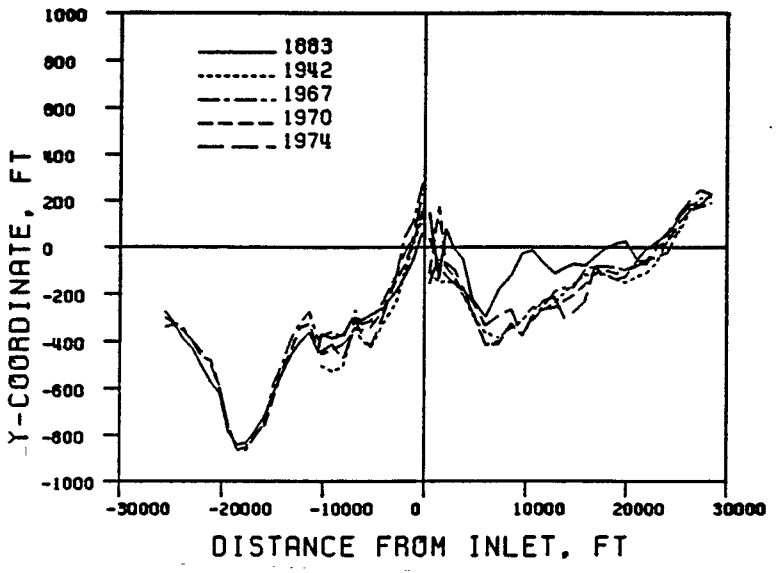

Figure 61: Jupiter Inlet: Shoreline Position vs. time.

that this is less than 20 percent of the estimated net littoral transport rates of 230,000 yd^3/yr (USAE) and 240,000 yd^3/yr (Walton) to the south.

The ebb tidal shoal offshore of Jupiter Inlet is relatively small, approximately 0.4 million yd^3 (1978). No flood tidal shoal exists, due to the maintenance dredging.

Inlet migration was accounted for when performing even/odd analysis for surveys that bracketed the 1917–1922 interval corresponding to the last major inlet migration. Figure 62 shows the results for 1883–1966/67. (Unfortunately, data were not available for subintervals of this period). Substantial erosion is seen for over two miles on the downdrift shore. The even function reflects the net loss of sediment that has resulted.

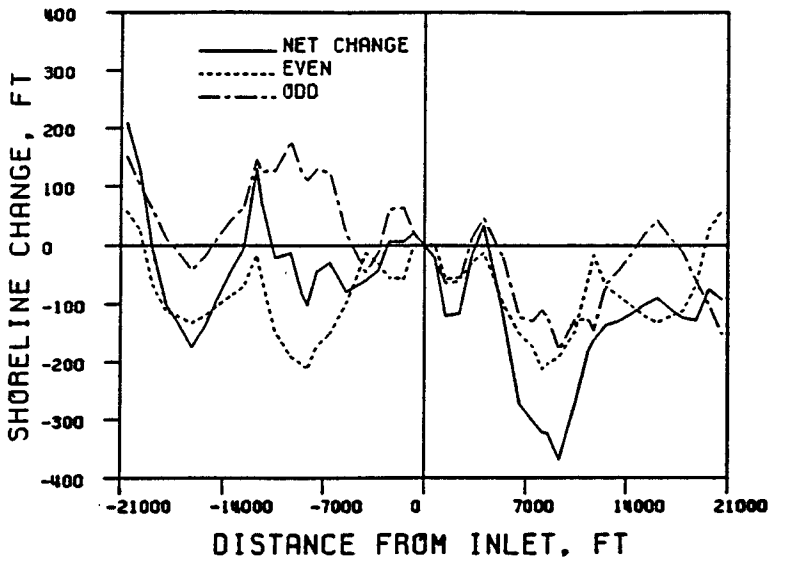

Figure 62: Jupiter Inlet: Even/Odd analysis of shoreline change, 1883–1966/67.

5.12 Boca Raton Inlet

Boca Raton Inlet is a natural inlet that was quite shallow during the infrequent periods that it was open prior to stabilization. It was dredged in 1925–26 and stabilized by jetties in 1930–31. Periodic dredging has been required since that time, but records of quantities are elusive. South Lake Worth Inlet is 14.5 miles to the north, Hillsboro Inlet is 5.4 miles to the south.

The north jetty was extended by 180 feet in 1975, and then modified in 1980 to contain a 65-foot weir section. A beachfill of 297,000 yd^3 of material was placed on the south beach in 1985. The sources of this material were the inlet and the ebb tidal shoal, the latter providing 244,000 yd^3 of the total. A dredge is currently maintained to bypass sediment to the south beach. Available dredging records indicate that approximately 1.1 million yd^3 was placed on the south beach during the years 1940–1985. This would correspond to an average annual bypassing rate of slightly more than 24,000 yd^3/yr. The ebb tidal shoal contains roughly 1.1 million yd^3 of material (1981).

Estimates of the net longshore sediment transport rate for the area range

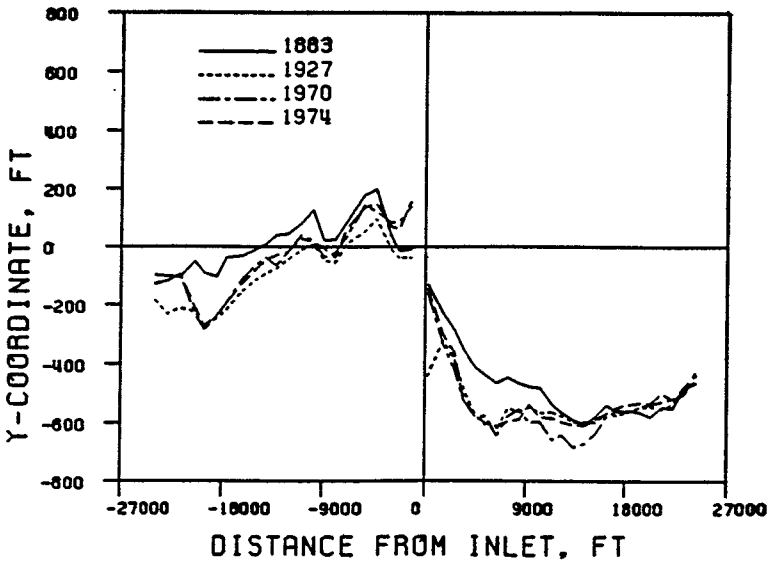

Figure 63: Boca Raton Inlet: Shoreline position vs. time.

from 150,000 yd^3/yr (USAE) to 280,000 yd^3/yr (Walton) to the south. Comparing this to the average bypassing rate, it should be expected that an updrift offset would exist, and this is indeed the case (Figure 64). The magnitude of the shoreline change is, however, relatively small (less than 50 feet), except for the region immediately updrift of the north jetty, for the interval 1927–1970. It appears that increased bypassing rates during this period would have removed the bias from the shoreline signature.

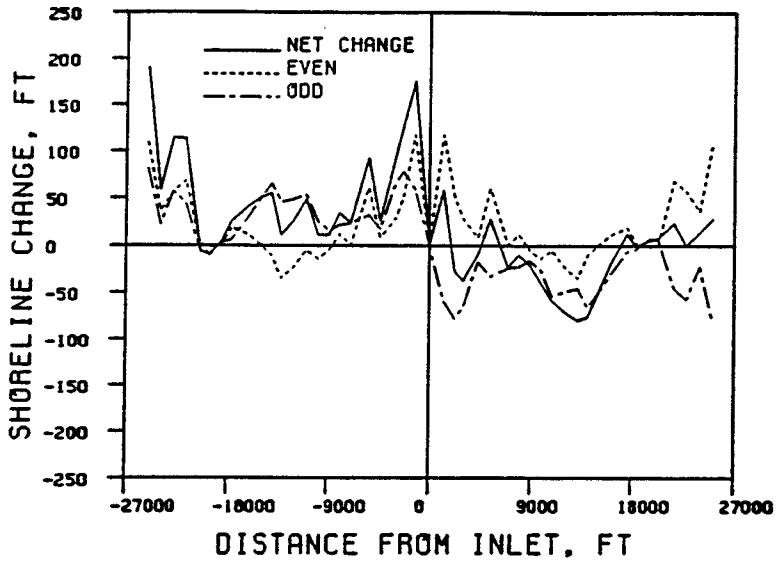

Figure 64: Boca Raton Inlet: Even/Odd analysis of shoreline change, 1927–1970.

5.13 Hillsboro Inlet

Hillsboro Inlet is a natural inlet that has been stabilized through the addition of rock jetties. The inlet is afforded some natural protection through the existence of a rock reef running close to shore, nearly shore–parallel. This reef has played a significant role in the evolution of the adjacent beaches. Note the unusual shoreline orientation shown in both the photo and in Figure 65. The nearest neighboring inlets are Boca Raton Inlet, 5.4 miles to the north, and Port Everglades, 11.5 miles to the south.

A rock groin was constructed on the north side of the inlet to protect the lighthouse in 1930. A wooden groin was built on the south side of the inlet in 1952. The existing rock jetties north and south of the inlet were constructed in 1966. The north jetty makes use of a portion of the reef as a weir section, allowing sand to deposit in a sheltered settling basin for subsequent dredging. Sand has been bypassed from this basin to the south beach since 1959 by a pipeline dredge situated in the inlet. The current average bypassing rate is 70,000 yd^3/yr, less than the estimated southward littoral transport rates of 100,000 yd^3/yr (USAE) and 280,000 yd^3/yr (Walton). In addition to the bypassed material, a total of 2.2 million yd^3 has been dredged. Of this

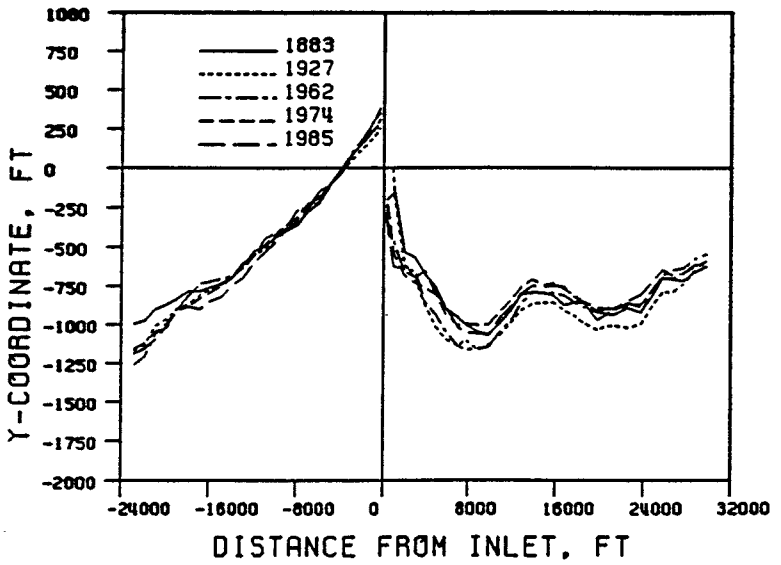

Figure 65: Hillsboro Inlet: Shoreline position vs. time.

dredged material, 1.6 million yd^3 has been placed on the south beach. There are presently no significant ebb or flood tidal shoals.

There is an extensive groin field that extends to about 17,000 feet north of the inlet. There are also several small groins located about 2500 feet south of the inlet.

Examining the plots of shoreline change, it can be seen that there was erosion immediately updrift of the inlet prior to construction of the groin north of the inlet in 1930 (Figure 66). Subsequent to construction of this groin, the updrift (north) shore was stabilized, while erosion is seen immediately downdrift as the downdrift shoreline adjusted to the new sediment budget. (Figure 67). The shoreline changes for the 1927–1962 interval are less than roughly 50 feet over much of the region, which can be considered small–scale variation or "noise". Bypassing by the pipeline dredge has led to recovery of the downdrift shore at some expense to the updrift shore, as can be seen by the plot for 1962–1974 (Figure 68). This has the effect of reversing the typical pattern for the odd component of shoreline change — it now shows a downdrift rather than updrift offset.

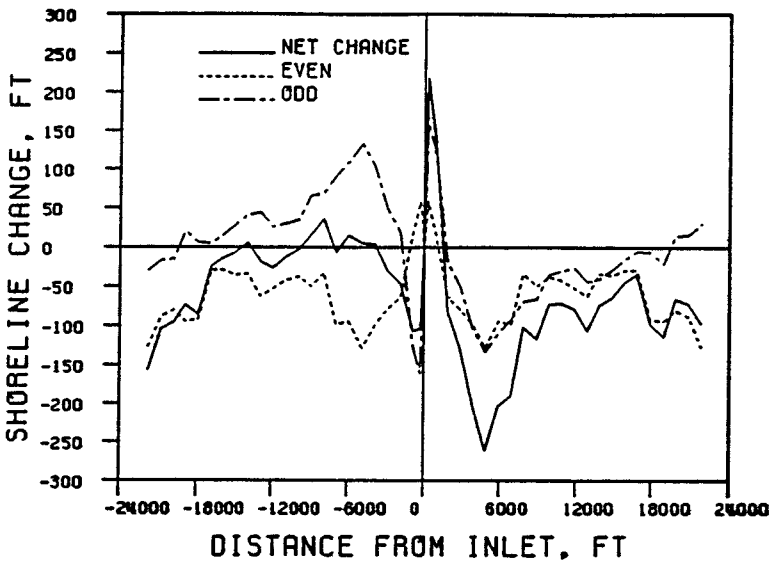

Figure 66: Hillsboro Inlet: Even/Odd analysis of shoreline change, 1883–1927.

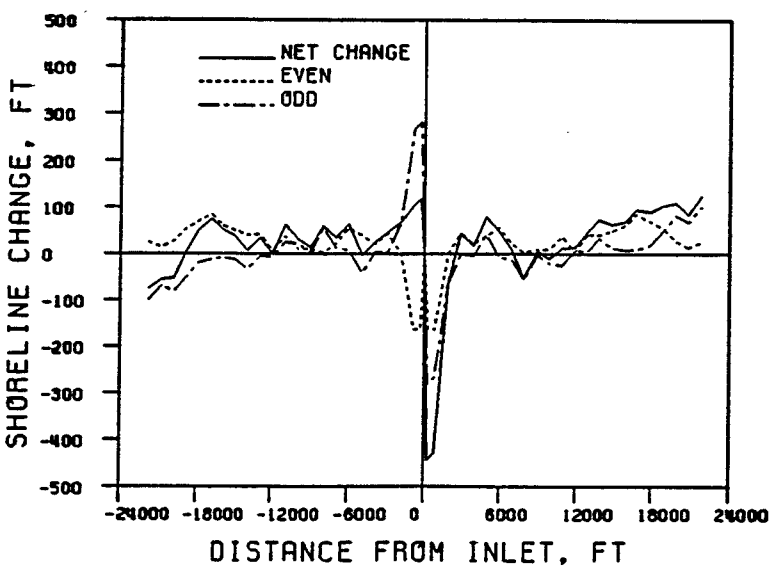

Figure 67: Hillsboro Inlet: Even/Odd analysis of shoreline change, 1927–1962.

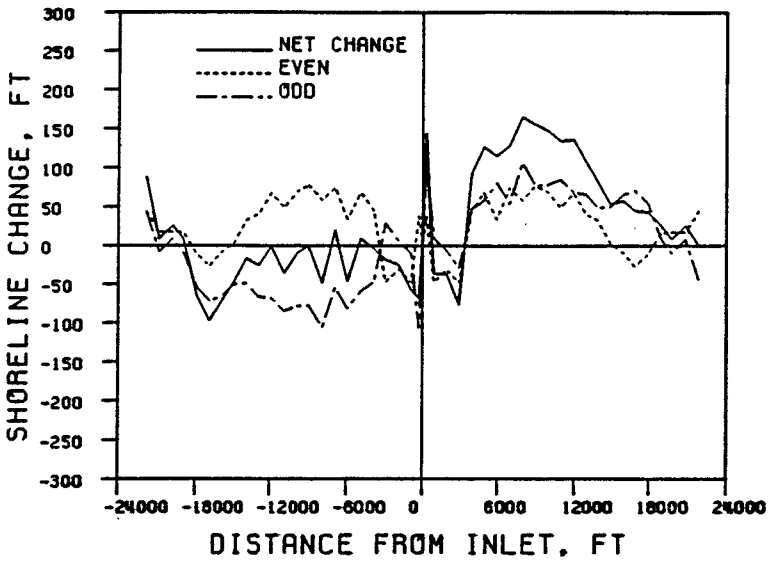

Figure 68: Hillsboro Inlet: Even/Odd analysis of shoreline change, 1962–1974.

5.14 Bakers Haulover

Bakers Haulover was created in 1925 by dredging through a narrow section of beach near the northern end of Biscayne Bay. Small stabilizing structures were built at that time. The inlet is approximately 9.3 miles north of Government Cut (Miami Harbor Entrance), and 13.3 miles south of Port Everglades. Sheet– pile jetties 325 ft. apart were completed in 1928; a major hurricane in 1926 had destroyed the original structures. Both jetties are now of rubble–mound construction, with the south jetty including a concrete cap. The south jetty was extended to a length of 800 ft. in 1975. The north jetty was extended in 1986, but is slightly smaller than the south jetty.

The net longshore sediment transport rate for this area has been estimated at 20,000 yd^3/yr (USAE) to 270,000 yd^3/yr (Walton) to the south. Beaches on both sides experienced erosion immediately adjacent to the jetties subsequent to construction (Figure 70). Much of this material was probably incorporated into the ebb and flood tidal shoals. The ebb shoal had a size of 0.6 million yd^3 in 1969. Between the years 1937–1978, 2.7 million yd^3 was dredged from the inlet. Most of this was placed on the adjacent beaches.

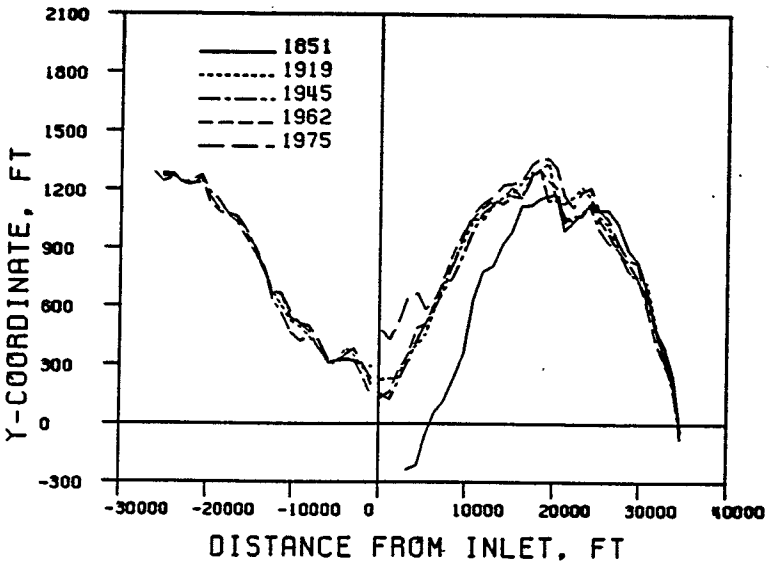

Figure 69: Bakers Haulover: Shoreline position vs. time.

The south beach has benefitted significantly from the Miami Beach Restoration Project, as can be seen in Figure 71. The south jetty has proven effective at trapping the sediment that has moved north from this project.

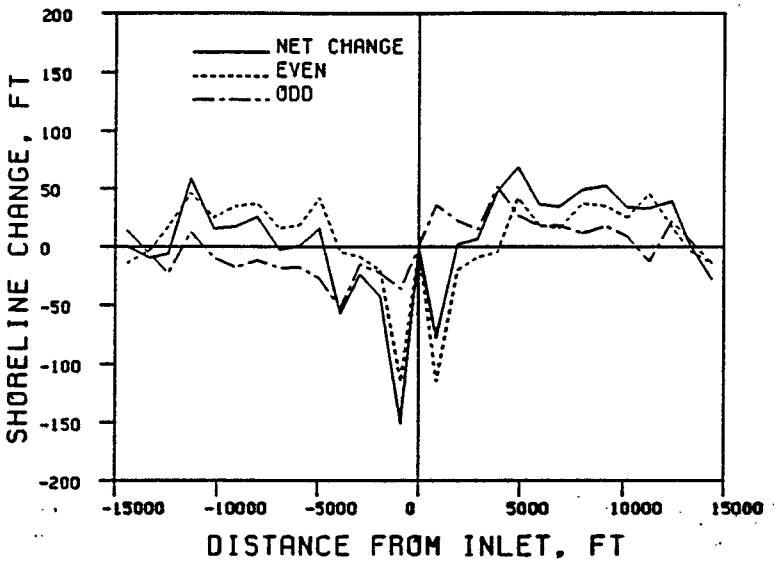

Figure 70: Bakers Haulover: Even/Odd analysis of shoreline change, 1919–1962.

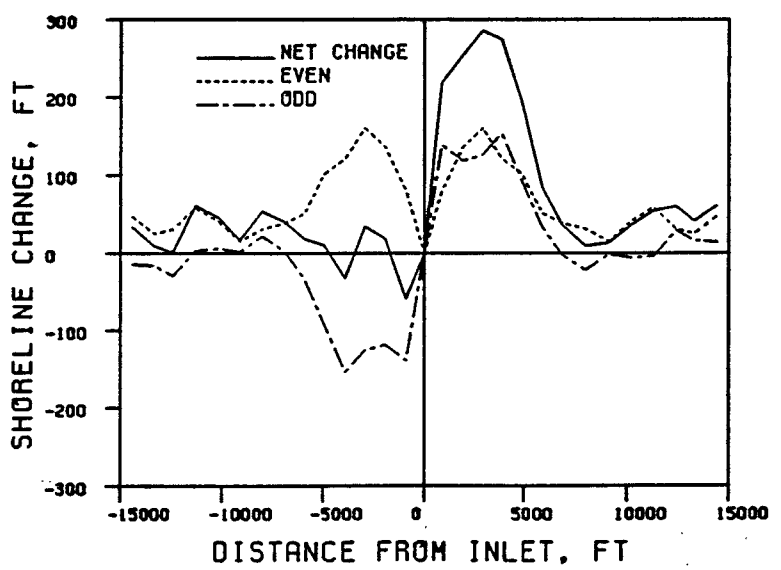

Figure 71: Bakers Haulover: Even/Odd analysis of shoreline change, 1919–1975.

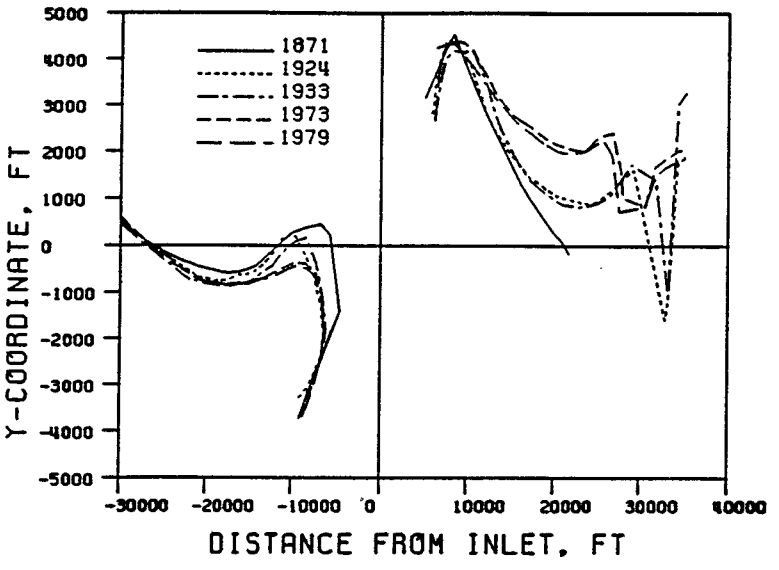

Figure 72: Nassau Sound: Shoreline position vs. time.

5.15 Nassau Sound

Nassau Sound is an unmodified, natural inlet which connects the Amelia and Nassau Rivers to the Atlantic Ocean. It separates Amelia Island, to the north, and Little Talbot Island, to the south, spanning a distance of more than two miles. This wide opening is interrupted by Bird Island, an emerging flood shoal. The primary entrance channel is approximately 5600 feet wide and varies in depth up to 20 feet. The behavior of this inlet is unaffected by man–made structures, and it is quite dynamic, making interpretation of past shoreline changes and prediction of future changes difficult. The nearest inlets are St. Mary's Entrance, 13.8 miles to the north, and Ft. George Inlet, 5.6 miles to the south.

Over the past 100+ years, the main channel at Nassau Sound has been shifting northward as the south end of Amelia Island has eroded and the north end of Little Talbot Island accreted. During this time, the ebb tidal shoal reduced slightly in size, but remains quite large, having an estimated volume of 40.5 million yd^3 in 1973. The net longshore sediment transport rate for the area has been estimated at 230,000 yd^3/yr to the south (Walton).

Plots of shoreline position vs. time (Figure 72) show that the southern shore of Amelia Island retreated northward roughly 2000 feet from 1871–

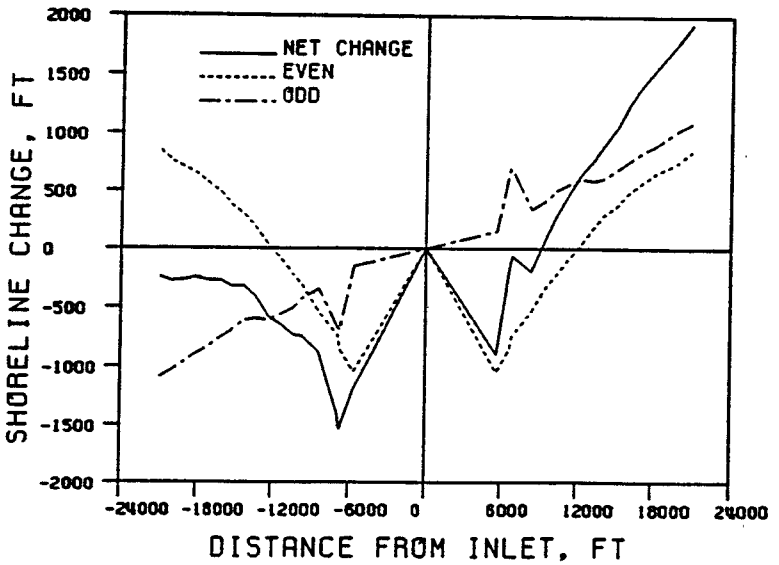

Figure 73: Nassau Sound: Even/Odd analysis of shoreline change: 1871–1979.

1979. The northern shore of Little Talbot Island accreted about 1000 feet during the same period. Similar erosional/accretional trends are seen along the open coasts of both islands. Thus there is a downdrift offset, contrary to the pattern often seen at tidal inlets. This is reflected in the odd function, shown in Figure 73 for the interval 1871–1979. Also note in Figure 72 that the position of Ft. George Inlet is about 30,000 ft. south of Nassau Sound.

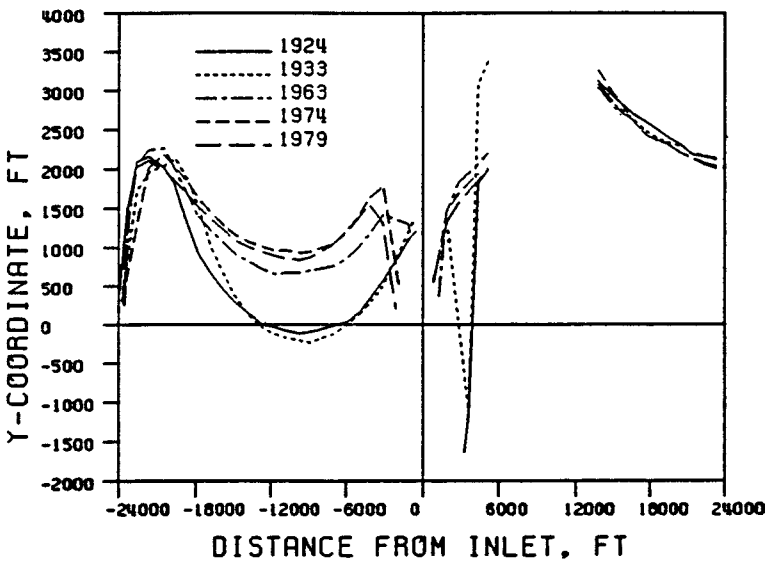

Figure 74: Ft. George Inlet/St. John's River Entrance: Shoreline position vs. time. Ft. George Inlet is at the coordinate system origin.

5.16 Ft. George Inlet — St. John's River Entrance

Ft. George Inlet and St. John's River Entrance will be treated together because of their proximity to one another. The center of Ft. George Inlet is approximately 5.6 miles south of Nassau Sound and roughly one mile north of the north jetty at St. John's River Entrance. St. Augustine Inlet lies 34.5 miles south of St. John's River Entrance. The ebb tidal shoals for Ft. George Inlet and St. John's River Entrance lie close together, and must be considered as one system. Figure 74 shows the shoreline adjacent to Ft. George Inlet and St. John's River Entrance for various dates. Data were unavailable for the 8000 ft. downdrift of St. John's River Entrance.

Both are natural inlets. St. John's River Entrance is a federal navigation project currently maintained to a depth of 42 feet and stabilized on both sides by substantial jetties. The jetties were first constructed between 1881–1890, with the north jetty built to a length of 9400 feet and the south jetty 6800 feet. Both jetties were lengthened in 1895 and again in 1937. The north and south jetties are presently 14,300 feet and 11,200 feet, respectively. The north jetty was sand–tightened in 1934 by placement of a concrete cap.

Ft. George Inlet has no training structures and has not been dredged,

but has been affected by the presence of the north jetty at St. John's River Entrance. It migrated northward roughly 2500 feet during the period 1924–1979, eroding the southern end of Little Talbot Island in the process. A spit with large dunes has grown north from the north jetty of St. John's River Entrance as Ft. George Inlet has migrated northward (see photo). This spit comprises a substantial amount of sand. The channel depth in Ft. George Inlet is approximately 8 feet.

The net longshore transport rate for the area has been estimated at 250,000 to 480,000 yd^3/yr to the south (Walton and USAE, respectively). The ebb tidal shoal was estimated to triple in size from 1874–1978, and was estimated at 174 million yd^3 for 1978. Nearly half of this volume accumulated after the channel at St. John's River Entrance was first dredged to its present 42 ft. depth in 1965. 26.4 million yd^3 was dredged from St. John's River Entrance between 1925 and 1985. Most of this was disposed of at sea, with 1.5 million yd^3 being placed on the south beach. Most of this nourishment occurred during the years 1980–1985.

The lack of data immediately downdrift of St. John's River Entrance precluded any meaningful application of the even/odd analysis technique, but the results of such an application at this site would be of little value because of its complexity. Each inlet lies within the other's zone of influence, one migrates while the other is stabilized, and the north jetty at St. John's River Entrance was quite "leaky" for many years, prior to sand-tightening. A thorough understanding of the processes affecting these inlets would require a detailed analysis that is beyond the scope of this study.

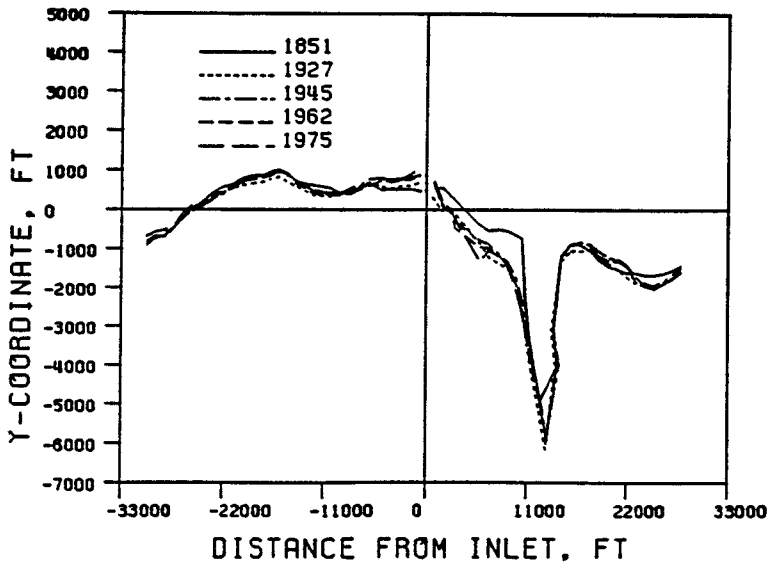

Figure 75: Government Cut: Shoreline position vs. time.

5.17 Government Cut — Miami Harbor Entrance

Government Cut was created in the early 1900's by dredging a channel across the southern end of Miami Beach, to provide a navigable entrance to Biscayne Bay from the Atlantic Ocean. It is approximately 9.3 miles south of Bakers Haulover. Initial plans called for an 18–ft. channel stabilized by a north jetty, but shoaling of material in the channel indicated a need for an additional jetty on the south side of the cut. A south jetty was planned by 1907. The channel has been deepened and widened several times, and both jetties have been extended since their initial construction. The entrance channel is currently maintained at a depth of 38 ft. and a width of 500 ft. The north jetty is 3000 ft. in length, and the south jetty 2000 ft. in length. Estimates of the net longshore sediment transport rate range from 20,000 yd^3/yr (USAE) to 270,000 yd^3/yr (Walton) to the south. The ebb tidal shoal is very small, with offshore reefs making estimation of its size difficult.

The geography of the Government Cut area makes it a rather unique case when examining beach response. Downdrift of the entrance is Fisher Island, which has an ocean–facing coast only about 3100 ft. in length, is bordered on the north by the south jetty for Government Cut, and is bordered on the south by Norris Cut, an unstabilized tidal entrance. Fisher Island has seen

considerable man–made improvements, consists primarily of fill material, and cannot be considered to exist in its natural state.

The beach north of Government Cut has experienced a net gain in material since construction of the inlet. This is due to impoundment of material updrift of the north jetty. Some of this material existed naturally on the updrift beach, and the rest is a result of the Miami Beach restoration project, completed in 1981. The shoreline of Miami Beach has an extensive network of seawalls and groins, exerting their influence during periods of minimum beach width.

6 Conclusion

Accurate prediction of shoreline changes resulting from the presence of tidal inlets remains a challenge for future research. Even confident interpretation of historical changes often requires careful consideration of all the physical processes affecting an area. This study has presented historical shoreline changes for 18 of Florida's east coast tidal inlets, a method for examining these changes, and two techniques that could be used in a predictive mode.

Resolution of measured shoreline changes into two components is one of many ways of examining such data. Dividing shoreline changes into even and odd components has been demonstrated as a method allowing examination of changes attributable, primarily, to the interruption of longshore sediment transport by an inlet. This method has the advantage of being simple to apply, but does not explicitly reveal any information regarding the physical processes affecting the site.

Of the 18 inlets studied, only one, Nassau Sound, may truly be called unmodified. Because of the large width and lack of structures at Nassau Sound, estimation of sediment bypassing rates is difficult. Ft. George Inlet and Matanzas Inlet are the only others studied that have not had structures built for training, but both are affected by man–made structures. Quantitative modelling of shoreline changes at inlets such as these will require accurate representation of the boundary conditions at the inlet.

It was expected that most of the stabilized inlets would provide signals that contained odd functions exhibiting the updrift offset predicted by the analytical solution. This was the case, with several exceptions which were understandable after consideration of the history of the area (e.g. St. Augustine Inlet, Ponce de Leon Inlet). Mechanical bypassing is being used at several inlets in attempts to negate this offset, but the bypassed quantities often appear to be inadequate. Detailed, long–term records of bypassed quantities and frequent surveys of shoreline position should be made to improve future studies.

None of the inlets satisfy all the assumptions included in the analytical solution, but this solution appears reasonable at inlets that approximate the impermeable jetty assumption. Although the best–fit analytical solution is, by definition, forced to agree with the odd function of shoreline change, it appears to yield reasonable values for the relevant wave parameters. Long–term, *directional* wave data could increase confidence in the results.

The numerical model presented attempted to address several processes neglected by the analytical solution, but thought to be important to shore-

line evolution around a tidal inlet: wave refraction and diffraction, wave energy dissipation due to breaking on the ebb tidal shoal, and temporal variation in the incident wave climate. Lack of suitable wave data precluded inclusion of the latter process, a major limitation. The wave transformation processes included in the model may be considered a "first–cut", since they require some rather weak assumptions (linear wave theory valid up to breaking; spilling breaker assumption; no wave–driven currents), but may provide a stepping–stone to more refined methods.

By studying the history of an inlet, and evaluating the even and odd components of shoreline change around it, much can be learned about the physical processes shaping the area. With future refinements in the predictive methods, quantitative prediction of changes will become possible.

REFERENCES

Abramowitz, M., and Stegun, I.A., 1972. "Handbook of Mathematical Functions", Dover Publications, New York, NY.

Berek, E.P., and Dean, R.G., 1982. "Field Investigation of Longshore Transport Distribution", Proceedings of the 18th Coastal Engineering Conference, Cape Town, Republic of South Africa, Volume II, pp. 1620–1639.

Coastal and Oceanographic Engineering Laboratory, University of Florida, Gainesville, Florida. "Coastal Engineering Study of Jupiter Inlet, Palm Beach County, Florida", May, 1969.

Dean, J.L., and Pope, J., 1987. "The Redington Shores Breakwater Project: Initial Response", Coastal Sediments '87, Nicholas C. Kraus, Ed., American Society of Civil Engineers, New York, NY.

Dean, R.G., 1989. Class notes for a course on Littoral Processes. Coastal and Oceanographic Engineering Department, University of Florida, Gainesville, Florida.

Dean, R.G., 1988. "Sediment Interaction at Modified Coastal Inlets: Processes and Policies," in *Hydrodynamics and Sediment Dynamics of Tidal Inlets*, David G. Aubrey and Lee Weisher, eds. Lecture Notes on Coastal and Estuarine Studies 29, Springer–Verlag, New York.

Dean, R.G., and M.P. O'Brien, 1987a. "Florida's East Coast Inlets: Shoreline Effects and Recommended Action", Coastal and Oceanographic Engineering Department, University of Florida, Gainesville, Florida, December, 1987.

Dean, R.G., and M.P. O'Brien, 1987b. "Florida's West Coast Inlets: Shoreline Effects and Recommended Action", Coastal and Oceanographic Engineering Department, University of Florida, Gainesville, Florida, December, 1987.

Dean, R.G., and E.M. Maurmeyer, 1983. "Models for Beach Profile Response," Chapter 7 in *Handbook of Coastal Processes and Erosion*, P.D. Komar, Ed. CRC Press, Boca Raton, Florida.

Douglas, Barry A., 1989. "Prediction of Shoreline Changes near Tidal Inlets," Master of Science thesis, Coastal and Oceanographic Engineering Department, University of Florida, Gainesville, Florida.

Department of Coastal Engineering, Engineering and Industrial Experiment Station, College of Engineering, University of Florida, "The Effect of South Lake Worth Inlet and its Bypassing Plant on Adjacent Shores: Present and New Installations", July 21, 1965.

Harlem, P.W., 1979. "Aerial Photographic Interpretation of the Historical Changes in Northern Biscayne Bay, Florida: 1925–1976", University of Miami Sea Grant, Miami, Florida.

Hunt, S.D., "Port Canaveral Entrance: Glossary of Inlets Report No. 9", Department of Coastal and Oceanographic Engineering, University of Florida, Gainesville, Florida. Florida Sea Grant College, December, 1980.

Jones, C.P., and Mehta, A.J., 1978. "Ponce de Leon Inlet: Glossary of Inlets Report No. 6", Department of Coastal and Oceanographic Engineering, University of Florida, Gainesville, Florida, February, 1978.

Larson, M., Hanson, H., and Kraus, N.C., 1987. "Analytical Solutions to the One–Line Model of Shoreline Change", Technical Report CERC–87–15, Coastal Engineering Research Center, U.S. Army Corps of Engineers, Vicksburg, Mississippi.

Marino, J.N., 1986. "Inlet Ebb Shoal Volumes Related to Coastal Physical Parameters", Thesis, Coastal and Oceanographic Engineering Department, University of Florida, Gainesville, Florida.

Marino, J.N., and Mehta, A.J., 1986. "Sediment Volumes Around Florida's East Coast Tidal Inlets: Final Report", Coastal and Oceanographic Engineering Department, University of Florida, Gainesville, Florida, July, 1986.

Mehta, A.J., Adams, W.D., and Jones, C.P., 1976. "Sebastian Inlet: Glossary of Inlets Report No. 3", Coastal and Oceanographic Engineering Laboratory, University of Florida, Gainesville, Florida, August, 1976.

Mehta, A.J., and Jones, C.P., 1977. "Matanzas Inlet: Glossary of Inlets Report No. 5", Florida Sea Grant Program, May, 1977.

Mei, C.C., 1989."The Applied Dynamics of Ocean Surface Waves", World Scientific, Singapore.

Pelnard–Considère, R., 1956. "Essai de Théorie de l'Evolution des Forms de Rivages en Plage de Sable et de Galets", 4th Journées de l'Hydraulique, les Energies de la Mer, Question III, Rapport No. 1, pp. 289–298.

Penney, W.G., and Price, A.T., 1952. "The Diffraction Theory of Sea Waves and the Shelter Afforded by Breakwaters", Royal Society of London.

Perlin, M., and Dean, R.G., 1983. "A Numerical Model to Simulate Sediment Transport in the Vicinity of Coastal Structures", Miscellaneous Report No. 83–10, Coastal Engineering Research Center, U.S. Army Corps of Engineers, Ft. Belvoir, Virginia, May, 1983.

Purpura, J.A., and Chiu, T.Y., 1977. "Second Report on the Performance of the Ponce de Leon Inlet, Florida, Improvement System", Coastal and Oceanographic Engineering Laboratory, University of Florida, Gainesville, Florida, July, 1977.

Walker, J.R., and Dunham, J.W., 1977. "Lake Worth Inlet — Case Study", Coastal Sediments '77, American Society of Civil Engineers, New York, NY.

Walton, T.L., and Adams, 1976. "Capacity of Inlet Outer Bars to Store Sand," Proceedings of the 15th Coastal Engineering Conference, Honolulu, Hawaii. American Society of Civil Engineers, New York, NY.

Walton, T.L., 1974a. "St. Lucie Inlet: Glossary of Inlets Report No. 1", Florida Sea Grant Report Number 2, July, 1974.

Walton, T.L., 1974b. "Fort Pierce Inlet: Glossary of Inlets Report No. 2", Florida Sea Grant Report Number 3, July, 1974.

Walton, T.L., 1976. "Littoral Drift Estimates Along the Coastline of Florida", Florida Sea Grant Report Number 13, August, 1976.

Walton, T.L., 1977. "Beach Nourishment in Florida and on the Lower Atlantic and Gulf Coasts", Florida Sea Grant Technical Paper No. 2, December, 1977.

Winer, Harley S., 1988. "Numerical Modelling of Wave–Induced Currents Using a Parabolic Wave Equation", Coastal and Oceanographic Engineering Department, University of Florida, Gainesville, Florida.

Yan, Yixin, 1987. "Numerical Modeling of Current and Wave Interactions of an Inlet–Beach System", Coastal and Oceanographic Engineering Department, University of Florida, Gainesville, Florida.